NASA/CR—1999-208880 PWA 6420–107

Acoustic Reflection and Transmission of 2–Dimensional Rotors and Stators, Including Mode and Frequency Scattering Effects

Donald B. Hanson
United Technologies Corporation, East Hartford, Connecticut

Prepared under Contract NAS3–26618

National Aeronautics and
Space Administration

Glenn Research Center

March 1999

Available from

NASA Center for Aerospace Information
7121 Standard Drive
Hanover, MD 21076
Price Code: A04

National Technical Information Service
5285 Port Royal Road
Springfield, VA 22100
Price Code: A04

FORWARD

The goal of Task 4/4a of NASA's Large Engine Technology Contract (Contract NAS3-26618) has been to develop a design method for turbofan harmonic noise. The method is based on theory to the extent that it permits calculations at the high frequencies and wavenumbers required for modern engines. Grid requirements and high computer times preclude direct use of Computational Fluid Dynamic and, instead, techniques from classical duct acoustics and cascade unsteady aerodynamics have been adapted to the task. Based on earlier work, we felt that the new method had to include the effect of swirl between the rotor and stator and the effect of unsteady rotor/stator coupling. This lead us to a scheme in which the acoustic elements of a fan (inlet, rotor, stator, nozzle) of a fan are analyzed first as isolated elements and then coupled by matching eigenmodes at planes between the elements. The end product of this work is TFaNS - the Theoretical Fan Noise prediction and design System, which is reported separately by D. A. Topol: "Development and Evaluation of a Coupled Fan Noise Design System," AIAA Paper No. 97-1611.

At the heart of the prediction system is the scattering behavior of the blade rows. This encompasses conversion of vortical waves (wakes) from the rotor into acoustic waves at the stator as well as acoustic reflection and transmission properties of both blade rows. In the regime of interest for fan design, blade row scattering includes mode and frequency scattering. These phenomena have been recognized in the past but never characterized extensively. Hence, an important part of the current work has been to explore this scattering behavior and to provide a report that can be used to understand the elements of TFaNS and to form a basis for future work with more advanced representations of blade row. This report is based strictly on 2D analysis and is divided into 2 parts: Part 1 provides theoretical background and a few computed examples so that the basic physics can be understood. This part is a reprint of an AIAA paper. Part 2 provides an extensive series of scattering curves documenting behavior over a range of mode orders and blade passing frequency harmonics. The curves are annotated to aid in physical interpretation with reference to theory developed in Part 1.

The actual code used for scattering in TFaNS has been developed by H. D. Meyer as documented in a separate report: "Final Report under Contract NAS3-26618," December, 1997. Meyer treats scattering in a annular duct via a quasi-3D technique: input and output waves are 3D, blade unsteady loading response is handled by 2D strip analysis, and coupling of the loading to duct modes is by the 3D duct Green's function. The present report and Meyer's report have been coordinated to use the same test cases and a similar notation and presentation format.

The project manager at NASA-Lewis for this work was Dennis Huff.

TABLE OF CONTENTS

AIAA/CEAS 97-1610
Acoustic Reflection and Transmission of Rotors and Stators Including Mode and Frequency Scattering

D. B. Hanson
Pratt & Whitney
East Hartford, CT, USA

18th AIAA
Aeroacoustics Conference
May 12-14, 1997
Atlanta, Georgia

ACOUSTIC REFLECTION AND TRANSMISSION OF ROTORS AND STATORS INCLUDING MODE AND FREQUENCY SCATTERING

Donald B. Hanson*
Pratt & Whitney
East Hartford, Connecticut

Abstract

In an earlier paper, a reduced order modeling scheme was presented for unsteady acoustic and vortical coupling between adjacent blade rows in a turbomachine. The essential behavior of the system is governed by modal scattering coefficients (i.e. reflection and transmission coefficients) of the rotor, stator, inlet, and nozzle, which are calculated as if they were connected to non-reflecting ducts. The objective of this paper is to identify fundamental behavior of these scattering coefficients for a better understanding of the role of blade row reflection and transmission in noise generation. A 2D flat plate unsteady cascade model is used for the analysis with the expectation that the general behavior presented herein will carry over to models that include more realistic flow and geometry.

It is shown that stators scatter input waves into many modes at the same frequency whereas rotors scatter on frequency, or harmonic order. Important cases are shown where the rotor reflection coefficient is greater than unity: a mode at blade passing frequency (BPF) traveling from the stator with unit sound power is reflected by the rotor with more than unit power at 2×BPF and 3×BPF. Analysis is presented to explain this unexpected phenomenon. Scattering curves are presented in a format chosen for design use and for physical interpretation. To aid in interpretation of the curves, formulas are derived for special conditions where wavefronts are parallel or perpendicular to the rotor or stator chords.

Introduction

For the purposes of predicting fan noise, we consider the engine to be as sketched in Figure 1 where we identify various "acoustic elements": inlet, rotor, stator, and nozzle. Much of the fan noise is caused by rotor wakes interacting with the stator. Useful prediction models for rotor/stator interaction noise have been developed in earlier models based on classical analysis methods: references 1 and 2, which were early precursors of the current model, treated rotor periodic wakes, stator loading response, and coupling to duct modes under the assumptions of uniform axial flow and no reflections or transmission losses from the other acoustic elements.

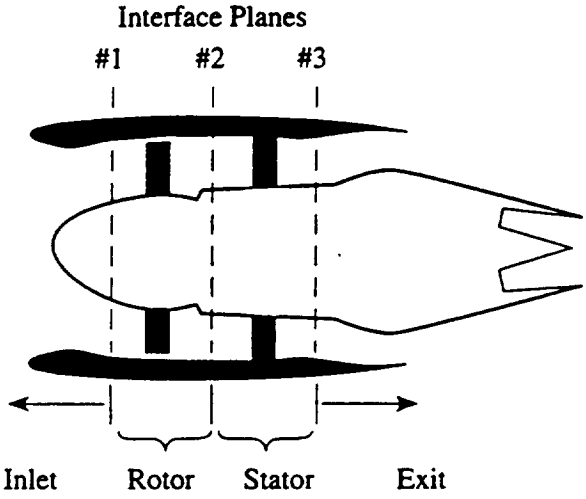

Figure 1. "Acoustic elements" for a coupled fan noise model.

Later (reference 3), coupling to Eversman's inlet and nozzle radiation codes[4,5] permitted computation of harmonic directivity patterns, still ignoring reflections back into the source region.

More recently, emphasis has been on including effects of unsteady coupling between the various acoustic elements according to the scheme presented in reference 6. Here, each of the acoustic elements is treated in isolation to compute its input/output relationship in terms of modal reflection and transmission coefficients. Then the elements are coupled at the interface planes by solving a linear system that matches the input to each element with the output of its neighbors. This coupling system is described in detail in the references and is summarized in the background section below. Overall evaluation of the fan noise prediction system is described in a companion paper by Topol (reference 7). The purpose of the present paper is to gain a better understanding of just one aspect of the coupling physics: behavior of the reflection and transmission coefficients (or, more generally, scattering coefficients) for the rotor and stator blade rows. We go beyond the type of information presented in other related studies and include scattering into modes and frequencies that are different from those of the input waves

Blade row scattering behavior is computed with flat plate cascade theory (an adaptation of the theory of S. N. Smith, ref. 8) and steady loading (with the attendant turning of the flow) is modeled via actuator disks coupled to the blade rows. This simplistic modeling provides a

*Technical Fellow-Acoustics, Associate Fellow -AIAA

basic understanding of the physics and kinematics of scattering and has been used to interpret the behavior of the fan noise prediction system. It is hoped that this work will also provide a model for future studies with more sophisticated computational procedures, i.e. CFD methods. This paper can show only a few examples of scattering but a supplemental NASA report[9] includes a large catalog of scattering curves. Furthermore, a separate report by H. D. Meyer[10] includes a quasi-3D model with scattering on radial modes.

The background section below reviews the coupling scheme and notation in enough detail that scattering coefficients can be defined clearly. That is followed by a section that explains the data presentation format and reasoning behind it. A review of mode kinematics is given and then formulas are derived for interpreting the scattering curves in terms of wave angles. The "results" section presents representative scattering curves with discussion and interpretation. Finally, there is an analysis of sound power issues, including an explanation of how a reflected acoustic power from a rotor can exceed the input power.

Background on Blade Row Coupling and Definition of Scattering Coefficients

This section reviews the coupling scheme used in the Theoretical Fan Noise Prediction System (TFaNS) in enough detail to define notation used for the scattering coefficients that are the subject of this report. Readers interested in a complete description of the coupling scheme should consult reference 6 or 7. In the coupling method, perturbations at the various interface planes in the fan are expanded in eigenmode series. The complex amplitude coefficients of the series are to be found in the coupling solution. Scattering coefficients are defined as ratios of these modal pressure amplitude coefficients. The scattering curves presented in this paper are in terms of power ratios rather than pressure ratios.

In Figure 1 there are 4 acoustic elements: inlet, rotor, stator, and nozzle. These are joined at interface planes indexed by r= 1, 2, and 3. At each of these planes the total perturbation in 2D uniform flow can be written as the sum of harmonic pressure waves and vortical waves. These are indexed, following Smith's notation, by T= 1 (for upstream going pressure waves), T = 2 (for downstream going pressure waves), and T = 3 (for vortical waves).

For pressure waves (T= 1,2):

$$p_T^r(x,\phi,t) = p_o \sum_{n=-\infty}^{\infty} \sum_{k=-\infty}^{\infty} A_T^r(n,k) e^{i[\alpha_T^r(n,k)(x-x_T^r)+\psi_{n,k}]} \tag{1}$$

Vortical waves (T= 3) are defined in terms of their axial velocity component (rather than directly in terms of the vorticity):

$$u_T^r(x,\phi,t) = a_o \sum_{n=-\infty}^{\infty} \sum_{k=-\infty}^{\infty} A_T^r(n,k) e^{i[\alpha_T^r(n,k)(x-x_T^r)+\psi_{n,k}]} \tag{2}$$

although only the pressure waves are treated in this paper. In the above equations, x, φ, and t represent the narrow annular duct coordinates and time, n is the BPF harmonic index, and k counts the circumferential modes. p_o and a_o are reference pressure and speed of sound that can be defined by the user but are usually taken to be their sea level, standard day values. α, with its indices, represents axial wavenumber and is discussed in later sections. x_T^r is the origin for each wave, taken at the interface plane where the wave exits an acoustic element. (This convention keeps the exponential behavior of cut off waves from yielding very large scattering coefficients.) Finally,

$$\psi_{n,k} = -m\phi + n\Omega t \tag{3}$$

is called the kinematic phase since it describes the mode spin characteristics.

$$m = nB - kV \tag{4}$$

is circumferential mode order per the familiar Tyler/Sofrin spinning mode theory.

The significance of equations 1 and 2 is that they *define* the complex amplitude coefficients $A_T^r(n,k)$. The ordered array of these coefficients is called the state vector and its knowledge specifies the perturbations at the interface planes. Scattering coefficients are defined according to the following notation.

$$A_{T'}^{r'}(n',k') \leftarrow S_{T',T}^{r',r}(n',k';n,k) A_T^r(n,k) \tag{5}$$

This is read: "a wave of type T at interface plane r with harmonic index n and circumferential order $m = nB\text{-}kV$ scatters into a wave of type T' at interface plane r' with harmonic index n' and circumferential mode order $m' = n'B\text{-}k'V$". The left arrow is used rather than an = sign because each input wave scatters into more than one output wave. The system equation incorporating these scattering coefficients is given in figure 2. $B_T^r(n,k)$ is the source vector, which is considered known or prescribed and has the same form as the state vector $A_T^r(n,k)$. The source vector could represent wakes from the rotor or it could represent stator output waves in an uncoupled environment, i.e. noise as calculated for an isolated stator with wake excitation. System equation A = S × A + B in figure 2 is interpreted to mean "the state vector A is the sum of the scattered waves and the source wave B".

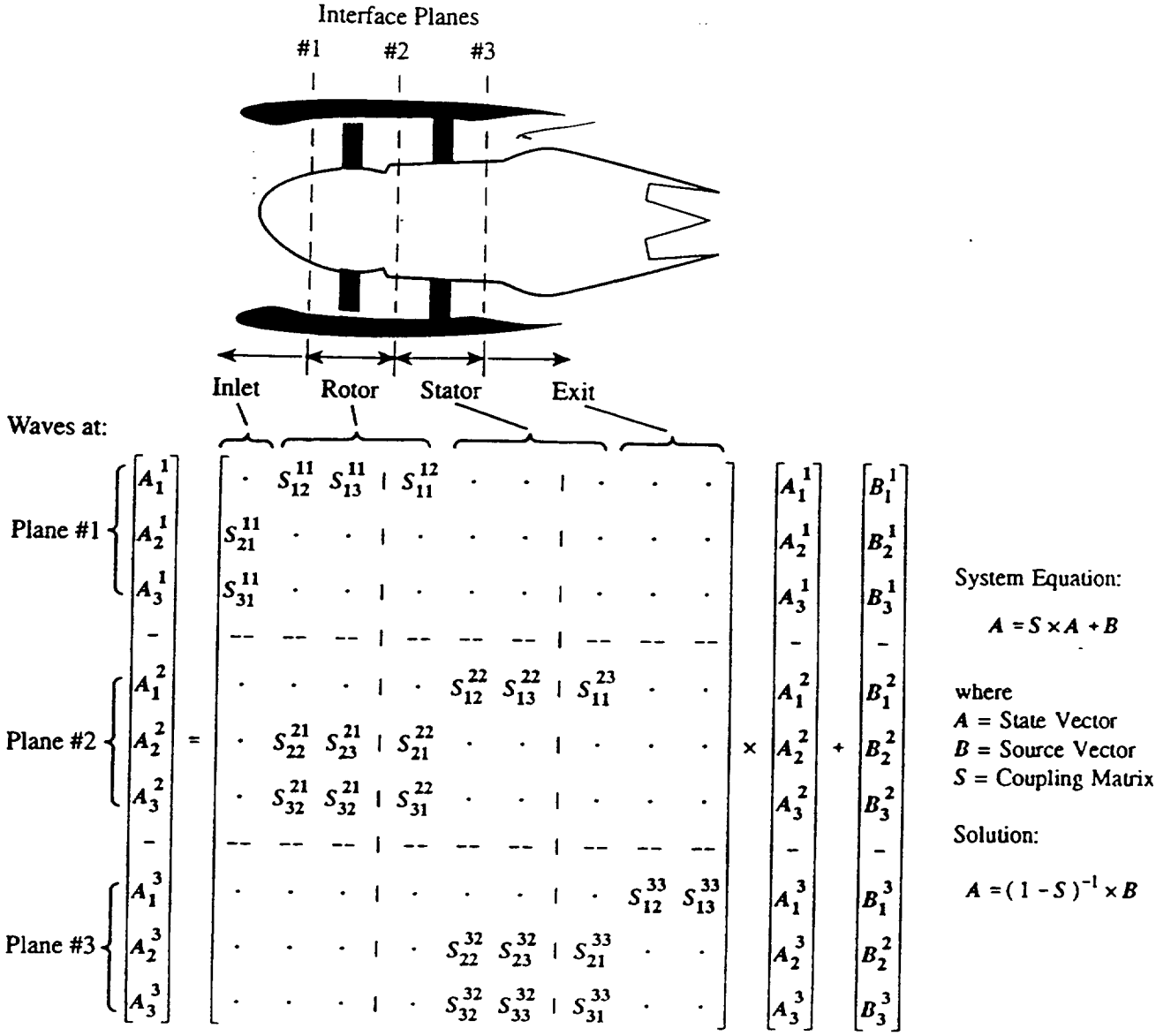

Figure 2. Generalized coupling scheme for fan noise from ref. 6.

Certain scattering rules apply. Waves either reflect back to the input plane or transmit to adjacent planes, i.e. $r' = r$ or $r' = r \pm 1$. Each wave type T scatters into all wave types T'. Scattering on the n,k indices is as follows:

$$\begin{array}{lccl} \text{inlet:} & n,k & \leftarrow & n,k \\ \text{nozzle:} & n,k & \leftarrow & n,k \\ \text{rotor:} & n',k & \leftarrow & n,k \\ \text{stator:} & n,k' & \leftarrow & n,k \end{array} \qquad (6)$$

Inlets and nozzles do not scatter on these indices because of their assumed axisymmetry. Rotors scatter on harmonic order but not on the k index. Stators scatter on k but not on frequency. In 3D, there is additional scattering or radial mode order. These rules are discussed in more detail in reference 6.

As mentioned in the introduction, scattering coefficients are computed by use of Smith's 2D unsteady cascade theory adapted for use with actuator disks that address turning of the mean flow. In this application, an actuator disk is a plane where the mean flow properties jump to represent the gap-averaged change across either a rotor or stator. For example, the stator model is built up conceptually by starting with the disk separating the flow in region 2 (the swirl region) from the flow in region 3 (the exit region). The flow on each side of the disk is uniform with properties representing the gap-averaged flow upstream and downsteam of the stator. Mean flow conditions are considered known and are prescribed from a separate aerodynamic analysis. The acoustic properties of the actuator disk are found by requiring that mass and momentum be conserved across the disk to first order in the perturbations. (More detail is given in ref. 9.) Conservation of mass and 2

components of momentum across the disk for any wave input requires scattering into 3 output wave types (the same as described above). Scattering coefficients are computed according to equation 5, with scattering only on wave type (T into T'). Turning of the mean flow is associated with the mean loading on the stator. Unsteady loading is handled with Smith's unsteady cascade theory. The scattering properties of the cascade are determined, again according to equation 5, and the cascade and actuator disk are combined into a single acoustic element representing the stator by matching the unsteady output of each sub-element to the input of the other.

Format for Scattering Curves and Sample Results

This section explains the format to be used for reflection and transmission (scattering) coefficient curves and explains why it is different from formats used in other studies. It also presents a sample curve to illustrate the major features of interest such as mode scattering, cutoff points, and peaks and valleys associated with alignment of the waves with the cascade chordlines. Formulas to help identify these special features are derived later.

Smith's Reflection/Transmission Curves - Figure 3 shows reflection and transmission curves from Smith's report that have often been reproduced by other investigators and referenced in reports. The coefficients represent ratios of output wave pressure amplitude to input wave amplitude for constant geometry, Mach number, and reduced frequency while interblade phase angle is varied. This is a reasonable format considering that the fundamental variables of Smith's analysis are

Gap/chord ratio:	$G = g/c$
Stagger angle:	θ
Mach number:	$M = W/a$
Reduced frequency:	$\hat{\omega} = \omega c / W$
Interblade phase angle:	σ

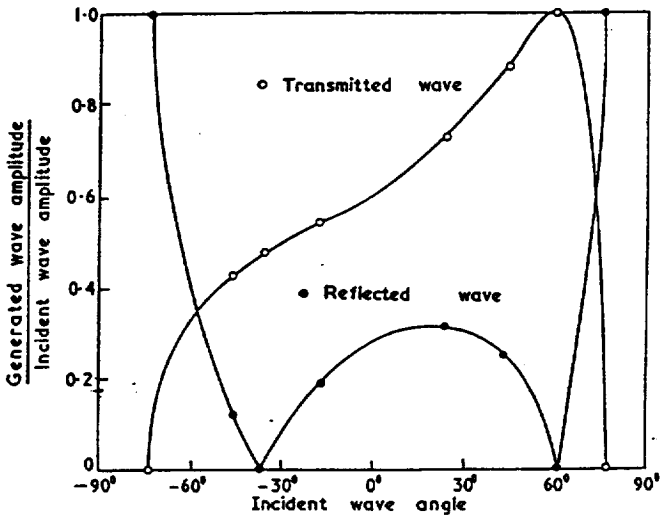

Figure 3. Smith's reflection and transmission curves. $G = 1, \theta = 60°, M = 0.5, \hat{\omega} = \pi / 2$

In generation of the curves, the first 4 parameters were held constant and the last was varied to vary incident wave angle. The frequency chosen by Smith was such that only one mode propagates. Hence, the mode scattering phenomena highlighted in the present paper does not occur, although Smith's theory includes the effect. Note from the curves that, in general, the sum of the reflection and transmission coefficients is not = 1.

Rotor/Stator Interaction Noise Analyses - In typical rotor/stator interaction analyses, geometry and frequency are inter-related in such a way that constant *reduced* frequency is not appropriate for noise studies. Consider the geometry and flow sketched in Figure 4 applied to an annulus of radius R. Often the solidities (or gap/chord ratios) of the 2 blade rows are fixed by aerodynamic requirements (at least within narrow limits). Also, the flow angles and Mach numbers are set by pressure ratio and tip speed constraints. In a typical acoustic design study, the stator would be varied by changing vane number V at constant gap/chord ratio. Since reduced frequency depends on chord, it will vary if stator gap/chord ratio is held constant. Hence, the strategy for the present study was to hold flow angles and Mach numbers constant (per the Mach triangle in Figure 4) and to vary vane/blade ratio at constant rotor gap/chord G. Then reduced frequency can be computed from the other parameters using $\omega = nB\Omega$:

$$\hat{\omega} \equiv \frac{\omega c}{W} = \frac{nB\Omega c}{Ma} = \frac{nB\Omega R / a}{M} \frac{c}{R} = 2\pi \frac{nB}{V} \frac{M_T}{M} \Big/ G \qquad (7)$$

Interblade phase angle for the cascade theory is σ = -

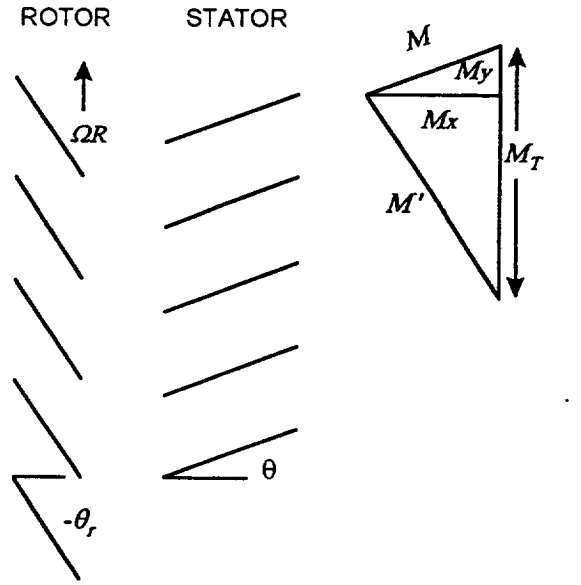

Figure 4. Mach numbers and flow angles for rotor and stator. Blades & vanes are aligned with flow.

$2\pi nB/V$. The role of $M_T \equiv \Omega R/a$ is to set frequency.

The rotor experiences radian frequency $\omega = kV\Omega$. In this case the reduced frequency becomes

$$\hat{\omega}_r \equiv \frac{\omega c_r}{W'} = \frac{kV\Omega c_r}{M'a} = \frac{kV\Omega R/a}{M'} \frac{c_r}{R} = 2\pi \frac{kV}{B} \frac{M_T}{M'} \Big/ G_r \tag{8}$$

In this case the interblade phase angle is $2\pi kV/B$, the sign difference being caused difference in the sign of relative motion of the adjacent blade row. From the discussion above, it can be deduced that scattering behavior depends only on vane/blade ratio, not on V and B individually.

Figure 5 shows representative curves in the standard form of this study. The basic B - V interaction mode (i.e. $m=nB-kV$ with $n=k=1$) was input to the stator from

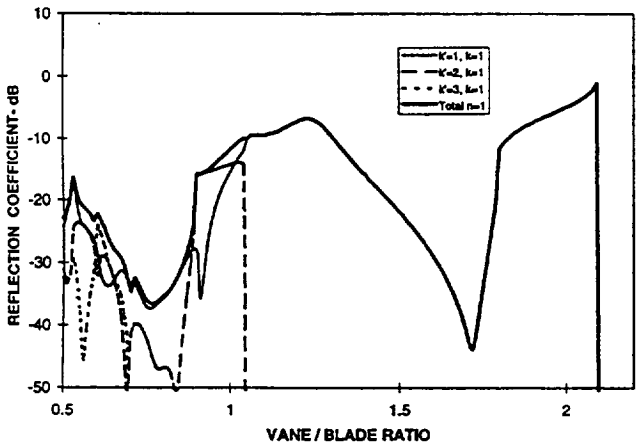

Figure 5. Sample reflection curves for stator with input of fundmental *B-V* mode *(n,k=1,1)*. Scattering into many modes *(n;k'=1;1,2,3...)*.

the rotor side (region 2) and traveled downstream to reflect at the stator into many waves (of which 3 are shown). The curves give the ratio of power in the output waves to power in the input wave with 0 dB representing unit reflection ratio. We point out a few features of Figure 5 before providing the detailed means to analyze scattering curves in the following section. First, note that the input wave cuts off at $V/B = 2.1$ and the $k' = 2$ and 3 output waves cut off at $V/B = 1.05$ and 0.70, respectively. Also, note the dip in all of the reflection curves around $V/B = 0.75$. This is the point where the input wave is oriented to pass through the stator without scattering (wavefronts are normal to the chord lines). Finally, the dip at $V/B = 1.7$ is where the reflected wave is oriented for poor coupling to the unsteady loading dipoles (again, wavefronts normal to chords).

Wavenumbers, Wave Angles, and Cutoff

In this section we develop relationships needed to interpret scattering curves in terms of vane/blade ratio and the relevant Mach numbers. For example, by comparing angles of wavefronts with stagger angles, conditions of high transmission or reflection can be predicted. Special formulas are derived for the "Venetian blind" condition where waves pass through a cascade unaffected, the "modal" condition where waves are weakly reflected because the loading dipoles are parallel to the wave fronts, and the "broadside" condition where wavefronts are parallel to the airfoil chords.

Circumferential Wavenumber and Mode Spin Characteristics - In Smith's original paper, waves are specified via complex coefficients multiplying exponentials of the general form

$$e^{i(\alpha x+\beta y+\omega t)} \tag{9}$$

where α and β are axial and tangential wavenumbers and ω is the radian frequency. For turbomachinery application, the frequency in the stator reference frame is

$$\omega = nB\Omega \tag{10}$$

where Ω is the shaft rotational frequency, B is the number of rotor blades, and n is harmonic order. Also, we wrap the tangential coordinate onto a narrow annulus of radius R so that $y = R\varphi$ and $\beta y = \beta R\varphi$. For the required periodicity in φ, βR must be an integer. We choose

$$\beta R = -m \tag{11}$$

so that the exponential above becomes

$$e^{i(\alpha x - m\phi + nB\Omega t)} \tag{12}$$

The circumferential mode order m is known from standard fan acoustic theory to be

$$m = nB - kV \tag{13}$$

where V is the vane count and k is an integer index. The mode spin behavior can be deduced from the φ, t portion of the exponential. If we track the zero phase point on a wave, the equation of motion (in the $x = 0$ plane) is

$$m\phi_o = nB\Omega t \tag{14}$$

from which the mode angular speed $\Omega_{mode} = \partial\phi_o / \partial t$ is

$$\Omega_{mode} = \frac{nB\Omega}{m} \tag{15}$$

Thus, the sign convention chosen above is such that the mode spins in the same direction as the rotor shaft for positive m (and positive harmonic order n). Because

m can have either sign, modes can be co-rotating (with the rotor) or counter-rotating.

Axial Wavenumber and Cutoff - Smith gives the axial wavenumber as

$$\alpha_{1,2} = \frac{1}{a^2 - U^2}\left[U(\omega + V\beta) \pm a\sqrt{(\omega + V\beta)^2 - (a^2 - U^2)\beta^2}\right] \tag{16}$$

For propagating waves, the 1 subscript and the upper sign apply to upstream going waves and the 2 subscript and the lower sign apply to downstream going waves. Here, U and V are axial and tangential mean flow velocity (soon to be replaced by aM_x and aM_y). If we define a non-dimensional α in parallel with the circumferential wave number m, then Equation 16 becomes

$$\bar{\alpha}_{1,2} \equiv \alpha_{1,2}R = \frac{1}{1 - M_x^2} \times$$
$$\left[M_x(nBM_T - mM_y) \pm \sqrt{(nBM_T - mM_y)^2 - (1 - M_x^2)m^2}\right] \tag{17}$$

where $M_T = \Omega R/a$ is the rotor tip Mach number and $\omega R/a = nBM_T$ is the non-dimensional frequency commonly used in duct acoustics.

When the square root in Equation 17 is real, the wavenumber is real and the mode propagates unattenuated in the x direction; when the square root is imaginary, the mode decays exponentially. The dividing point, where the radicand is zero, is the cutoff condition:

$$(nBM_{T,cutoff} - mM_y)^2 = (1 - M_x^2)m^2 \tag{18}$$

The solution for the cutoff Mach number is

$$nBM_{T,cutoff} = \left[\pm\sqrt{1 - M_x^2} + M_y\right] \times m \tag{19}$$

which is sketched in Figure 6.

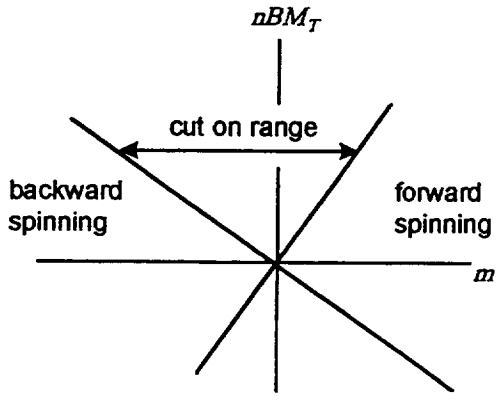

Figure 6. Mode order - frequency domain showing more modes cut on for spin against the swirl.

The 2 diagonal lines are the cutoff boundaries. The bias to the left, associated with a positive M_y (swirl in the direction of rotor rotation), shows for a given lobe count $|m|$ that backward spinning waves (m <0) cut on at lower frequencies than forward spinning waves. Stated differently, when the mode spins against the swirl, it cuts on at lower frequency.

Equation 19 can also be written to express the range of V/B for cut on modes:

$$\left(\frac{kV}{nB}\right)_{\text{cutoff}} = 1 - \frac{M_T}{M_y \pm \sqrt{1 - M_x^2}} \tag{20}$$

which is sketched in Figure 7 in a form to aid in interpreting the abcissas of the scattering curves.

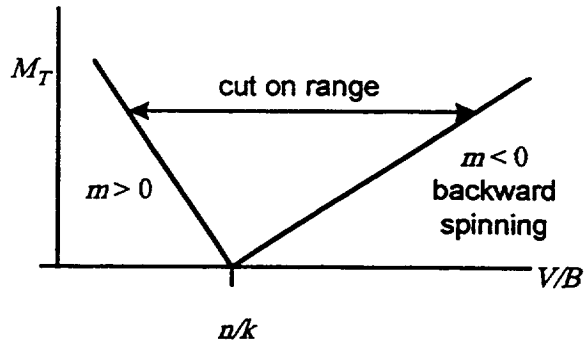

Figure 7. Cut on range in terms of V/B ratio and tip Mach number. Same abscissa used in scattering plots

Wavefront Slopes - In Equation 1 a wavefront is a line of constant phase at any fixed time. For example, $\alpha x + \beta y = 0$. Slopes of these lines in the x,y plane are $S_{1,2} = -\alpha/\beta = \bar{\alpha}_{1,2}/m$. From the above expressions, this is

$$S_{1,2} = \frac{1}{1 - M_x^2} \times$$
$$\left[M_x\left(\frac{nBM_T}{m} - M_y\right) \pm s_m\sqrt{\left(\frac{nBM_T}{m} - M_y\right)^2 - \left(1 - M_x^2\right)}\right] \tag{21}$$

where s_m is the sign of m and the upper/lower signs apply to up/downstream going waves.

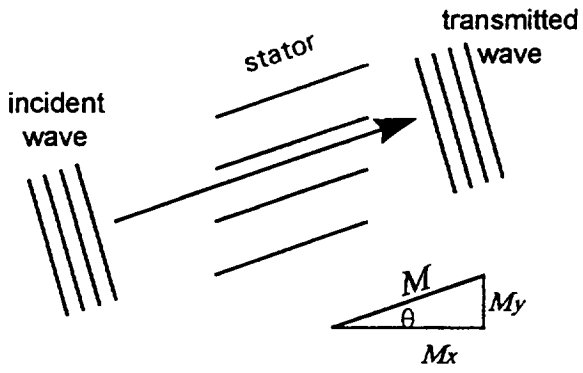

Figure 8. "Venetian blind" condition for stator. Incident wavefronts with slope $-Mx/My \perp$ chord

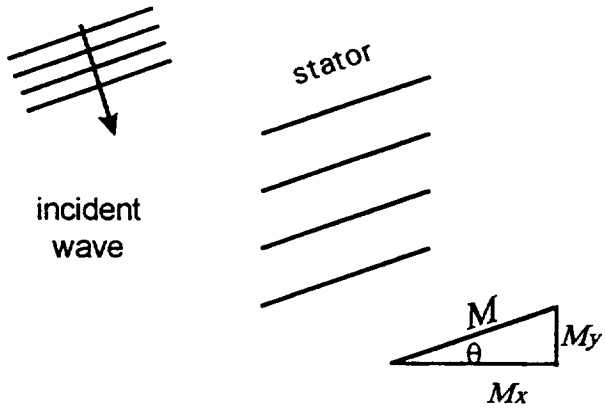

Figure 10. "Broadside" condition for stator. Incident wavefronts // chord. Wavefront slopes = My/Mx.

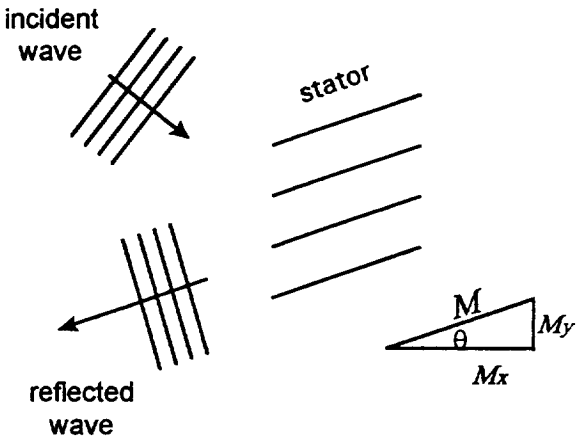

Figure 9. "Modal" condition for stator: reflected wavefront $\perp$ chord. Wavefront slope = $-Mx/My$.

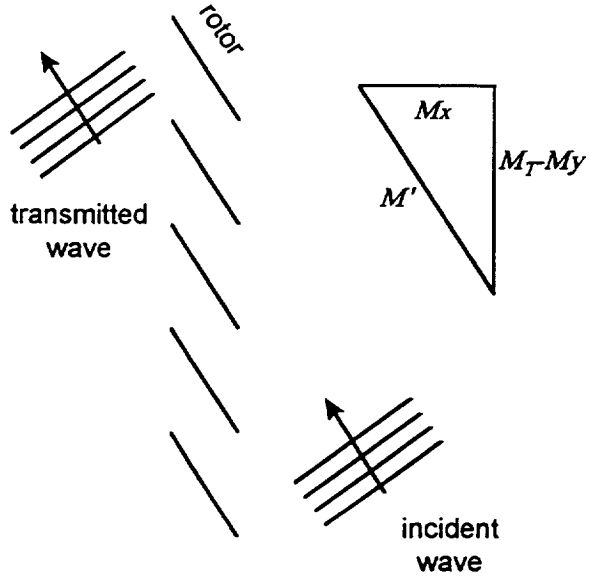

Figure 11. Venetian blind" condition for rotor. Incident wavefronts $\perp$ chord. Slope = $Mx/(M_T-My)$.

Special Angles and Vane/Blade Ratios

We expect scattering curves to exhibit certain behavior when wavefronts are parallel or perpendicular to the airfoils. The most obvious example is when waves perpendicular to the vanes impinge on the stator: we expect the wave to pass through the blade row without scattering as in Figure 8. We call this the "Venetian Blind" condition and the figure shows the required slope to be $-M_x/M_y$. A related, but less obvious, situation shown in Figure 9 is called the "modal" condition. Here the reflected waves are normal to the chords. With this alignment, the unsteady loading dipoles cannot couple to the reflected wave and reflection is weak. Again, the slope is $-M_x/M_y$.

In the "broadside" condition, waves are parallel to the chord lines as in Fig 10. For broadside incident waves, we expect high reflection (at least at high frequency).

The analogous conditions for the rotor are obvious extensions of the above. For example, the Venetian blind condition is shown in Figure 11. Here, from the Mach triangle, the blade chord slopes are $-(M_T-M_y)/M_x$.

Now, we set about finding formulas for vane/blade ratios that lead to wavefronts either parallel or perpendicular to the chordlines. This is done by solving Equation 21 for kV/nB in terms of the wavefront slope and inserting slopes from the sketches in Figures 8-10.

$$\frac{kV}{nB} = 1 - \frac{M_T}{M_y - M_x S \pm \sqrt{1+S^2}} \qquad (22)$$

The sign $\pm s_m$ in Equation 21 has been lost because of a squaring operation and a new $\pm$ has appeared from application of the quadratic formula. Hence, we must re-evaluate the sign choice based on physical arguments.

For waves perpendicular to the stator, we showed above in Figures 8 and 9 that $S = -M_x/M_y$. Substitution into Equation 22 leads to

$$\frac{kV}{nB} = 1 - \frac{M_T \sin\theta}{M \pm 1} \qquad (23)$$

To deal with the sign choice, consider the dowstream-going wave in Figure 8. The sketch shows that downstream-going waves are co-rotating, so that $m > 0$. Since $m=nB-kV$, positive m requires $kV < nB$ so that $kV/nB < 1$. This is given by the positive sign in equation 23 since the relative Mach number $M < 1$. Thus, the upper/lower sign in Equation 23 applies to the down/upsteam going wave.

For waves parallel to the stator, Figure 10 showed the required slope to be M_y/M_x. In this case, substitution into Equation 22 gives

$$\frac{kV}{nB} = 1 \pm M_T \cos\theta \qquad (24)$$

Here, by similar arguments, the upper/lower sign applies to the down/upstream-going wave.

For the rotor, a more appropriate form of Equation 22 can be derived:

$$\frac{nB}{kV} = 1 - \frac{M_T}{(M_T - M_y) + M_x S \pm \sqrt{1+S^2}} \qquad (25)$$

Substitution of slopes from Figure 11 gives the desired formulas. All of these results are summarized in Tables 1 and 2.

Finally, the cascade response theory can exhibit special behavior when the normal distance between 2 vanes or blades is equal to a half the free space sound wavelength. By noting that the normal spacing of the stator vanes is $gap \times \cos\theta$, the frequency is $nB\Omega/2\pi$, and the gap is $2\pi R/V$, this condition is easily found and is shown in the Tables 1 and 2.

Table 1. Special Conditions for the Stator*

Waves Parallel to Vanes	$\frac{kV}{nB} = 1 \mp M_T \cos\theta$
Waves Perpendicular to Vanes	$\frac{kV}{nB} = 1 \pm \frac{M_T \sin\theta}{1 \mp M}$
½ Wavelength Normal Vane Gap	$\frac{V}{nB} = 2M_T \cos\theta$

Table 2. Special Conditions for the Rotor*

Waves Parallel to Blades	$\frac{nB}{kV} = 1 \mp M_T \cos\theta_r$
Waves Perpendicular to Blades	$\frac{nB}{kV} = 1 \mp \frac{M_T \sin\theta_r}{1 \mp M'}$
½ Wavelength Normal Blade Gap	$\frac{B}{kV} = 2M_T \cos\theta_r$
*Upper/lower signs for up/downstream going waves Note: by convention, rotor angles are negative	

From these tables, we can find the vane/blade ratios at which waves will impinge broadside to the blades (waves parallel to blades), will slip through a blade row without scattering (waves perpendicular to blades), or will have low amplitude when scattered (again, waves perpendicular to blades).

Scattering Results

The present 2-dimensional study was coordinated with 2 other studies performed under the LET 4 contract. The first of these was a parallel study of scattering behavior using newly developed quasi-3D capability (ref. 10). That study, in turn, used geometry and operating conditions chosen to complement evaluation[7] of the TFaNS noise prediction system. In the latter case, most of the evaluation involved comparison with NASA Lewis' test data from the Pratt & Whitney 22 inch ADP model known as "Fan 1". The quasi-3D study used that fan geometry and 2 of the operating conditions, identified as the "mid-speed" and "high-speed" cases. The 2D study was based on the tip station of the same fan for the same 2 conditions. These are reported in detail in ref. 9; selected results from the high speed case are shown later in this paper.

Fan 1 has 18 blades and 45 vanes. However, in this study, vane/blade ratio was varied over the range of 0.5 to 2.5 while holding the gap/chord ratios constant. The geometry and flow were as follows.

Gap/chord rotor/stator:	0.962/0.917
Stagger rotor/stator:	51.3 °/ 30.5°
Pressure ratio:	1.278
Inlet axial Mach #:	0.510
Rotor rotational Mach #:	0.772

Given the inlet axial Mach number, the rotor rotational Mach number, and the pressure ratio, the remaining Mach numbers and flow angles were computed on the assumption of zero losses and axial exit flow with results shown in Table 3.

Table 3. 8750 RPM Condition

Mach Numbers	Upstream of Rotor	Between Rows	Dnstream of Stator
Axial, M_x	0.510	0.404	0.388
Swirl, M_y	0.000	0.238	0.000
Tip, M_T	0.772	0.742	0.733

Reflection and transmission curves for the stator and rotor are shown in Figures 12 and 13. Ordinates are in dB expressing the ratio of output power to power in the input wave. Thus, 0 dB represents unit reflection or transmission. Since emphasis is on rotor/stator coupling, input waves chosen for each blade row come from the direction of the other blade row. In all cases the input is the fundamental interaction mode at blade passing

frequency n, k = 1,1, which is to say the $m = B - V$ mode.

In Figure 12 the stator reflection curve is shown at the top and the transmission curve at the bottom. In accordance with the scattering rules in equation 6, the 1,1 input wave scatters into 1,1; 1,2; 1,3, etc. Application of Equation 20 to the operating conditions on page 8 shows the input wave in region 2 to be cut off at V/B = 2.10, which provides the upper limit on the reflection curves. In region 3 (downstream of the stator) cutoff is at V/B =1.8 as can be seen in the transmission curve. The k' = 2 and 3 modes cut off at ½ and 1/3 of these values, as required by equation 20. At cutoff of the 1,1 mode, the stator reflects all of the input energy (0 dB). Application of formulas in Table 1 on page 8 help identify prominent features of the curves. For example, downstream-going waves are perpendicular to the stator chords at V/B = 0.74 according to the middle formula in Table 1. This is the "Venetian blind" condition: the top curves shows all reflected waves are low in amplitude and the bottom curves show transmission of the input wave only into itself (no scattering into the other k' s). The same formula in Table 1 shows the upstream-going wave to be perpendicular to the chord at V/B = 1.71. This is the "modal" condition indicated by the major dip in the reflection curve: the reflected wave is oriented normal to the stator loading dipoles and thus cannot couple to it. Finally, the bottom formula in Table 1 shows that a ½ wavelength fits between 2 vanes at V/B = 1.28. The dip at V/B = 1.2 in the transmission appears to be related to this but the condition is not precise.

Figure 13 presents the rotor scattering curves in the same format. Now the n, k = 1,1 wave at BPF scatters into BPF, 2×BPF, and 3×BPF, all at k = 1. From formulas in Table 2, a minor dip can be identified at V/B = 0.9 where a half wave fits across the blade gap. The major dip at V/B = 1.54 is the "modal" condition: the fundamental wave input from the stator is reflected with wavefronts normal to the rotor chords. More interesting, however, is the fact that, with input energy at BPF only, the reflected energy is dominated by upper harmonics over most of the V/B range. This is discussed further in the next section. Finally, the rotor transmission curves shown at the bottom of Figure 13 indicate substantial transmission loss over most of the V/B range. However, most of the energy that does get

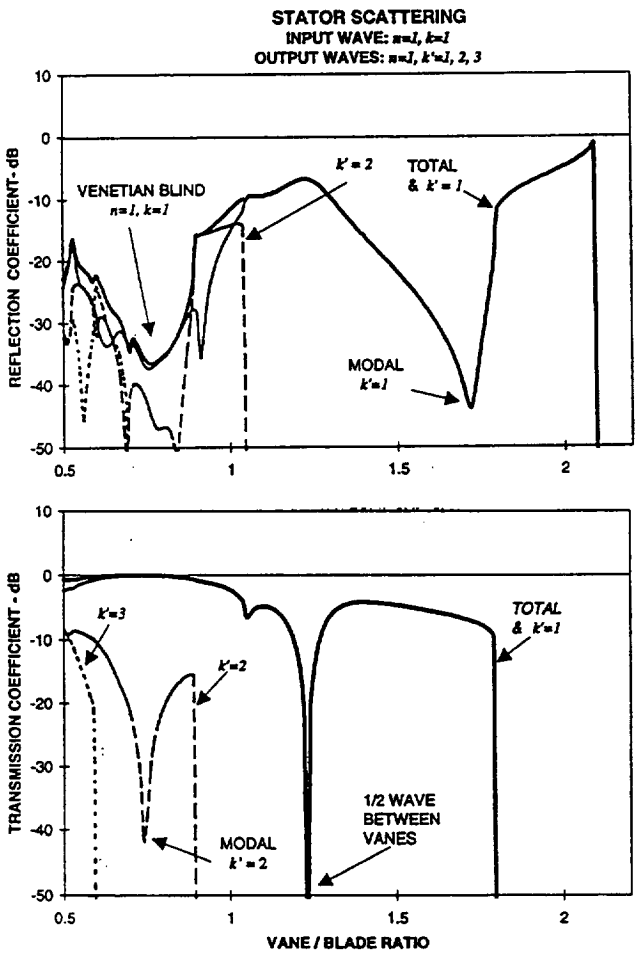

Figure 12. Stator scattering curves

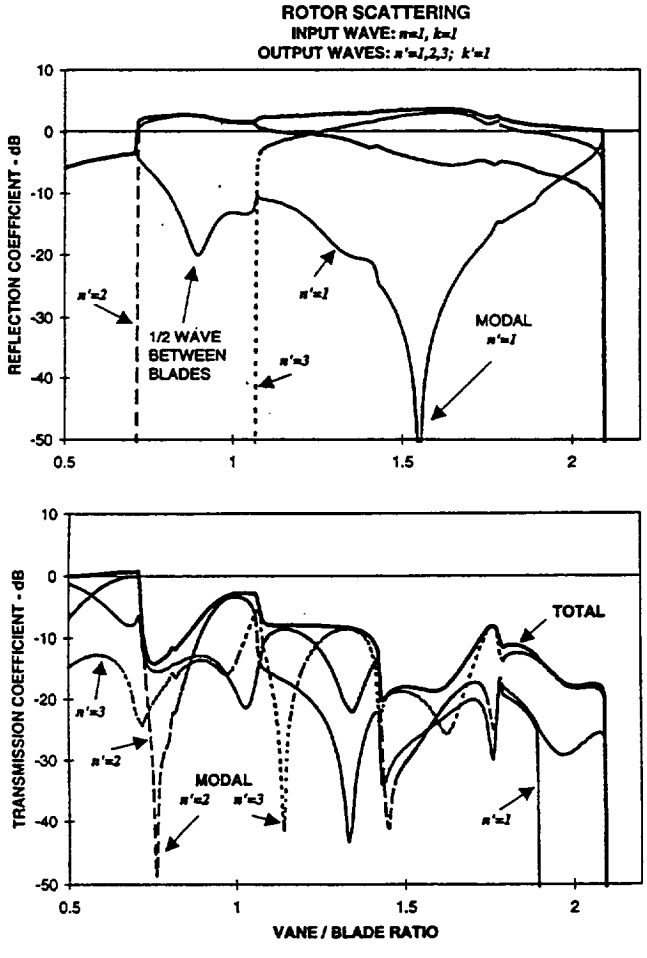

Figure 13. Rotor scattering curves

through the rotor is scattered up from BPF. Modal points for the forward scattered waves at 2×BPF and 3×BPF are called out at V/B = 0.76 and 1.14.

Sound Power Considerations

In Figure 13 portions of the rotor reflection curves pass above the 0 dB level. Since 0 dB represents unit power reflection coefficient, this indicates that the rotor is reflecting more acoustic power than that in the input wave. Values shown at +3 dB indicate that the energy reflected at 2×BPF and 3×BPF is *twice* the input energy at BPF. Since there are no simple "conservation of energy" principles that apply to moving surfaces, we should not be suspicious of this result. However, the result was unexpected and some analysis is presented in this section to explain it.

Power in the acoustic perturbations is evaluated according to the energy flux vector given in by Goldstein's *Aeroacoustics* (ref. 11)

$$\mathbf{I} = \left(\frac{p}{\rho_o} + \mathbf{u}\cdot\mathbf{U}\right)(\rho_o \mathbf{u} + \rho \mathbf{U}) \tag{26}$$

This is the instantaneous energy per unit area per unit time in the direction given by I. The perturbation pressure, density, and velocity are p, ρ, and u and ρ_o and U are the density and velocity of the background flow. The energy flux vector is space and time dependent. We are interested in its component in the x direction. Forming $I_x = \mathbf{I}\cdot\mathbf{i}_x$ and applying $\rho = p/a^2$ lead to

$$\begin{aligned} I_x = {} & (1+M_x^2)pu + \frac{M_x}{\rho_r a_r}p^2 \\ & + \rho_r a_r M_x u^2 + \rho_r a_r M_y\, uv + M_x M_y pv \end{aligned} \tag{27}$$

for the power flux in the x direction. Subscripts r in equation 27 refer to density and speed of sound in region r. When the pressure perturbation given by equation 1, and parallel expressions for the associated u and v velocity perturbations, are inserted into equation 27, the expression can be first averaged over time and then averaged over the duct cross sectional area (over φ, in this 2D case) to find the average power crossing any x = constant plane in the duct. Henceforth, this quantity is called "the power" and is in the usual form showing that the total power is the sum of the modal powers.

$$\overline{\overline{I_x}} = \frac{\rho_o a_o^3}{\gamma^2}\frac{A_r}{P_r}\sum_n \sum_k F_{nk}|A_{nk}|^2 \tag{28}$$

where γ is the ratio of specific heats for air. $A_r = a_r/a_o$ and $P_r = p_r/p_o$. Only propagating modes are included in the summation. Details of the derivation are given in the appendix. A related expression gives the mean squared pressure

$$\overline{\overline{p^2}} = p_o^2 \sum_n \sum_k |A_{nk}|^2 \tag{29}$$

Thus, factor F_{nk} represents the ratio between the modal power and modal mean squared pressure. The expression for this is derived in the appendix.

$$F_{nk} = \frac{\mp(1-M_x^2)^2\, nBM_T\sqrt{E}}{(nBM_T - mM_y \pm M_x\sqrt{E})^2} \tag{30}$$

where $\sqrt{E}$ is the square root that appears in the axial wavenumber in equation 17. Since E goes to zero at cutoff, F_{nk} does also. In equation 30, the upper/lower sign applies to up/downstream going waves. Since we dotted I into the unit x vector, we have the necessary result that flux on the downstream side is positive and on the upstream side is negative (both indicating flux away from the source).

The appendix also derives an expression corresponding to equation 30 from the point of view of an observer in the rotor coordinate system

$$\overline{\overline{I'_x}} = \frac{\rho_o a_o^3}{\gamma^2}\frac{A_r}{P_r}\sum_n \sum_k \hat{F}_{nk}|A_{nk}|^2 \tag{31}$$

where, of course, the pressure coefficients A_{nk} are the same in both rotor and stator coordinates. Factor $\hat{F}_{nk}$ is exactly the same as F_{nk} except that nB in the numerator of equation 30 is replaced by kV.

The power ratio plotted in the figures herein is given by 10 $\log_{10}$ of

$$\Re = \frac{F_{n'k'}|A_{n'k'}|^2}{F_{nk}|A_{nk}|^2} \tag{32}$$

which is the power of the scattered wave divided by the power of the input wave. An observer in the rotor frame would compute a different value

$$\hat{\Re} = \frac{\hat{F}_{n'k'}|A_{n'k'}|^2}{\hat{F}_{nk}|A_{nk}|^2} \tag{33}$$

The ratio of these ratios is $\Re/\hat{\Re} = n'k/nk'$. Since the rotor does not scatter on k, the ratio is simply

$$\frac{\Re}{\hat{\Re}} = \frac{n'}{n} \tag{34}$$

This is to say that the observer in the stator frame will compute a reflection (or transmission) coefficient n'/n times what the observer in the rotor frame computes. To the rotor observer, the blades are not moving and we

expect reflection ratios no greater than one. (This has been the case in the calculations of this study.) However, the change of reference frame results in higher power for cases of scattering up in frequency, as indicated by equation 34. Note that, in the scattering curves shown above, scattering of BPF into BPF did not exceed unit power ratio.

The physical interpretation of the above discussion is that the energy in the returning waves is increased by motion of the reflecting surfaces.

Concluding Remarks

The simple cascade model applied in this paper shows how acoustic reflection and transmission of blade rows involves scattering into modes and frequencies different from those of the input waves. This complex behavior can be interpreted with the aid of formulas derived herein that help identify peaks and valleys in the scattering curves based on orientation of wavefronts relative to the scattering blade chords. In particular, the vane/blade ratio where wavefronts are perpendicular to the chords provides conditions where waves can pass through rotors or stators without scattering and also conditions where incident waves are not reflected because of dipole alignment. It was shown that rotors tend to scatter up in BPF order and that reflected energy can exceed incident energy by a substantial amount. Although the analysis of this paper was based on a 2D flat plate cascade model, the kinematic and energy relations are more general and will carry over to more accurate representations of the cascades and flow.

Acknowledgment

This work was supported by NASA-Lewis under contract NAS3-26618 with Dennis Huff as project manager.

Appendix - Sound Power Formulas

Equation 27 gives the power per unit area in terms of the time dependent pressure and its associated velocity components. To derive the expression for the time average of this averaged over the duct cross section, we insert the series for p from equation 1 and the associated series for u and v. Then we average over time, integrate over the spatial angle φ, and re-arrange the expression to arrive at equation 30 of the main text.

The series for pressure is

$$p(x,\phi,t) = p_o \sum_n \sum_k A_{nk} e^{i[\alpha_{nk}x + \beta_{nk}\phi + nB\Omega t]} \quad (35)$$

and the associated equations for axial and transverse velocity perturbations can be written in parallel form

$$u(x,\phi,t) = a_o \sum_n \sum_k A_{nk} U_{nk} e^{i[\alpha_{nk}x + \beta_{nk}\phi + nB\Omega t]} \quad (36)$$

and

$$v(x,\phi,t) = a_o \sum_n \sum_k A_{nk} V_{nk} e^{i[\alpha_{nk}x + \beta_{nk}\phi + nB\Omega t]} \quad (37)$$

Here, $\beta_{nk} \equiv -(nB - kV) = -m$ is the negative of the spinning mode order. The axial wavenumber can be written

$$\alpha_{nk} = \frac{1}{1 - M_x^2}\left[M_x q \pm \sqrt{E}\right] \quad (38)$$

in which

$$q = nBM_T + M_Y \beta_{nk} \quad (39)$$

and

$$E = q^2 - (1 - M_x^2)\beta_{nk}^2 \quad (40)$$

Smith's paper (ref. 8) gives the relationships between velocity components and pressure in the pressure waves. In our notation, these are

$$U_{nk} = \frac{A_r}{\gamma P_r}\left(\frac{-\alpha_{nk}}{\lambda_{nk}}\right) \quad (41)$$

and

$$V_{nk} = \frac{A_r}{\gamma P_r}\left(\frac{-\beta_{nk}}{\lambda_{nk}}\right) \quad (42)$$

where we have defined

$$\lambda_{nk} = nBM_T + M_x \alpha_{nk} + M_y \beta_{nk} \quad (43)$$

In order to apply the derivation to either the rotor- or stator-fixed frame, we modify equation 27 slightly by adding a prime to M_y

$$I_x = (1 + M_x^2)pu + \frac{M_x}{\rho_r a_r} p^2 + \rho_r a_r M_x u^2 + \rho_r a_r M'_y uv + M_x M'_y pv \quad (44)$$

Thus, we can set $M'_y = M_y$, for the observer in stator-fixed coordinates, or to $M_y - M_T$ for the observer in rotor-fixed coordinates. Note in equation 44 that, for zero Mach number, the intensity becomes $I_x = pu$, the familiar result from classical acoustics.

In equation 44 each term involves a product of perturbation quantities, e.g. pu. Since the series representations of the perturbations are pure real (by virtue of using double sided series in n), we can just as well write this as $p^* u$, which is more convenient for the ensuing manipulations. When the expressions above for p, u, and v are substituted into equation 44, we find

$$I_x = \frac{\rho_o a_o^3}{\gamma^2}\frac{A_r}{P_r}\sum_n\sum_{n'}\sum_k\sum_{k'} F_{nn'kk'}A_{nk}A^*_{n'k'} \times e^{i[(\alpha_{nk}-\alpha_{n'k'})x+(\beta_{nk}-\beta_{n'k'})\phi+(n-n')B\Omega t]} \quad (46)$$

where γ is the ratio of specific heats for air and arose from $\rho_o a_o^2 = \gamma\, p_o$. Also,

$$F_{nn'kk'} = (1+M_x^2)\left(\frac{-\alpha_{n'k'}}{\lambda_{n'k'}}\right)+M_x+M_x\left(\frac{\alpha_{nk}\alpha_{n'k'}}{\lambda_{nk}\lambda_{n'k'}}\right) +M'_y\left(\frac{\alpha_{nk}\beta_{n'k'}}{\lambda_{nk}\lambda_{n'k'}}\right)+M_xM'_y\left(\frac{-\beta_{n'k'}}{\lambda_{n'k'}}\right) \quad (47)$$

When equation 45 is averaged over time, only terms with $n = n'$ survive and the φ exponential becomes $\exp i(k-k')V\phi$. Averaging over φ leaves only terms with $k = k'$. Thus, the exponential in equation 45 disappears completely and the quadruple sum is reduced to

$$\bar{\bar{I}}_x = \frac{\rho_o a_o^3}{\gamma^2}\frac{A_r}{P_r}\sum_n\sum_k F_{nk}|A_{nk}|^2 \quad (48)$$

where now

$$F_{nk} = (1+M_x^2)\left(\frac{-\alpha_{nk}}{\lambda_{nk}}\right)+M_x+M_x\left(\frac{\alpha_{nk}}{\lambda_{nk}}\right)^2 +M'_y\left(\frac{\alpha_{nk}\beta_{nk}}{\lambda_{nk}^2}\right)+M_xM'_y\left(\frac{-\beta_{nk}}{\lambda_{nk}}\right) \quad (49)$$

After applying the definitions for the α's, β's, and λ's and considerable manipulation, this can be written as

$$F_{nk} = \frac{\pm(1-M_x^2)^2[-(nBM_T+M_y\beta_{nk})+M'_y\beta_{nk}]\sqrt{E}}{(nBM_T+M_y\beta_{nk}\pm M_x\sqrt{E})^2} \quad (50)$$

For application to the observer in the stator reference frame, we set $M'_y = M_y$, in which case

$$F_{nk} = \frac{\mp(1-M_x^2)^2\, nBM_T\sqrt{E}}{(nBM_T+M_y\beta_{nk}\pm M_x\sqrt{E})^2} \quad (51)$$

which is the result quoted in the text in equation 30. For the observer in the rotor frame, we set $M'_y = M_y - M_T$ and we place a hat on F to distinguish the rotor result

$$\hat{F}_{nk} = \frac{\mp(1-M_x^2)^2\, kVM_T\sqrt{E}}{(nBM_T+M_y\beta_{nk}\pm M_x\sqrt{E})^2} \quad (52)$$

The upper/lower signs apply to up/downstream going waves. On the upstream side, the negative sign indicates power flux in the negative x direction: away from the source region. The only difference in these expressions is the factor nB for the stator where the rotor has kV. Thus, observers in the different reference frames will differ in their calculation of sound power for any mode by the factor nB/kV.

References

1 Meyer, H. D. and Envia, E., "Aeroacoustic Analysis of Turbofan Noise Generation," NASA CR-4715, March 1966.

2 Topol, D. A., "Rotor Wake/Stator Interaction Noise - Predictions *versus* Data," J. Aircraft Vol. 30, No. 5, pp. 728-735, September/October 1993.

3 Topol, D. A., "Development of a Fan Noise Design System - Part 2: Far-Field Radiation and System Evaluation," AIAA Paper No. 93-4416.

4 Roy, I. D. and Eversman, W. E., "Improved Finite Element Modeling of the Turbofan Engine Inlet Radiation Problem,:" ASME Journal of Vibration and Acoustics 117(1), pp 109-115, January 1995.

5 Eversman, W. E., "A Finite Element Formulation of Aft Fan Duct Acoustic Radiation," AIAA/CEAS Paper 97-1648.

6 Hanson, D. B., "Mode Trapping in Coupled 2D Cascades - Acoustic and Aerodynamic Results, AIAA Paper No. 93-4417.

7 Topol, D. A., "Development and Evaluation of a Coupled Fan Noise Design System," AIAA Paper No. 97-1611.

8 Smith, S. N., "Discrete Frequency Sound Generation in Axial Flow Turbomachines," Aeronautical Research Council Reports and Memoranda, R. & M. No. 3709, HMSO, London, 1973.

9 Hanson, D. B., Final report under NASA contract NAS3-26618, June 1997

10 Meyer, H. D., Final report under NASA contract NAS3-26618, December 1997.

11 Goldstein, M. E., *Aeroacoustics*, McGraw-Hill, New York, 1976.

PART 2
COMPENDIUM OF SCATTERING CURVES
(with Annotation and Discussion)

Summary

This part of the report lists the geometry and flow conditions for the scattering study, provides tables of special vane/blade ratios keyed to formulas from Part 1 for physical interpretation, and presents scattering curves for a range of mode orders and BPF harmonics at 2 operating conditions.

Scattering curves are in the format introduced in Part 1: reflection and transmission coefficients as power ratios in dB *versus* vane/blade ratio. The curves are annotated showing vane/blade ratios where various input and output waves are either parallel to or perpendicular to the chords of the scattering blade rows. Conditions for channel resonances are also identified.

Conclusions

A large number of scattering curves was examined to find if qualitative reflection and transmission behavior could be predicted based on intuitive expectations regarding wave alignment. For example, it might be expected that waves impinging broadside on vanes would reflect or scatter strongly and transmit weakly. This was not found to be the case. Similarly, the channel resonance condition (where organ pipe modes are set up between adjacent blades or vanes) produced nothing remarkable in the curves.

Regarding the broadside condition, perhaps the results should have not been a surprise. The methodology used here is equivalent to that of S. N. Smith (ref. 8) and reproduces the reflection/transmission curves in Figure 3. For this figure, the "Venetian blind condition" is at 60° where it can be seen that the wave transmits perfectly. The broadside condition is at 30° where it can be seen that the transmision loss is about 50% (6 dB); the reflection is very weak – less than 10% of the input wave amplitude. Thus, the results presented in this report are not in conflict with previous knowledge.

The condition that does produce predictable behavior is that for wavefronts perpendicular to chord lines (i.e., where waves propagate parallel to chords). For input waves, this is called the "Venetian blind condition". Here, incoming waves are not reflected but transmit with unit transmission coefficient at the input mode order and with no scattering into other modes or frequencies. When scattered waves are perpendicular to chords, we call this the "modal condition". Reflected wave energy goes to zero at the modal point and tends to be low in a wide range on either side. The result can be a wide valley in the reflection curve when only one mode is cut on.

2.1 GEOMETRY AND FLOW FOR 2 CASES USED IN STUDY

A fan with an upstream rotor and downstream stator is represented by flat plate cascades as in figure 14. Gap/chord ratio (inverse solidity) matches the tip station of the 22" ADP Fan 1. Flow into the rotor and out of the stator is axial; flow between blade rows has a tangential component associated with pressure ratio and tip speed of the rotor. Mean flow conditions are specified by inflow Mach number, tip rotational Mach number, and pressure ratio based on static conditions of a standard day. The remaining flow conditions in the 3 regions (upstream of rotor, between rotor and stator, and downstream of stator) are computed under the idealized assumption of 2D isentropic (lossless) flow, as explained in Appendix D. The jumps in the mean flow conditions occur at the rotor leading edge and stator trailing edge. Stagger angles of blades and vanes are computed under the assumption that they "weathervane" into the mean flow.

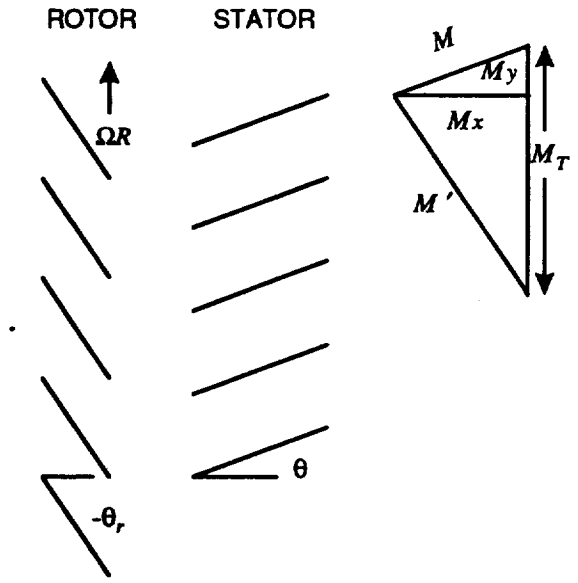

Figure 14. Geometry and flow of fan stage

Scattering curves were generated at the 2 conditions from NASA's test of ADP Fan 1 shown in Table 4.

Table 4. Geometry and Flow Conditions for Scattering Study

	Mid Speed	High Speed
Corrected RPM	7031 RPM	8750 RPM
Tip Mach Number	0.614	0.772
Inlet Axial Mach Number	0.404	0.510
Pressure Ratio	1.180	1.278
Gap/Chord: Rotor/Stator	0.962/0.917	0.962/0.917
Stagger Angle: Rotor/Stator	48.8°, 29.6°	51.3°, 30.5°
Static Pressure / $p_{STANDARD}$: Region 1, 2, 3	0.894, 1.055, 1.089	0.837, 1.099, 1.152
Total Pressure/Inlet P_{TOT} : Region 1, 2, 3	1.000, 1.180, 1.180	1.000, 1.278, 1.278
Speed of Sound/ $a_{STANDARD}$: Region 1, 2, 3	0.984, 1.008, 1.012	0.975, 1.014, 1.020
Mach Numbers		
Axial: M_{x1}, M_{x2}, M_{x3}	0.404, 0.350, 0.341	0.510, 0.404, 0.388
Swirl: M_{y1}, M_{y2}, M_{y3}	0.000, 0.199, 0.000	0.000, 0.238, 0.000
Tip Rot' : M_{T1}, M_{T2}, M_{T3}	0.614, 0.600, 0.597	0.772, 0.742, 0.738

2.2 SCATTERING CURVES FOR HIGH SPEED CASE

Part 1 of this report presented reflection and transmission curves for the high speed condition defined in Section 2.1. Results were given only for input of the fundamental wave: $n = 1$, $k = 1$ with scattering into the permitted combinations of $n' = 1,2,3$ and $k' = 1,2,3$. This section presents curves for more input waves: the 9 combinations of $n = 1,2,3$; $k = 1,2,3$ for the high speed case. Results for the mid speed case are in Section 2.3. In all cases the input waves originate in the region between rotor and stator.

Presentation of the scattering curves in Sections 2.2 and 2.3 is in pairs of facing pages for the same input mode as follows.

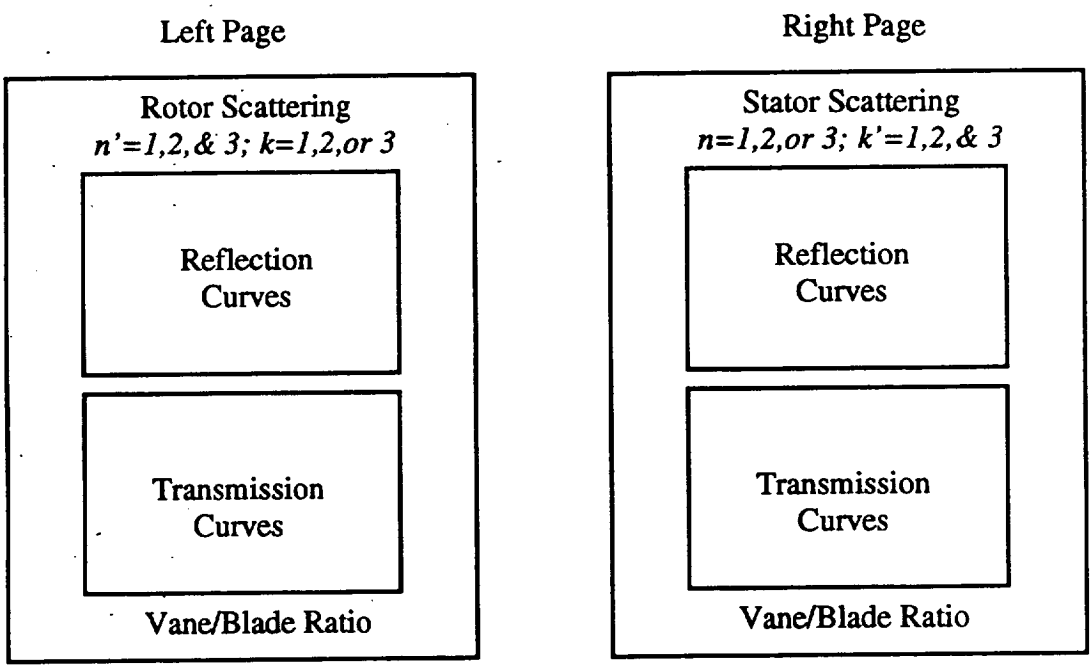

Scattering Curves for High Speed Case Table 5 gives figure numbers for the scattering curves and identifies input and output modes for each. Figures 15a and 15b are repeats of Figures 12 and 13 in Part 1.

Table 5. Figure Numbers - High Speed Case

	Rotor		Stator	
Input Mode n; k	Output Mode n'; k	Figure #	Output Mode n; k'	Figure #
1;1	1,2,3; 1	15a	1; 1,2,3	15b
1;2	1,2,3; 2	16a	1; 1,2,3	16b
1;3	1,2,3; 3	17a	1; 1,2,3	17b
2;1	1,2,3; 1	18a	2; 1,2,3	18b
2;2	1,2,3; 2	19a	2; 1,2,3	19b
2;3	1,2,3; 3	20a	2; 1,2,3	20b
3;1	1,2,3; 1	21a	3; 1,2,3	21b
3;2	1,2,3; 2	22a	3; 1,2,3	22b
3;3	1,2,3; 3	23a	3; 1,2,3	23b

Tables 1 and 2 of Part 1 gave formulas for vane/blade ratios at which the various input and output waves would be either parallel to or perpendicular to the chords of rotors or stators. The first step in study of the scattering curves is to apply these formulas and annotate the curves at these special vane/blade ratios. This will aid in interpreting the various peaks and valleys of the plots. Tables 6 and 7 below list the special vane/blade ratios for the high-speed condition.

Table 6. Vane/Blade Ratios for Special Angles Relative to STATOR

mode order	Waves ⊥ Vane Chords		Waves // Vane Chords	
n, k	Upgoing Wave	Downgoing	Upgoing Wave	Downgoing
1, 1	1.71	0.74	0.36	1.64
1, 2	0.85	0.37	0.18	0.82
1, 3	0.57	0.25	0.12	0.55
2, 1	3.42	1.49	0.72	3.28
2, 2	1.71	0.74	0.36	1.64
2, 3	1.14	0.50	0.24	1.09
3, 1	5.13	2.23	1.08	4.92
3, 2	2.56	1.12	0.54	2.46
3, 3	1.71	0.74	0.36	1.64

Table 7. Vane/Blade Ratios for Special Angles Relative to ROTOR

mode order	Waves ⊥ Vane Chords		Waves // Blade Chords	
n, k	Upgoing Wave	Downgoing	Upgoing Wave	Downgoing
1, 1	0.38	1.54	1.87	0.68
1, 2	0.19	0.77	0.93	0.34
1, 3	0.13	0.51	0.62	0.23
2, 1	0.76	3.09	3.73	1.37
2, 2	0.38	1.54	1.87	0.68
2, 3	0.25	1.03	1.24	0.46
3, 1	1.14	4.63	5.59	2.05
3, 2	0.57	2.32	2.79	1.03
3, 3	0.38	1.54	1.87	0.68

These points are marked on Figures 15-23 using the following code names whose meaning will become clear in the following discussion.

BSI	Broadside input wave
VBI	Venetian Blind input wave
MO	Modal - scattered wave index is shown
BSR	Broadside reflected wave - scattered wave index is shown
BST	Broadside transmitted wave - scattered wave index is shown

Rather than discussing each curve individually, we studied the 36 sets of curves in Figures 15-23 to find what generalizations could be made. There seems to be as much to say about what doesn't happen as about what does.

For example, nothing special seems to occur at spinning mode order $m = 0$. This is the plane wave condition computed for $nB = kV$, which intuition might tell us to avoid for design of quiet fans. This intuition is probably based on low speed fan design where any choice other than

$B = V$ leads to BPF being cut off. However, for high speed fans, cut on with $m = 0$ doesn't seem worse than cut on at other spinning mode orders.

In some simple acoustic problems it can be shown that the sum of the reflection and transmission coefficients is equal to 1. Simply stated: what is not transmitted is reflected. A quick look at the figures reveals that this is certainly not the case for blade row scattering. The sum of the reflection and transmission coefficients can be greater than or less than unity.

We might expect characteristic behavior for "Broadside" conditions (where wavefronts are parallel to the chord lines). For example, the BSI (Broadside input) condition sketched figure 1-10 might be expected to result in strong reflection and weak transmission. No such behavior was found is study of the curves. Also, for BSR (reflected wave parallel to chord) and BST (transmitted wave parallel to chord) there was no tendency toward peaks in the curves.

We examined the scattering curves to find if there is a tendency toward increased reflection at higher frequencies where ray acoustics might be valid. No such trend was found, probably because we are dealing with individual waves, not rays.

We looked for identifiable behavior when channels between adjacent vanes or blades would resonate like an organ pipe. Appendix C gives the conditions for standing waves in these channels and the computed vane/blade ratios are shown in Table 8.

Table 8. Vane/Blade Ratios for Channel Resonances

	ROTOR			STATOR		
q	k=1	k=2	k=3	n=1	n=2	n=3
1	0.38	0.19	0.13	2.07	4.15	6.22
2	0.76	0.38	0.25	1.04	2.07	3.11
3	1.13	0.57	0.38	0.69	1.38	2.07
4	1.51	0.76	0.50	0.52	1.04	1.56

In the table, q is the number of cycles in the standing wave pattern. To avoid clutter, these points are not marked on the figures but the reader can verify that nothing special occurs at conditions which could produce standing waves.

The conditions where the formulas of Part 1 reliably predict characteristic behavior are those for waves perpendicular to the chord lines. For the VBI (Venetian Blind input) condition sketched in figure 8, waves pass through the blade row without scattering (except for weak effects of the actuator disks). Thus, there is little reflection of any waves (see, for example the tops of Figures 15b or 18b); on the transmission side, the input wave passes through unchanged and there is no scattering into other waves (see bottoms of same figures). The VBI condition produces a prominent valley in the reflection curves, in some cases, showing its effect over the entire *V/B* range.

The modal conditions for transmission and reflection (here, the waves are also perpendicular to the chord lines) are reliable predictors of low wave strength although the effect is less dramatic than the VBI condition because they affect only one mode at a time. Figure 15b, however, shows a case where the modal behavior dominates the plot because it affects the only mode that is cut on.

Rotor Scattering - High Speed Case

Input Mode Order: *n=1; k=1* Output Modes: *n'=1,2,3; k=1*

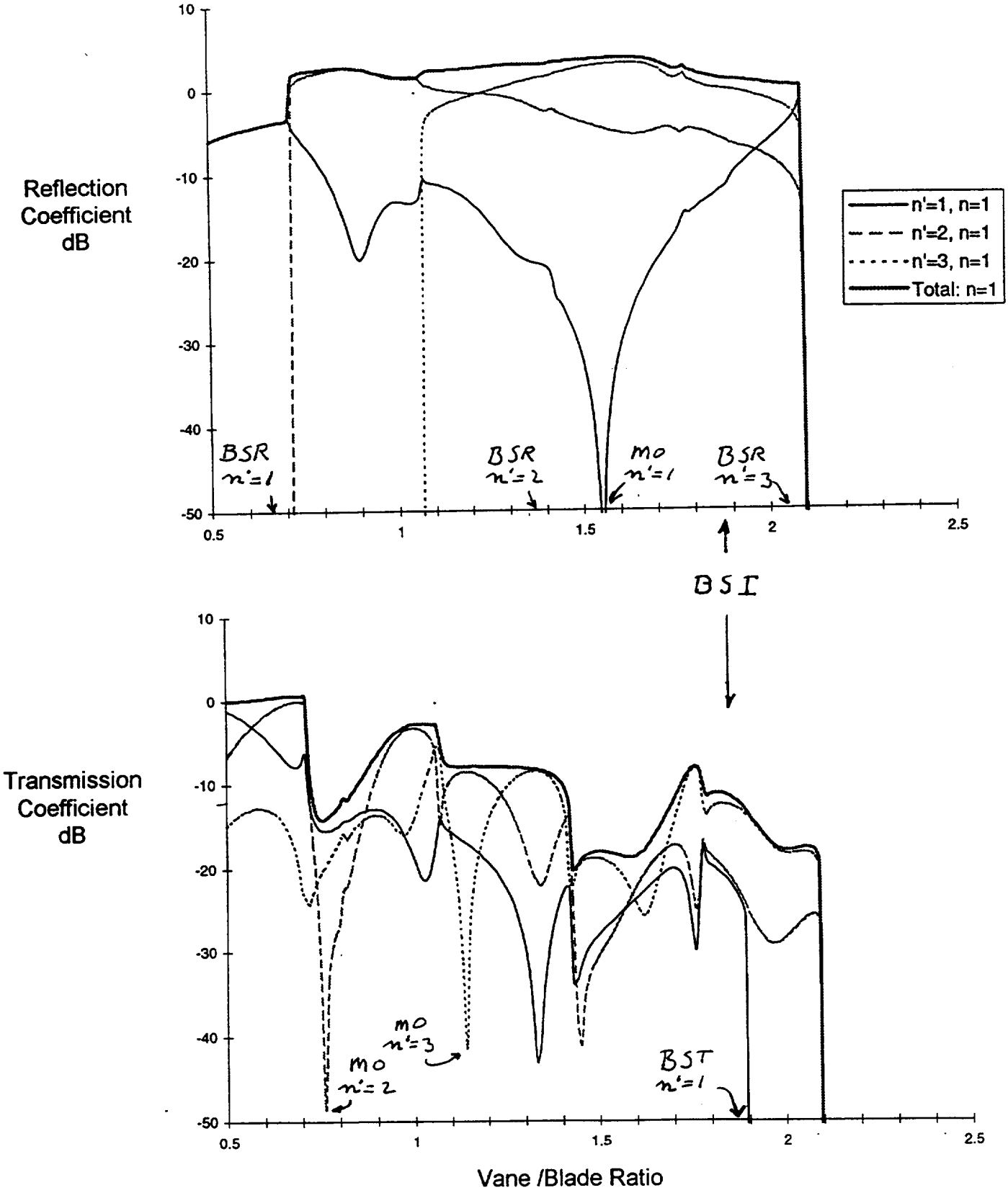

Figure 15a

Stator Scattering - High Speed Case

Input Mode Order: *n=1, k=1* Output Modes: *n=1; k'=1,2,3*

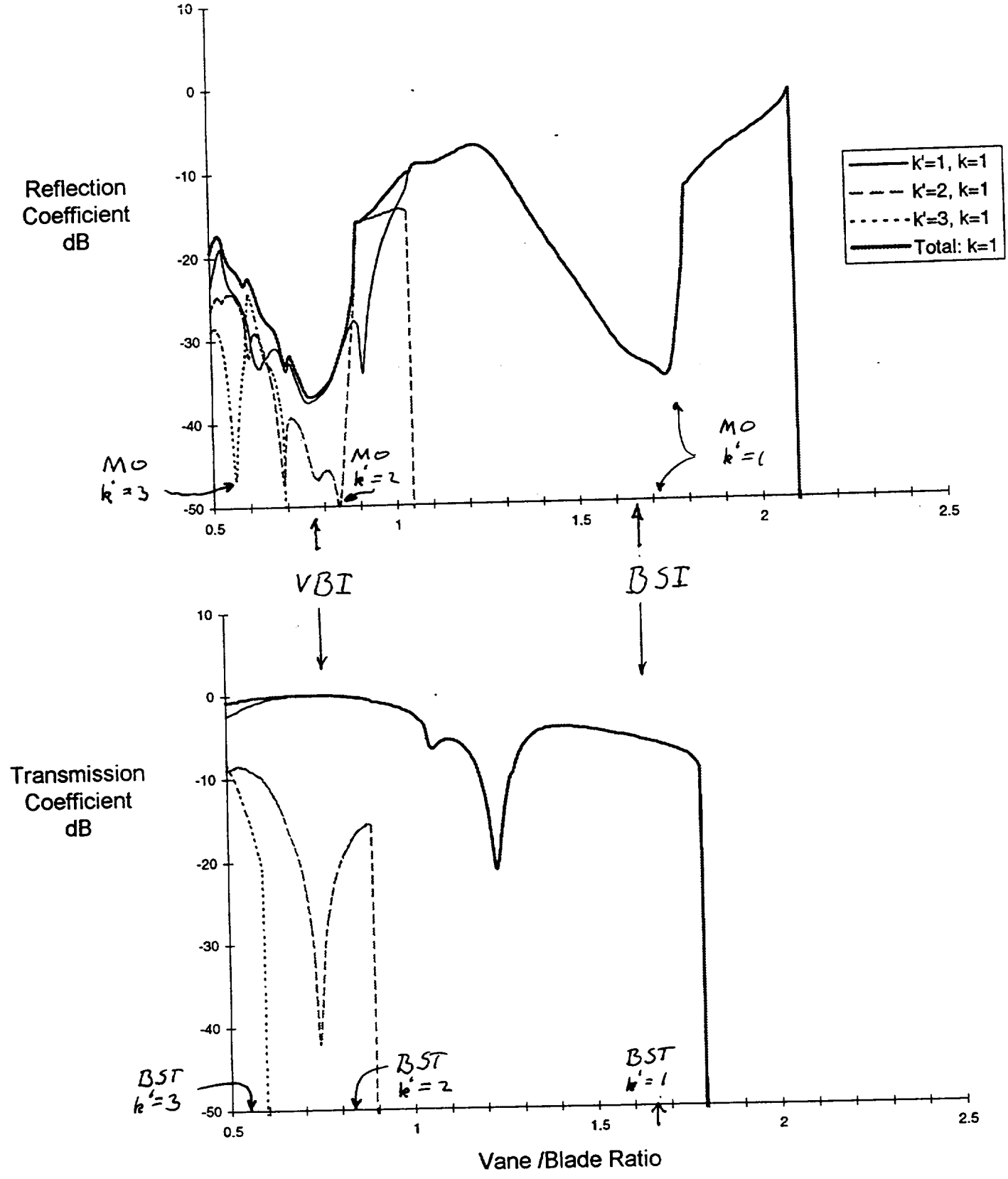

Figure 15B

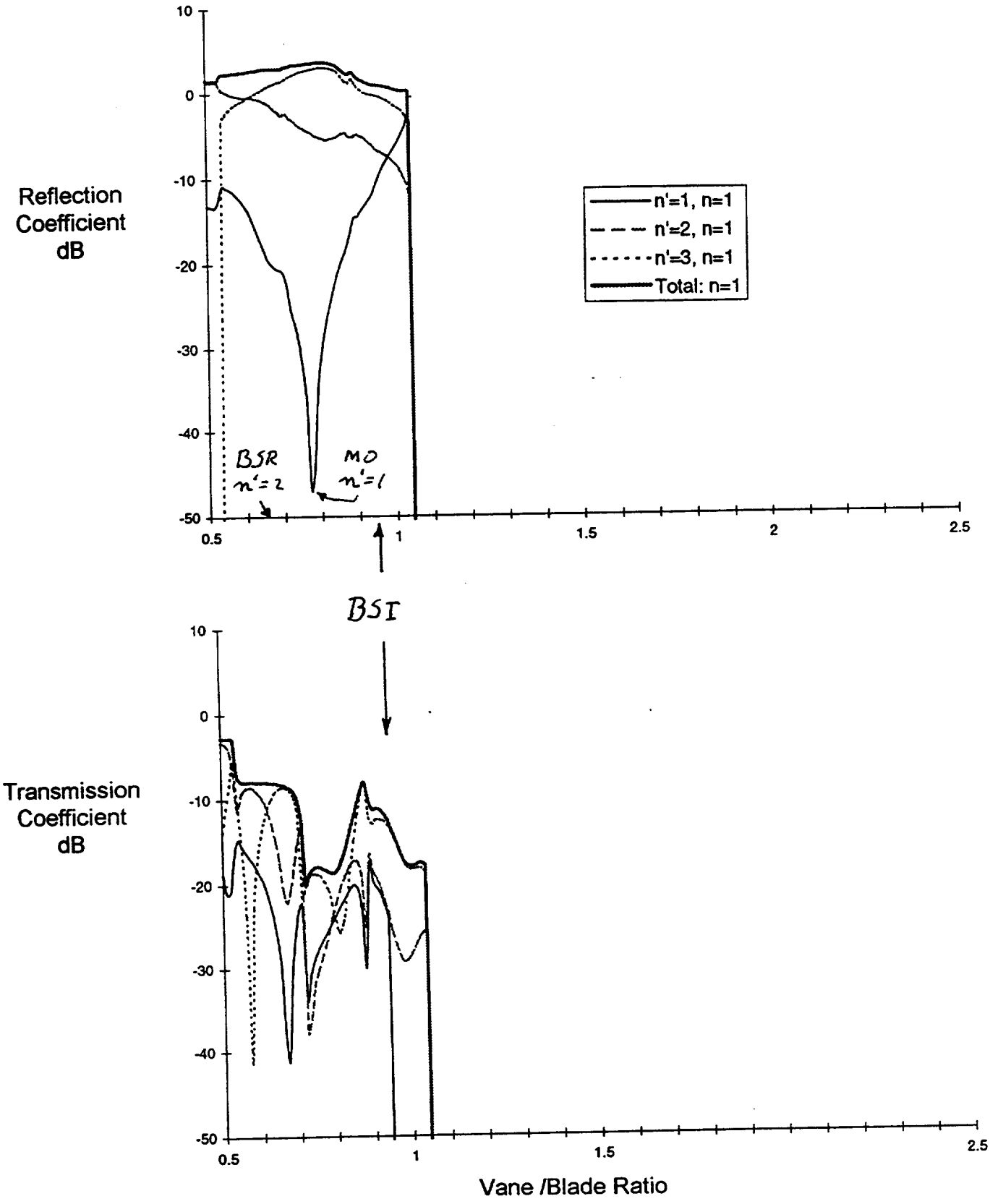
Rotor Scattering - High Speed Case
Input Mode Order: n=1; k=2 Output Modes: n'=1,2,3; k=2
Reflection Coefficient dB
10
0
-10
-20
-30
-40
-50
0.5
1
1.5
2
2.5
n'=1, n=1
n'=2, n=1
n'=3, n=1
Total: n=1
BSR n'=2
MO n'=1
BSI
Transmission Coefficient dB
Vane /Blade Ratio

Figure 16a

Stator Scattering - High Speed Case
Input Mode Order: *n=1, k=2* Output Modes: *n=1; k'=1,2,3*

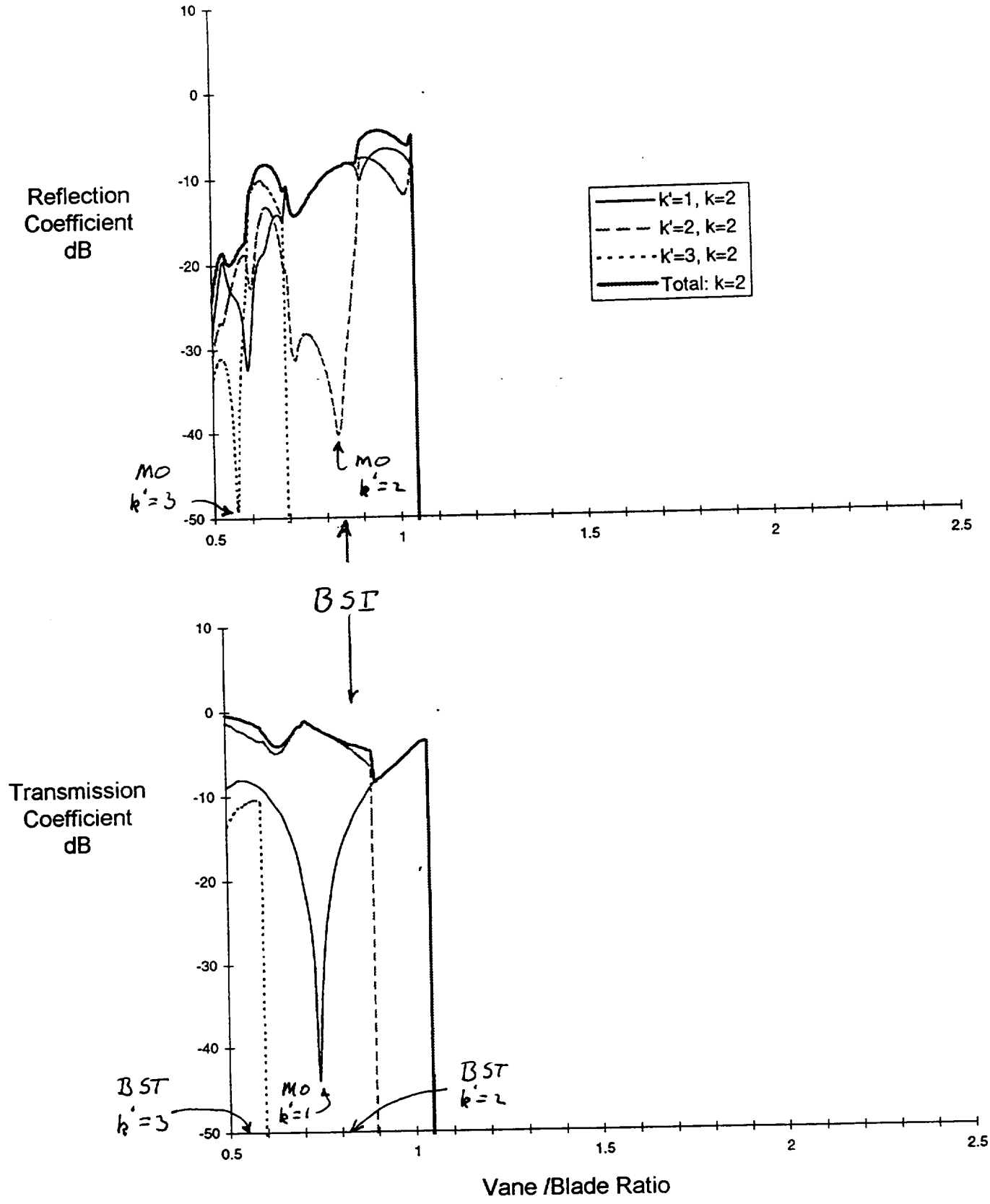

Figure 16b

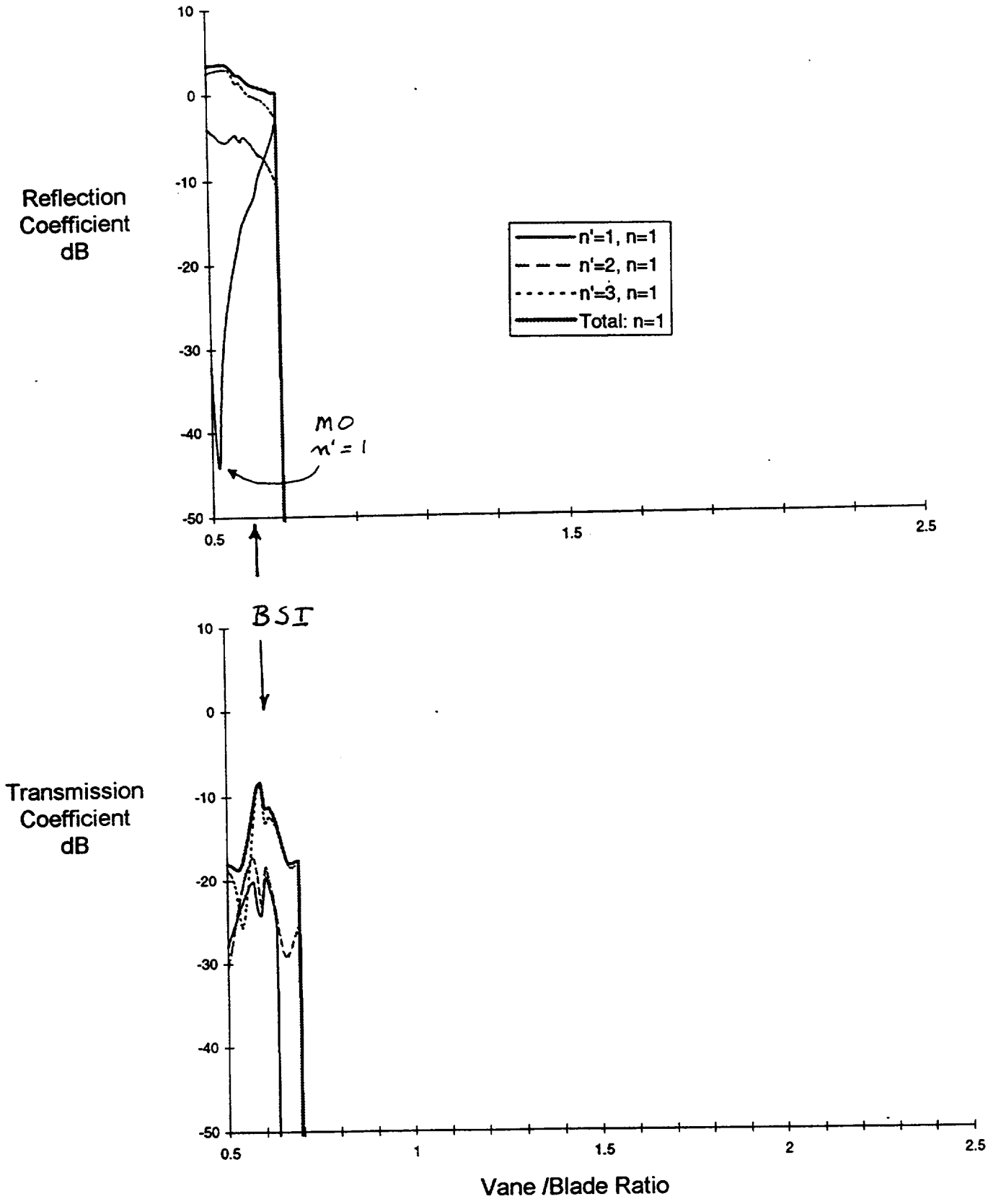
Rotor Scattering - High Speed Case
Input Mode Order: n=1; k=3 Output Modes: n'=1,2,3; k=3
Reflection Coefficient dB
10
0
-10
-20
-30
-40
-50
0.5
1.5
2.5
n'=1, n=1
n'=2, n=1
n'=3, n=1
Total: n=1
MO
n'=1
BSI
Transmission Coefficient dB
10
0
-10
-20
-30
-40
-50
0.5
1
1.5
2
2.5
Vane /Blade Ratio

Figure 17a

Stator Scattering - High Speed Case

Input Mode Order: *n=1, k=3* Output Modes: *n=1; k'=1,2,3*

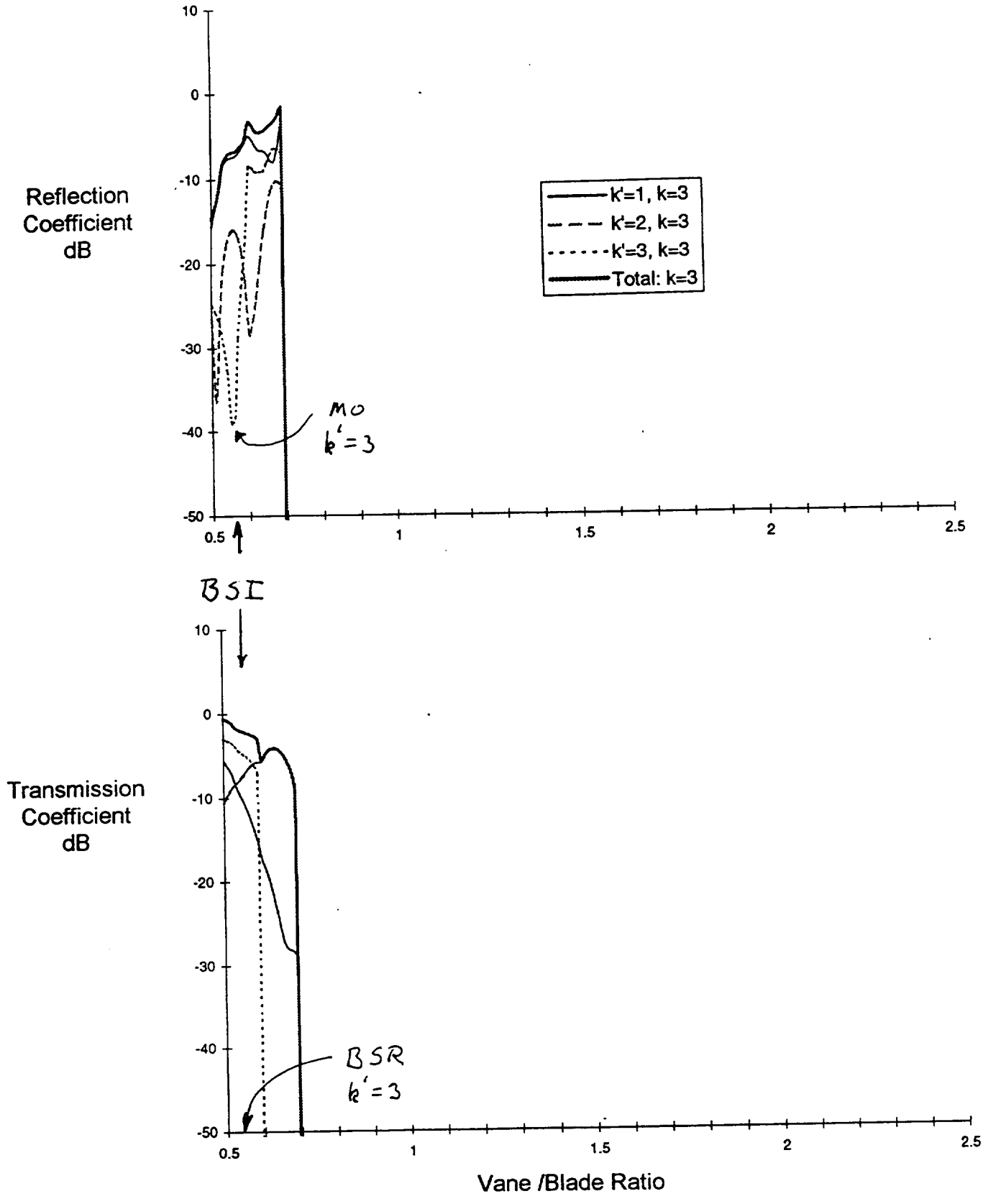

Figure 17b

Rotor Scattering - High Speed Case

Input Mode Order: *n=2; k=1* Output Modes: *n'=1,2,3; k=1*

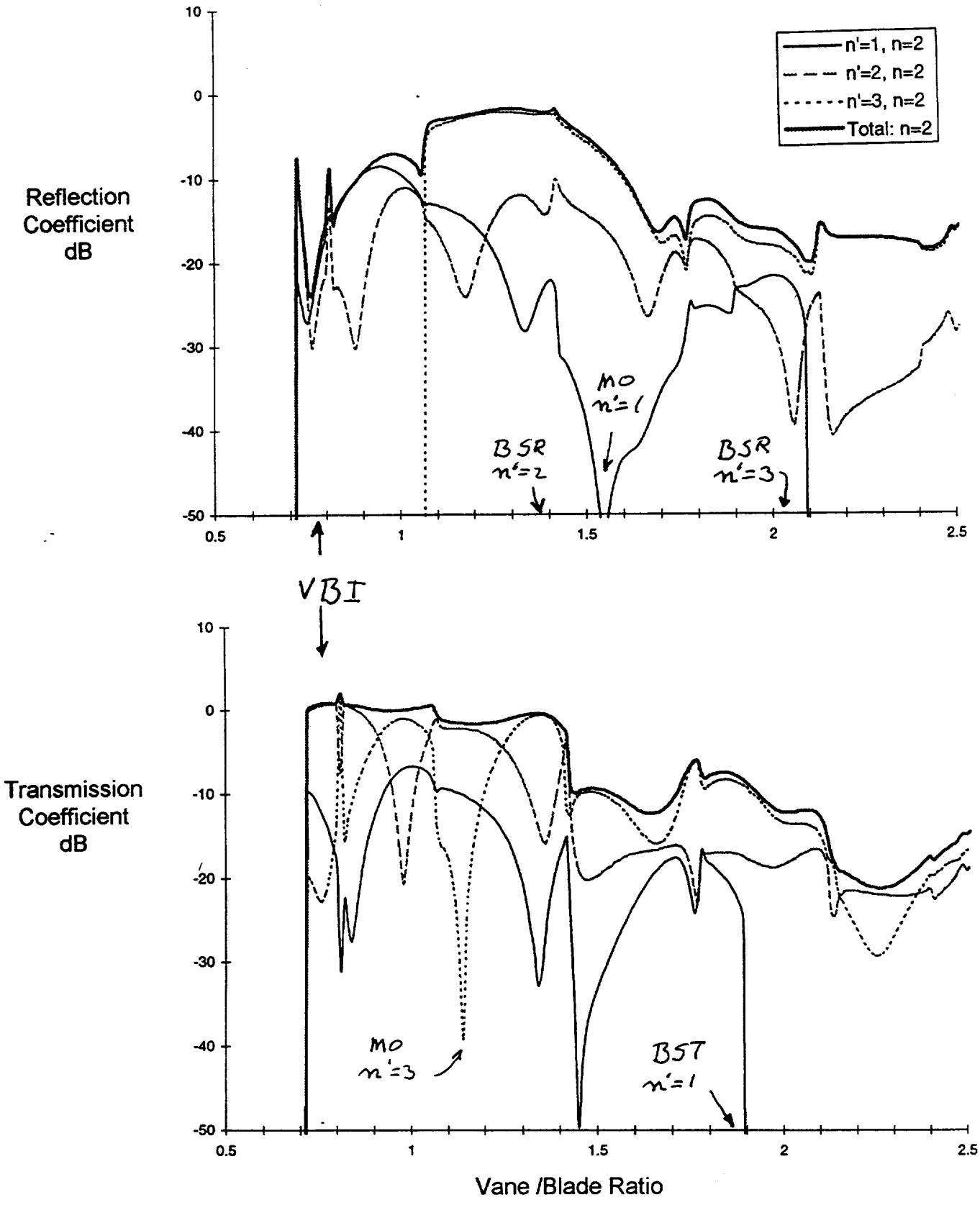

Figure 18a

Stator Scattering - High Speed Case

Input Mode Order: *n=2, k=1* Output Modes: *n=2; k'=1,2,3*

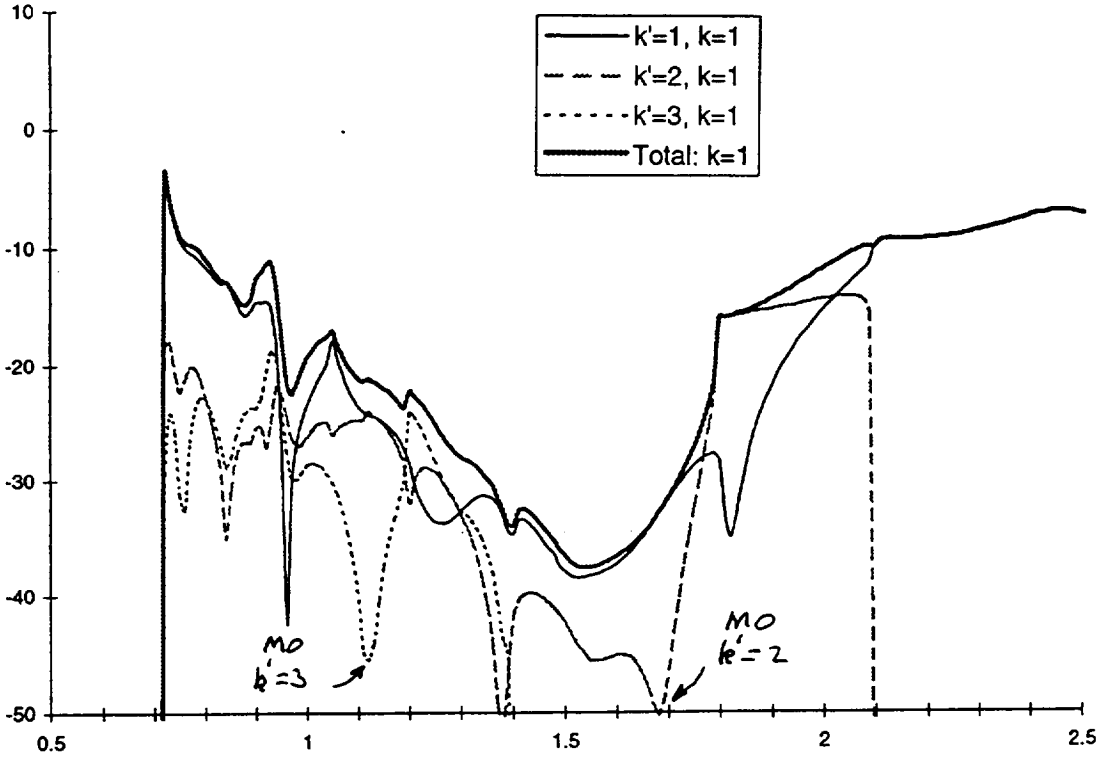

Reflection Coefficient dB

VBI

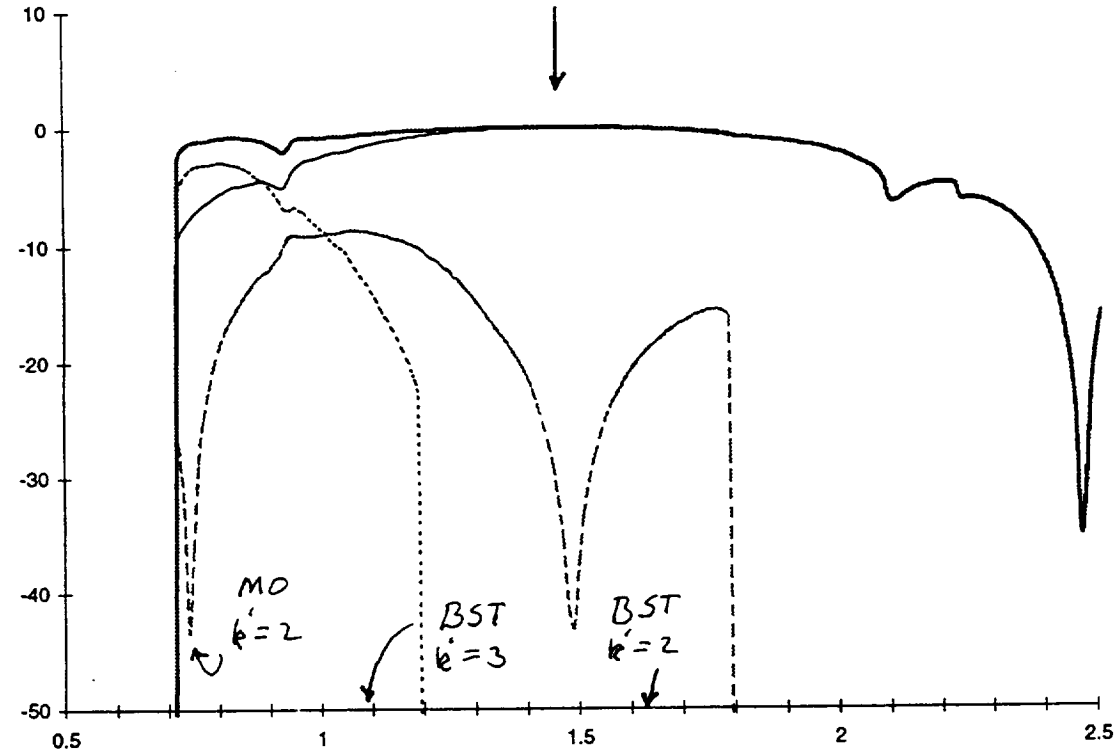

Transmission Coefficient dB

Vane /Blade Ratio

Figure 18b

Rotor Scattering - High Speed Case
Input Mode Order: *n=2; k=2* Output Modes: *n'=1,2,3; k=2*

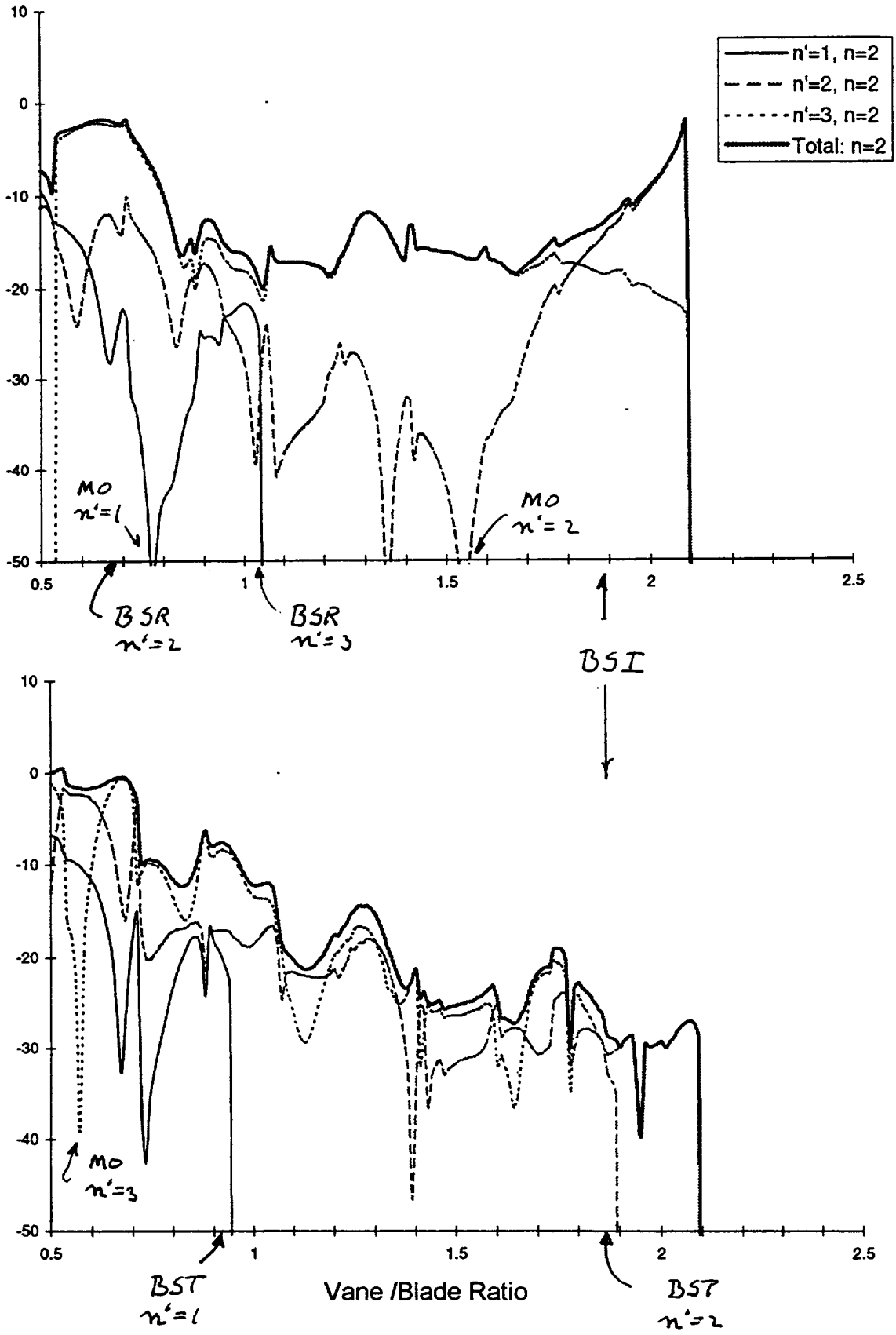

Figure 19a

Stator Scattering - High Speed Case

Input Mode Order: *n=2, k=2* Output Modes: *n=2; k'=1,2,3*

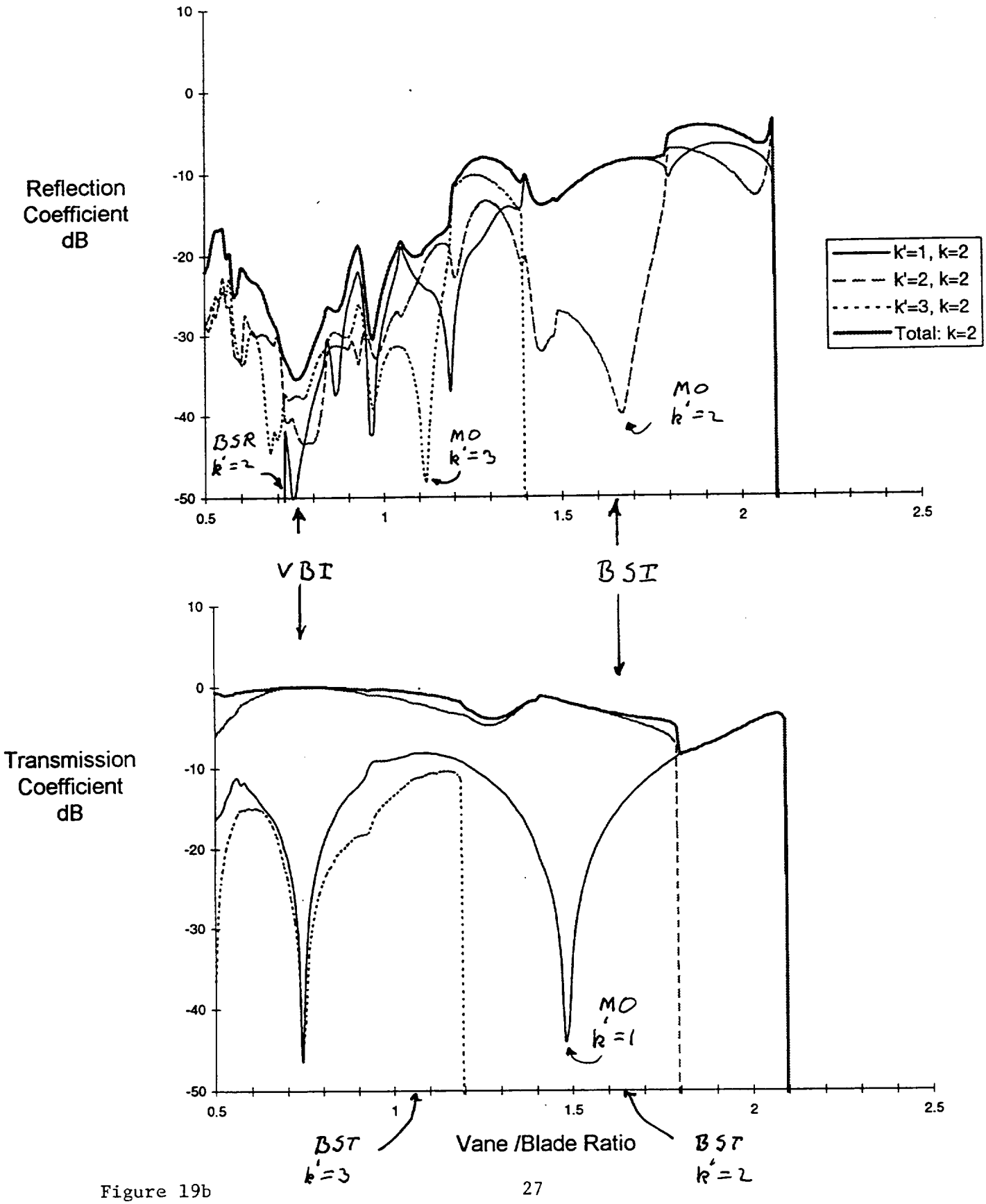

Figure 19b

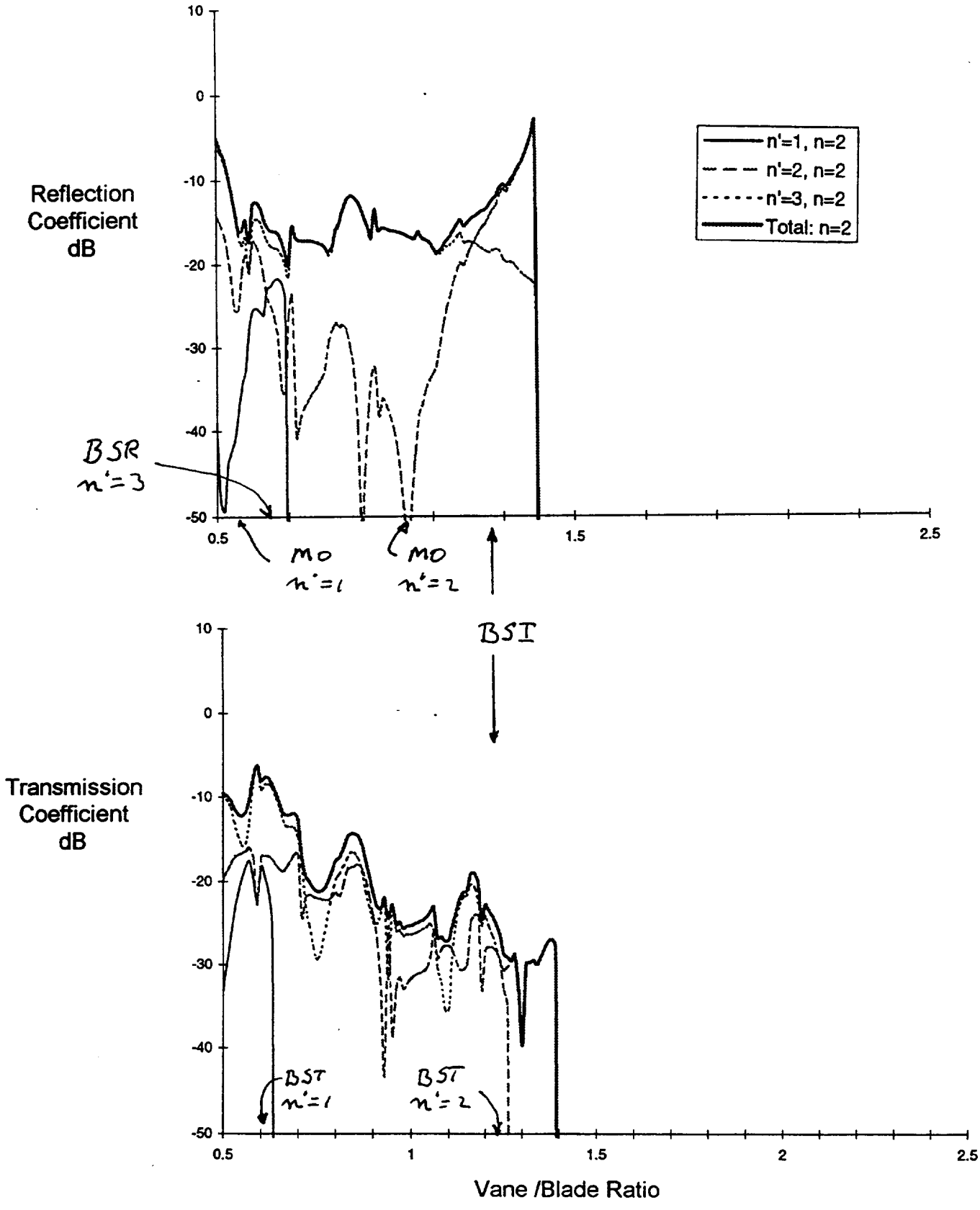
Rotor Scattering - High Speed Case
Input Mode Order: n=2; k=3 Output Modes: n'=1,2,3; k=3
Reflection Coefficient dB
n'=1, n=2
n'=2, n=2
n'=3, n=2
Total: n=2
BSR n'=3
MO n'=1
MO n'=2
BSI
Transmission Coefficient dB
BST n'=1
BST n'=2
Vane /Blade Ratio

Figure 20a

Stator Scattering - High Speed Case

Input Mode Order: *n=2, k=3* Output Modes: *n=2; k'=1,2,3*

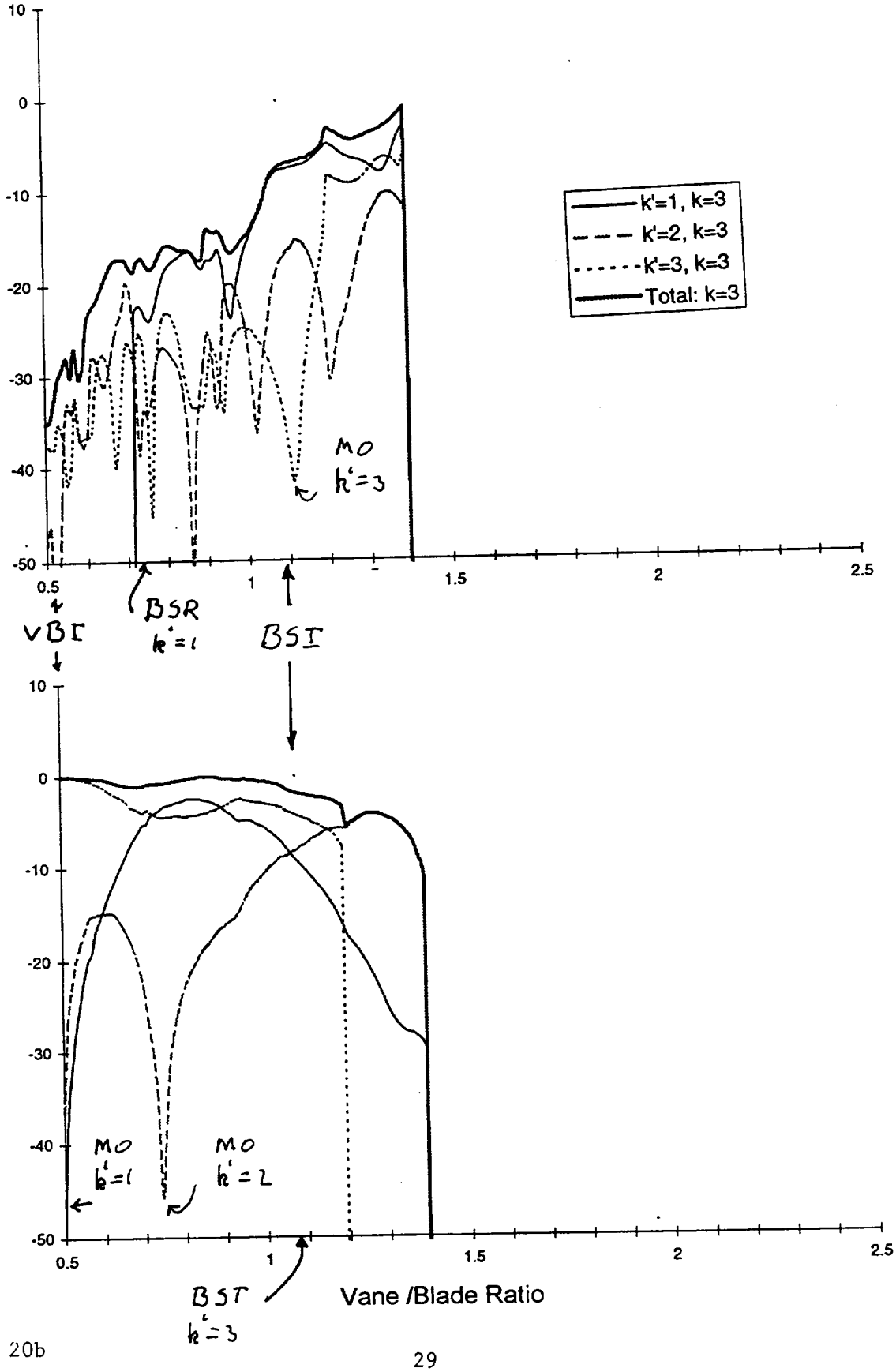

Figure 20b

Rotor Scattering - High Speed Case

Input Mode Order: *n=3; k=1* Output Modes: *n'=1,2,3; k=1*

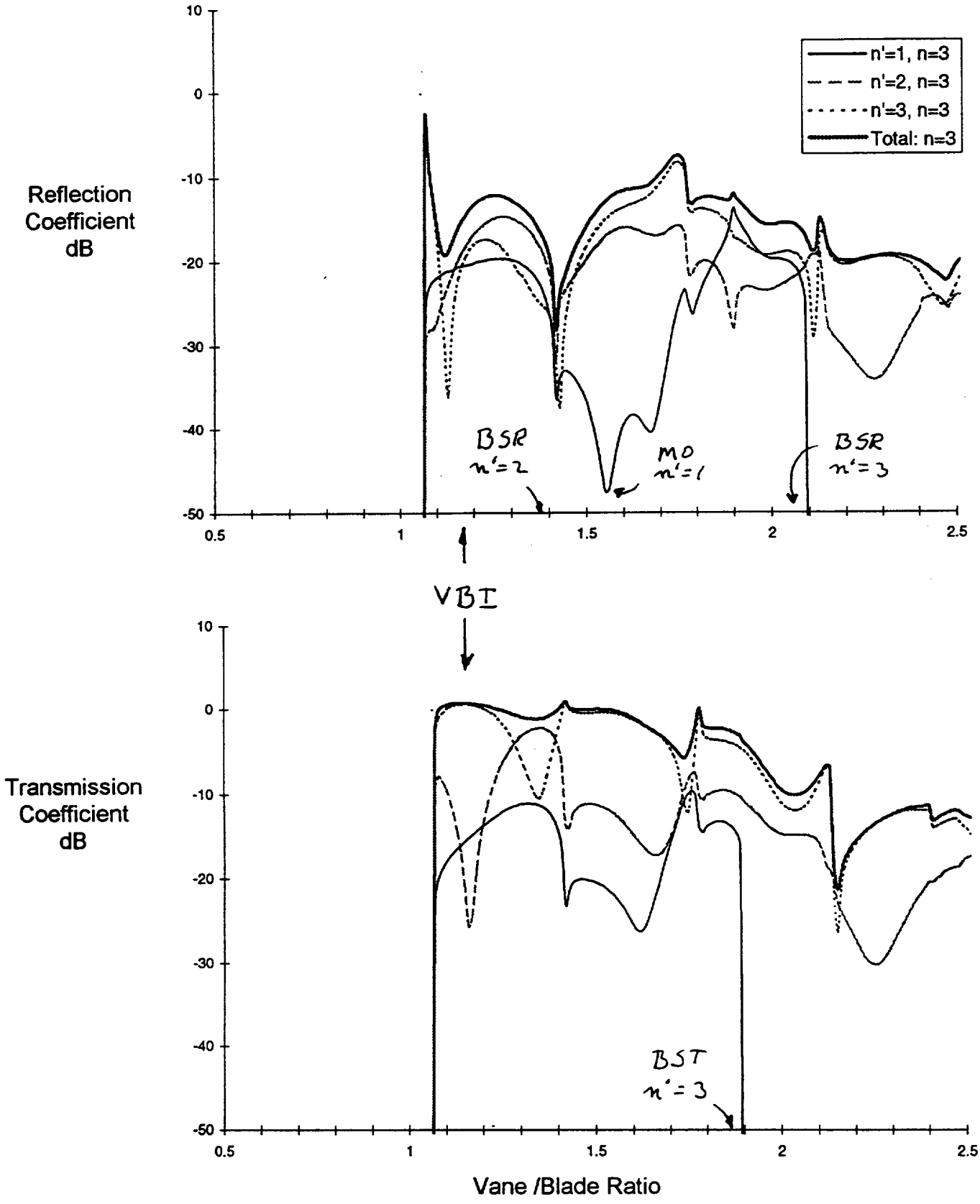

Figure 21a

Stator Scattering - High Speed Case

Input Mode Order: *n=3, k=1* Output Modes: *n=3; k'=1,2,3*

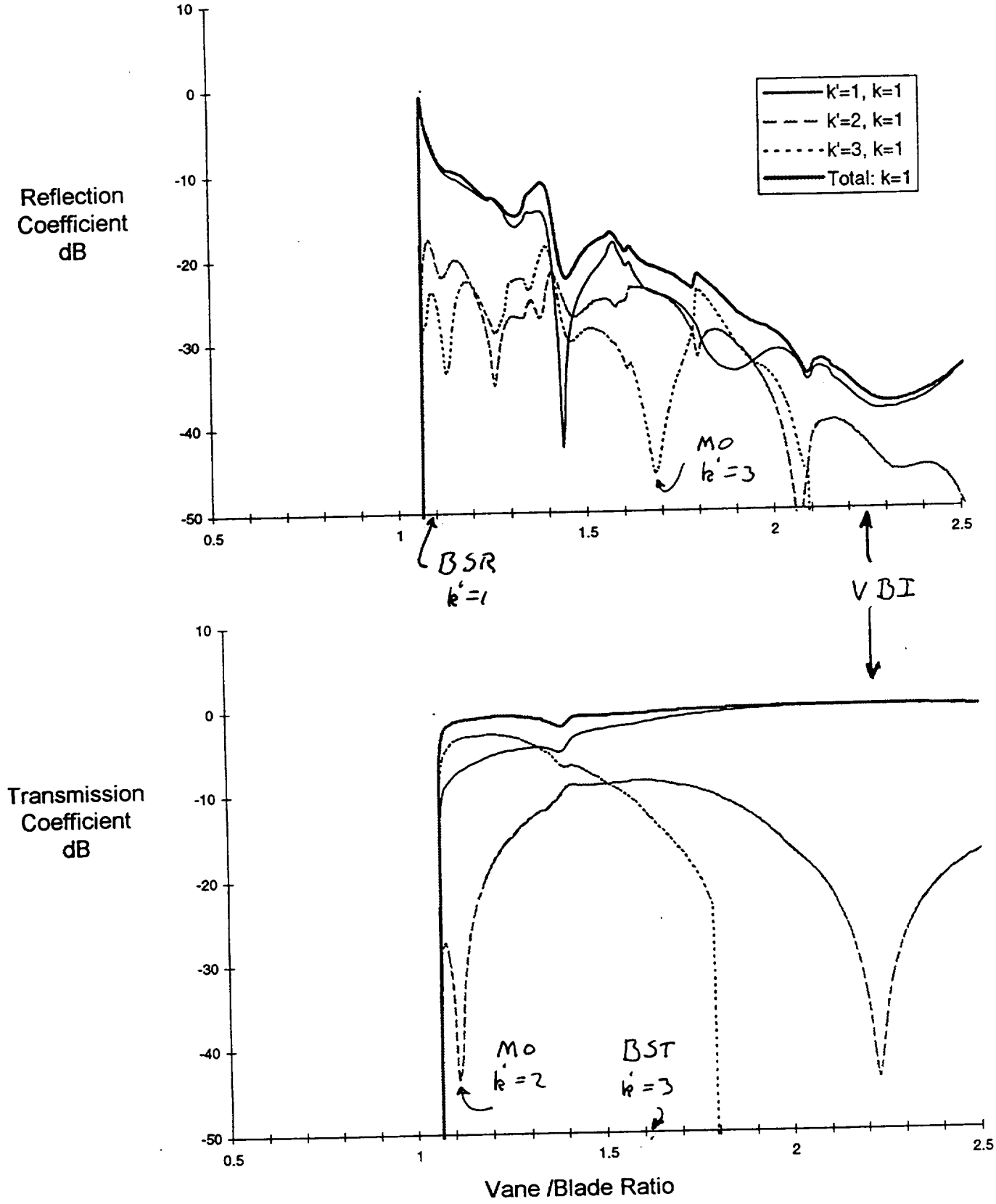

Figure 21b

Rotor Scattering - High Speed Case

Input Mode Order: *n=3; k=2* Output Modes: *n'=1,2,3; k=2*

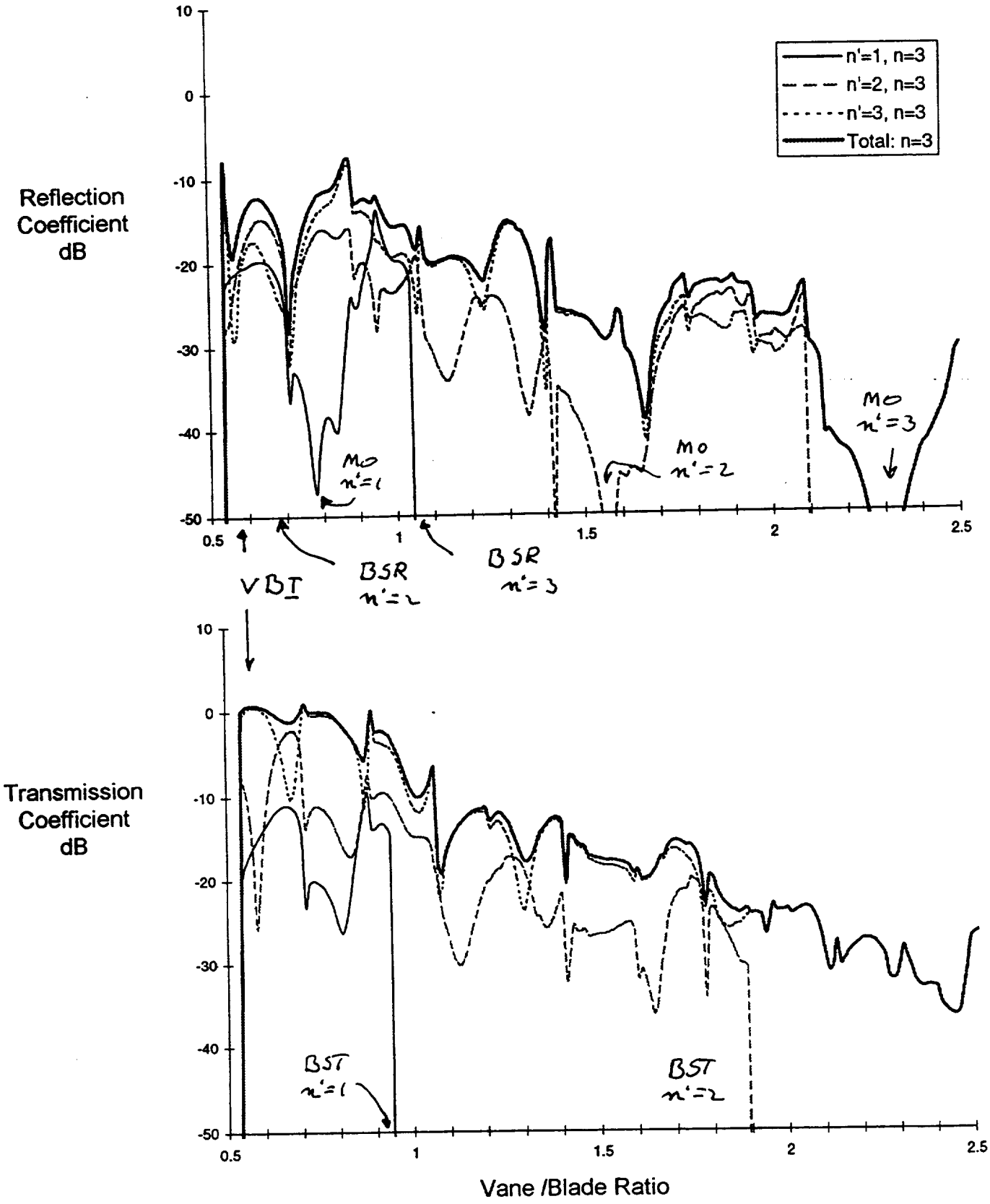

Figure 22a

Stator Scattering - High Speed Case

Input Mode Order: *n=3, k=2* Output Modes: *n=3; k'=1,2,3*

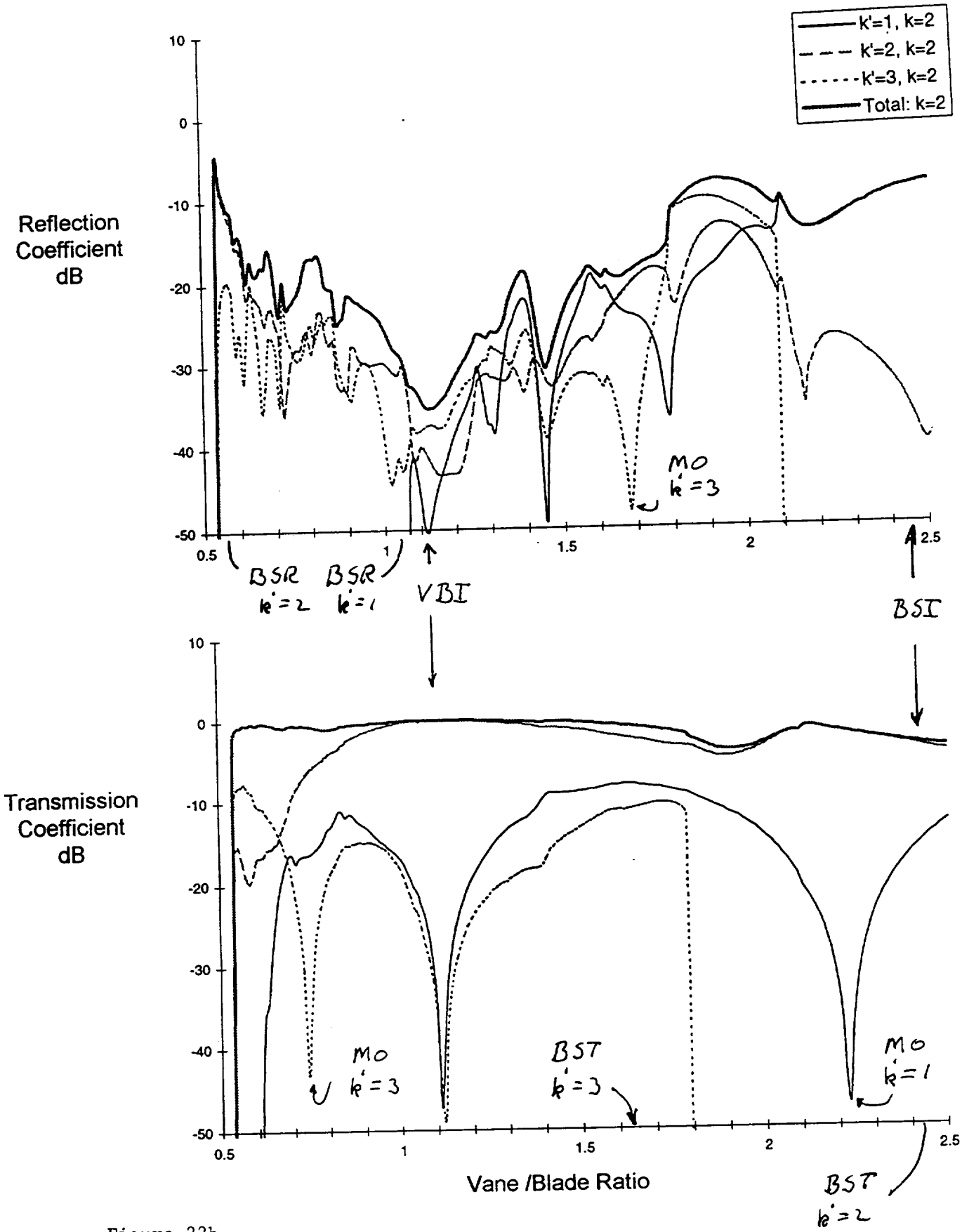

Figure 22b

Rotor Scattering - High Speed Case

Input Mode Order: *n=3; k=3* Output Modes: *n'=1,2,3; k=3*

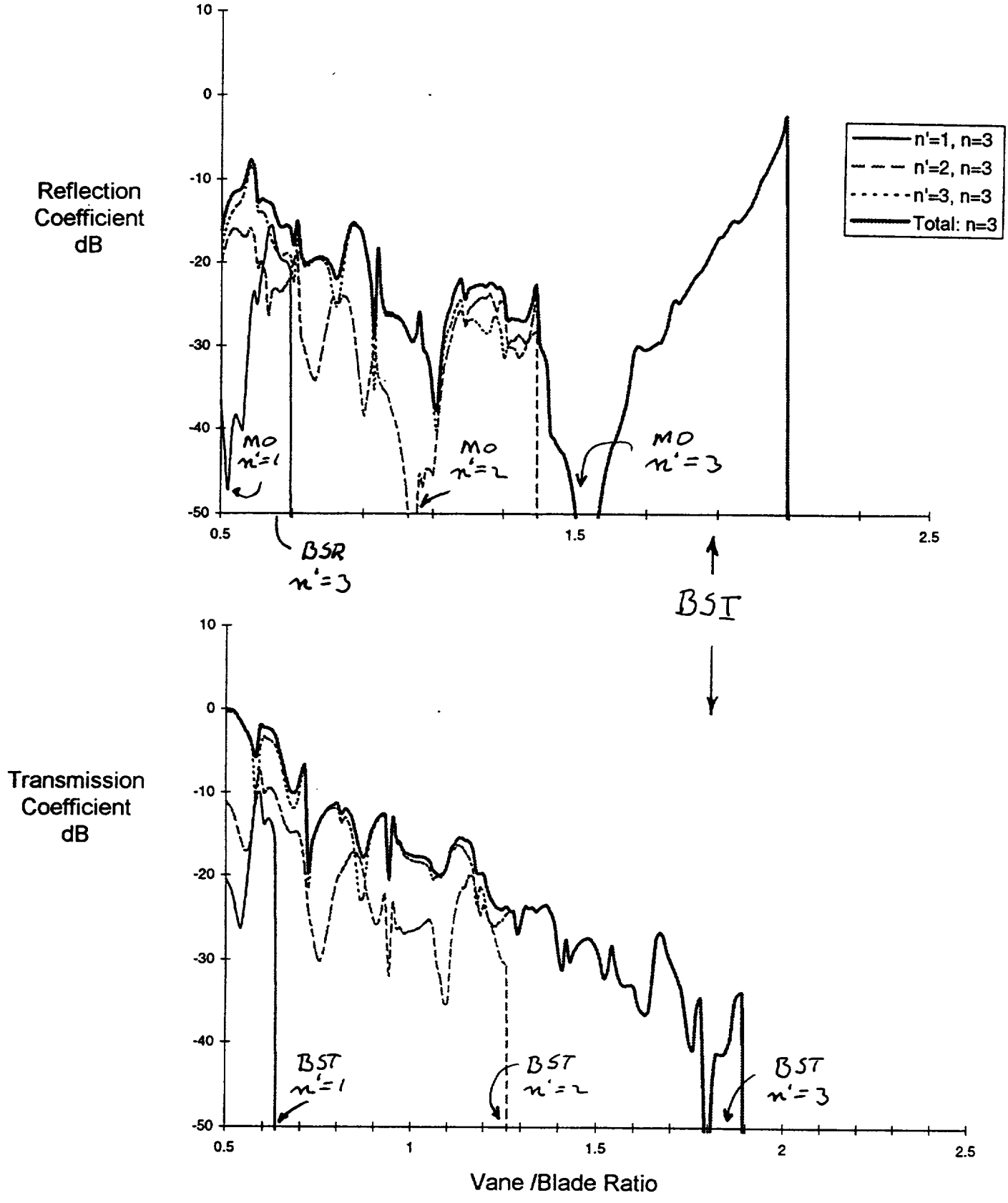

Figure 23a

Stator Scattering - High Speed Case
Input Mode Order: *n=3, k=3* Output Modes: *n=3; k'=1,2,3*

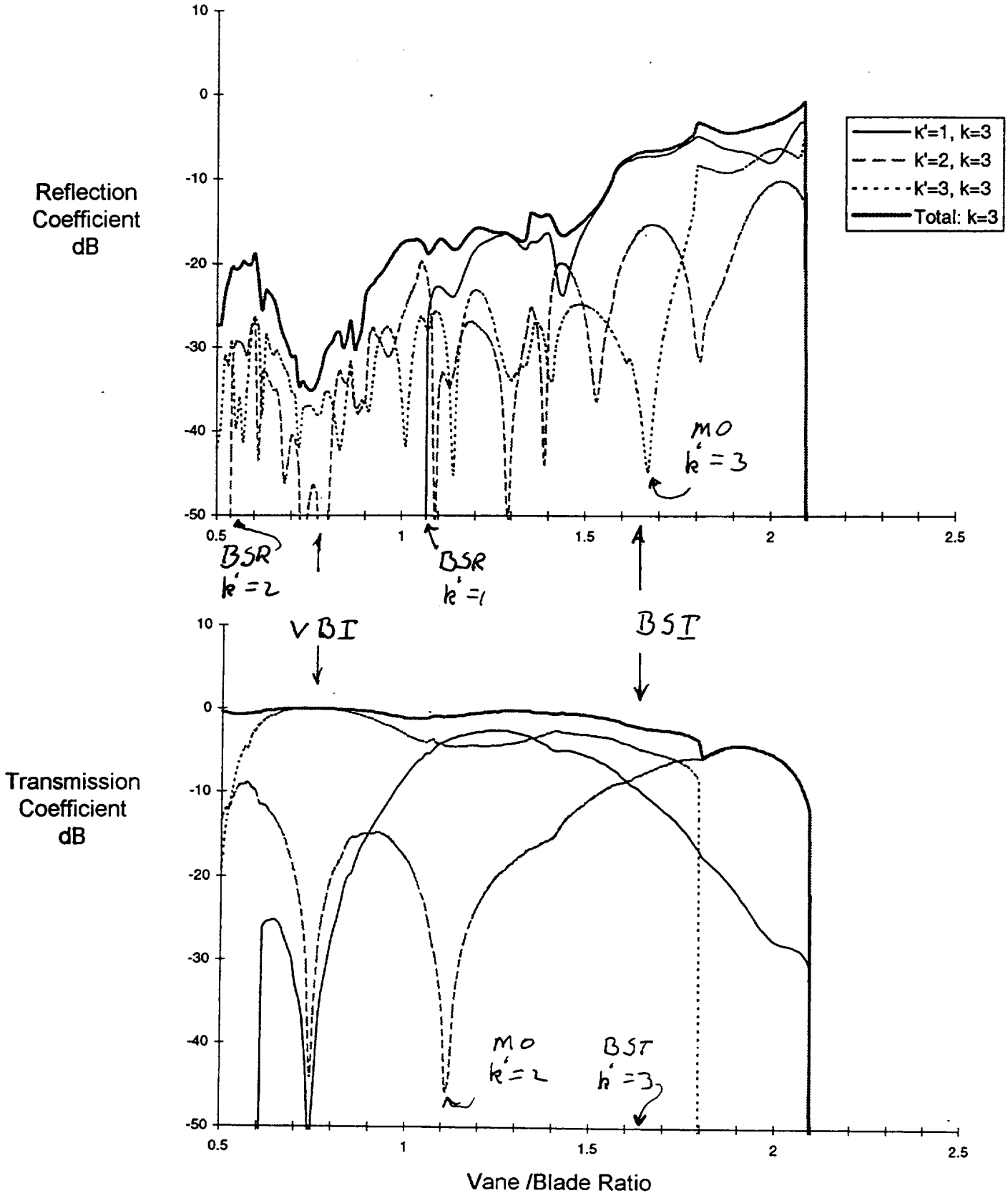

Figure 23b

2.3 SCATTERING CURVES FOR MID SPEED CASE

Scattering Curves for Mid Speed Case Curves for the mid speed case are presented in this section without discussion since they are similar to those just discussed the high speed case. Figure numbers and mode identification are given in Table 9 below and special vane/blade ratios are shown in Tables 10 and 11.

Table 9. Figure Numbers - Mid Speed Case

	Rotor		Stator	
Input Mode n; k	Output Mode n'; k	Figure #	Output Mode n; k'	Figure #
1;1	1,2,3; 1	24a	1; 1,2,3	24b
1;2	1,2,3; 2	25a	1; 1,2,3	25b
1;3	1,2,3; 3	26a	1; 1,2,3	26b
2;1	1,2,3; 1	27a	2; 1,2,3	27b
2;2	1,2,3; 2	28a	2; 1,2,3	28b
2;3	1,2,3; 3	29a	2; 1,2,3	29b
3;1	1,2,3; 1	30a	3; 1,2,3	30b
3;2	1,2,3; 2	31a	3; 1,2,3	31b
3;3	1,2,3; 3	32a	3; 1,2,3	32b

Table 10. Vane/Blade Ratios for Special Angles Relative to STATOR

mode order	Waves ⊥ Vane Chords		Waves // Vane Chords	
n, k	Upgoing Wave	Downgoing	Upgoing Wave	Downgoing
1, 1	1.50	0.79	0.48	1.52
1, 2	0.75	0.40	0.24	0.76
1, 3	0.50	0.26	0.16	0.51
2, 1	2.99	1.58	0.96	3.04
2, 2	1.50	0.79	0.48	1.52
2, 3	1.00	0.53	0.32	1.02
3, 1	4.49	2.37	1.43	4.57
3, 2	2.24	1.18	0.72	2.28
3, 3	1.50	0.79	0.48	1.52

Table 11. Vane/Blade Ratios for Special Angles Relative to ROTOR

mode order	Waves ⊥ Vane Chords		Waves // Rotor Chords	
n, k	Upgoing Wave	Downgoing	Upgoing Wave	Downgoing
1, 1	0.51	1.42	1.65	0.72
1, 2	0.25	0.71	0.83	0.36
1, 3	0.17	0.47	0.55	0.24
2, 1	1.02	2.84	3.31	1.43
2, 2	0.51	1.42	1.65	0.72
2, 3	0.34	0.95	1.10	0.48
3, 1	1.53	4.25	4.96	2.15
3, 2	0.76	2.13	2.84	1.08
3, 3	0.51	1.42	1.65	0.72

Rotor Scattering - Mid Speed Case
Input Mode Order: *n=1; k=1* Output Modes: *n'=1,2,3; k=1*

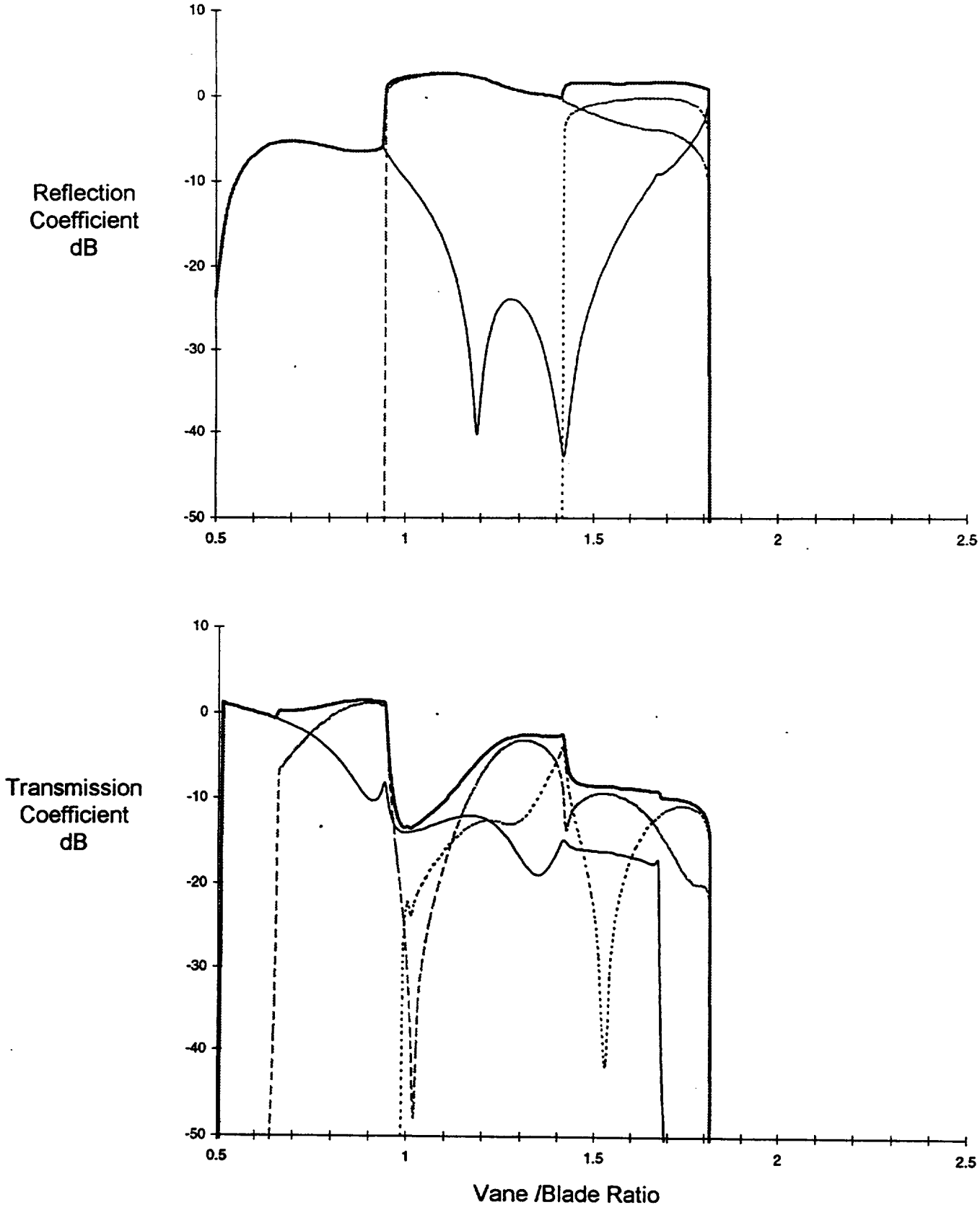

Figure 24a

Stator Scattering - Mid Speed Case
Input Mode Order: *n=1, k=1* Output Modes: *n=1; k'=1,2,3*

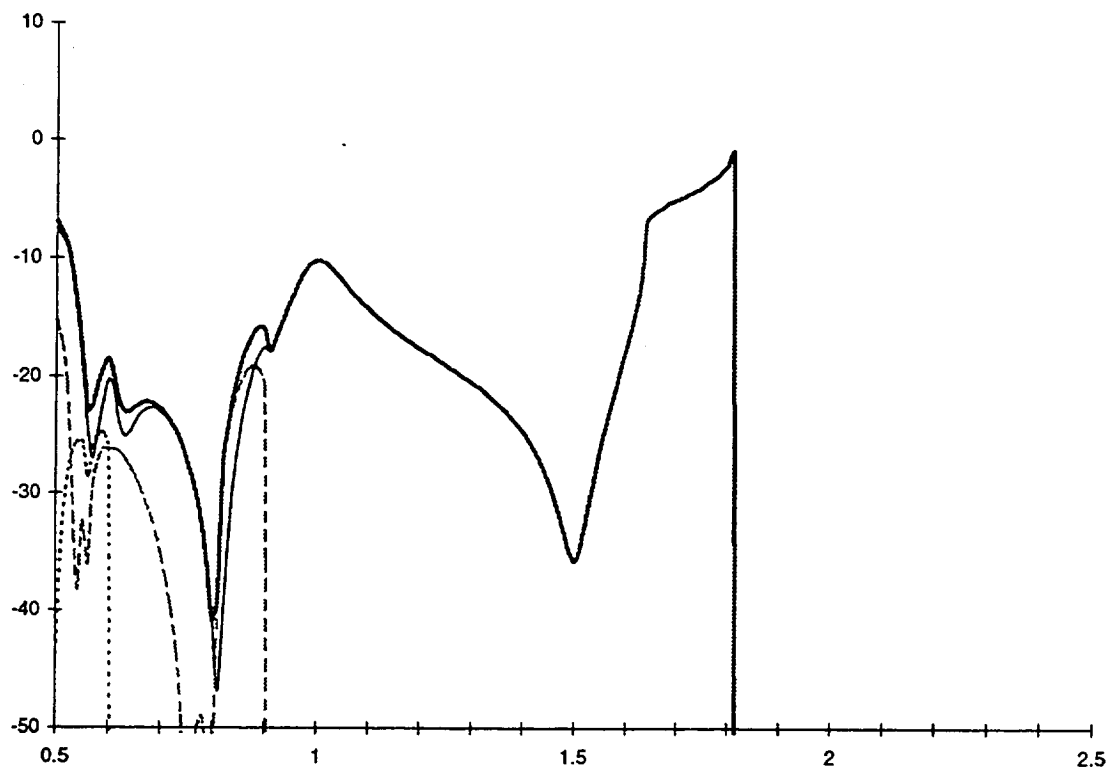

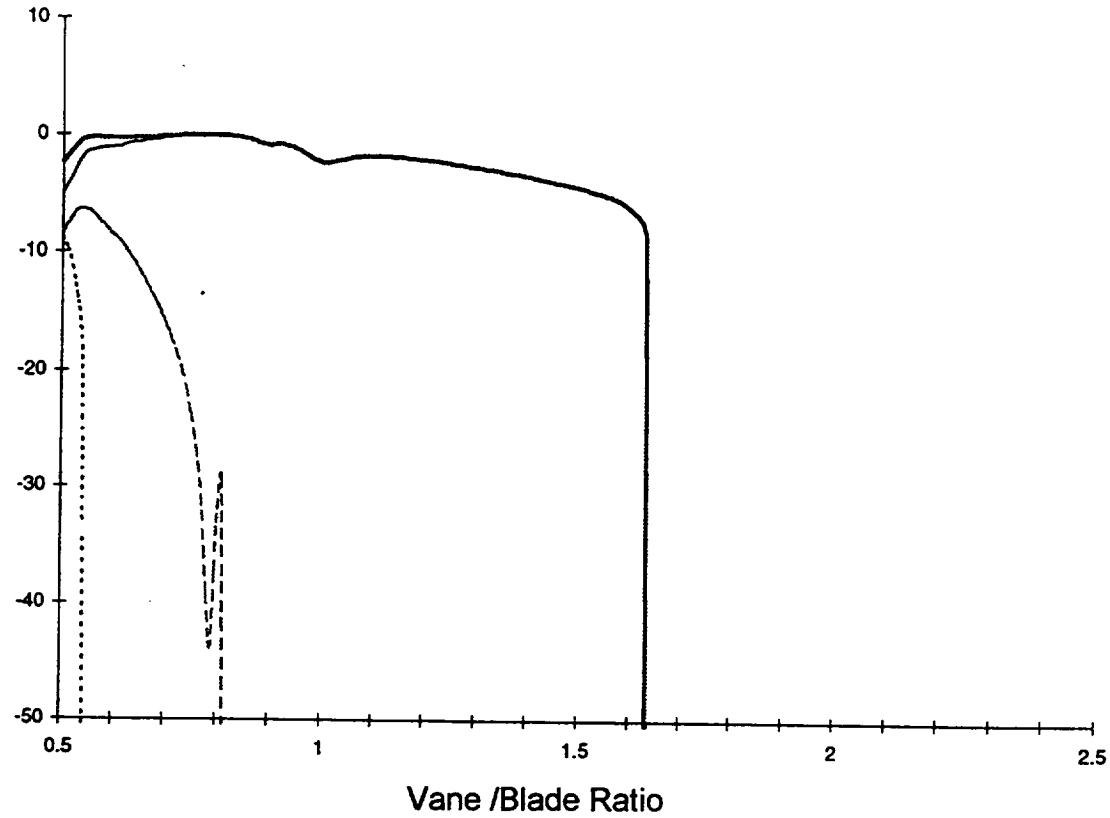

Figure 24b

Rotor Scattering - Mid Speed Case
Input Mode Order: *n=1; k=2* Output Modes: *n'=1,2,3; k=2*

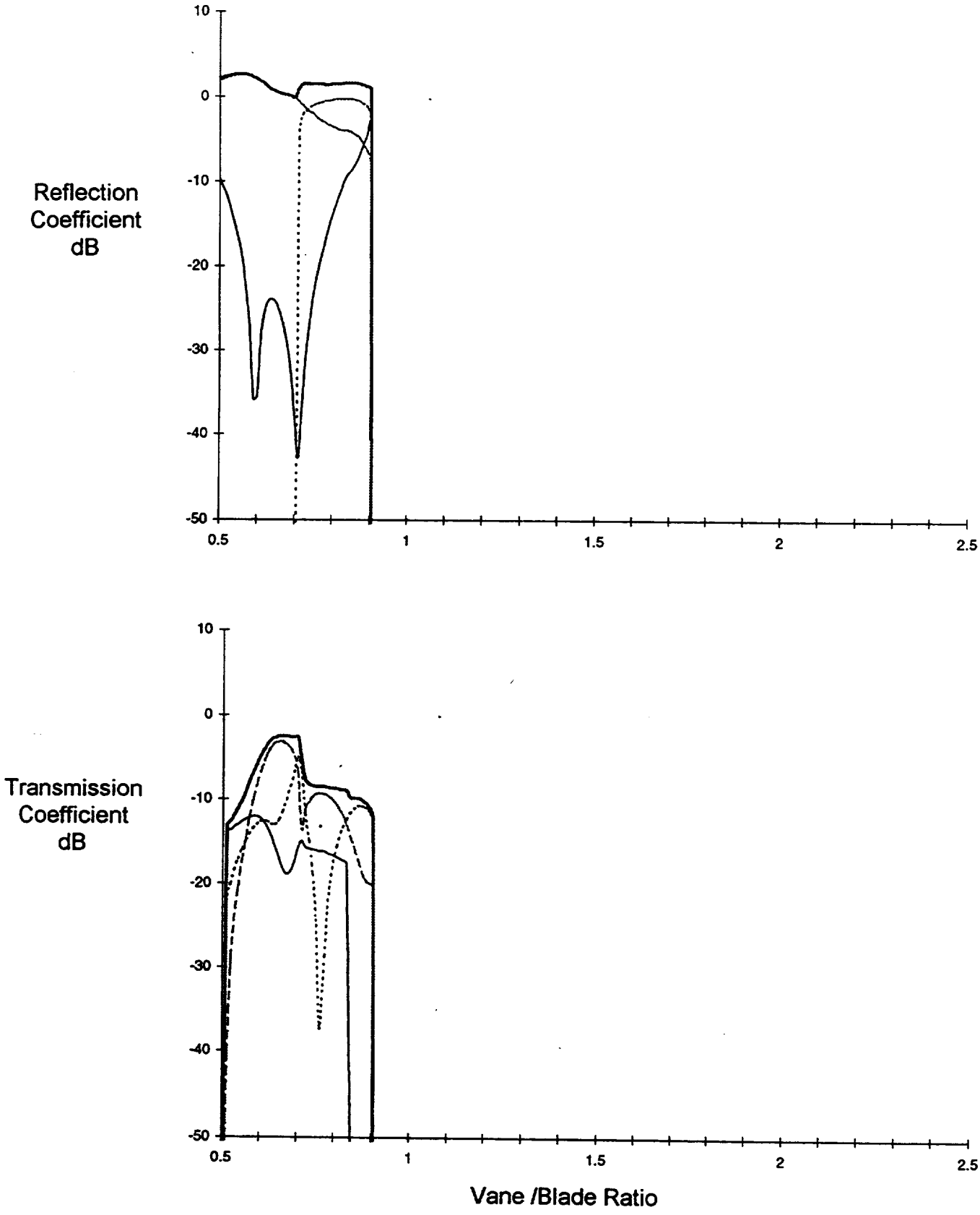

Figure 25a

Stator Scattering - Mid Speed Case
Input Mode Order: *n=1, k=2* Output Modes: *n=1; k'=1,2,3*

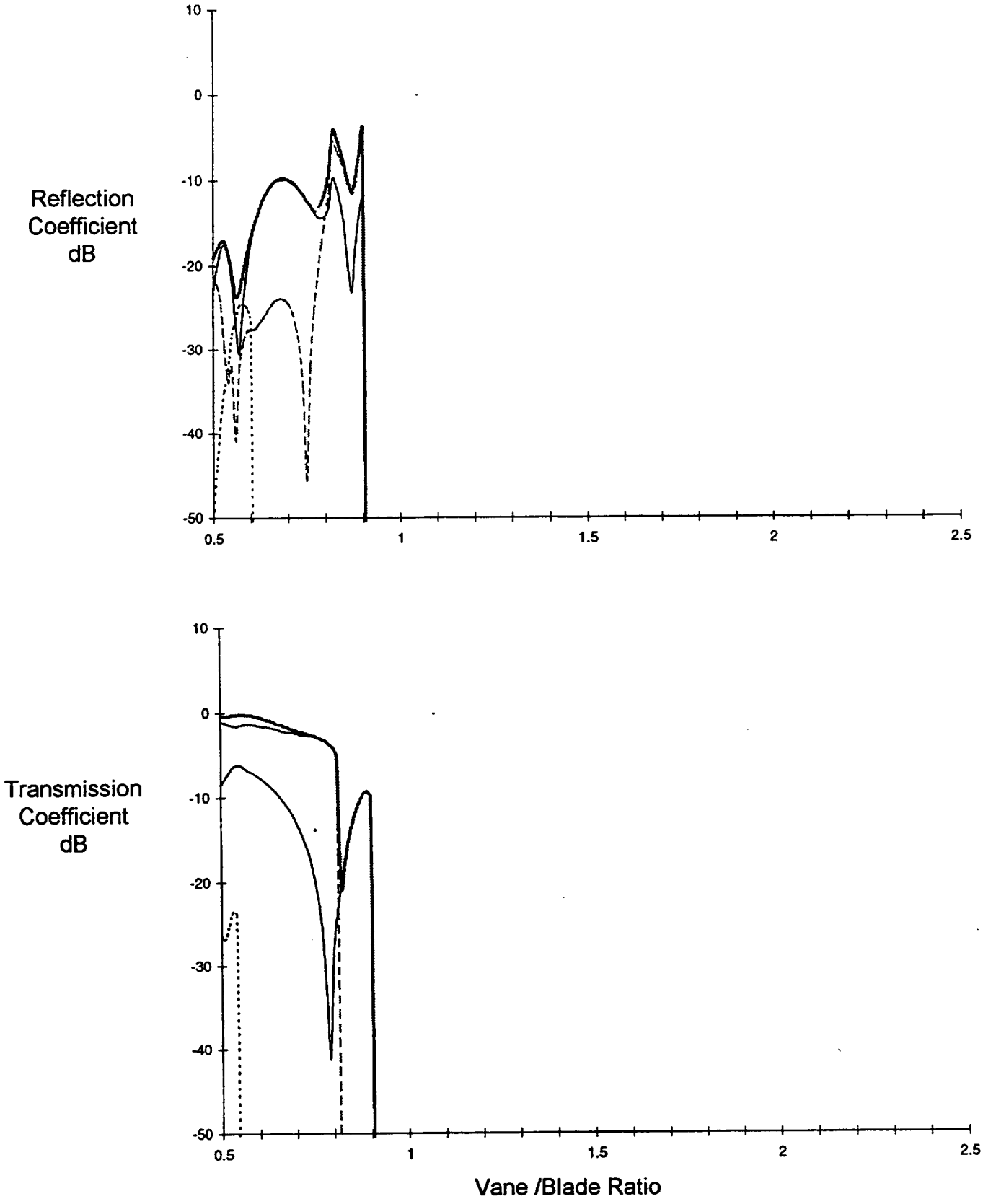

Figure 25b

Rotor Scattering - Mid Speed Case
Input Mode Order: *n=1; k=3* Output Modes: *n'=1,2,3; k=3*

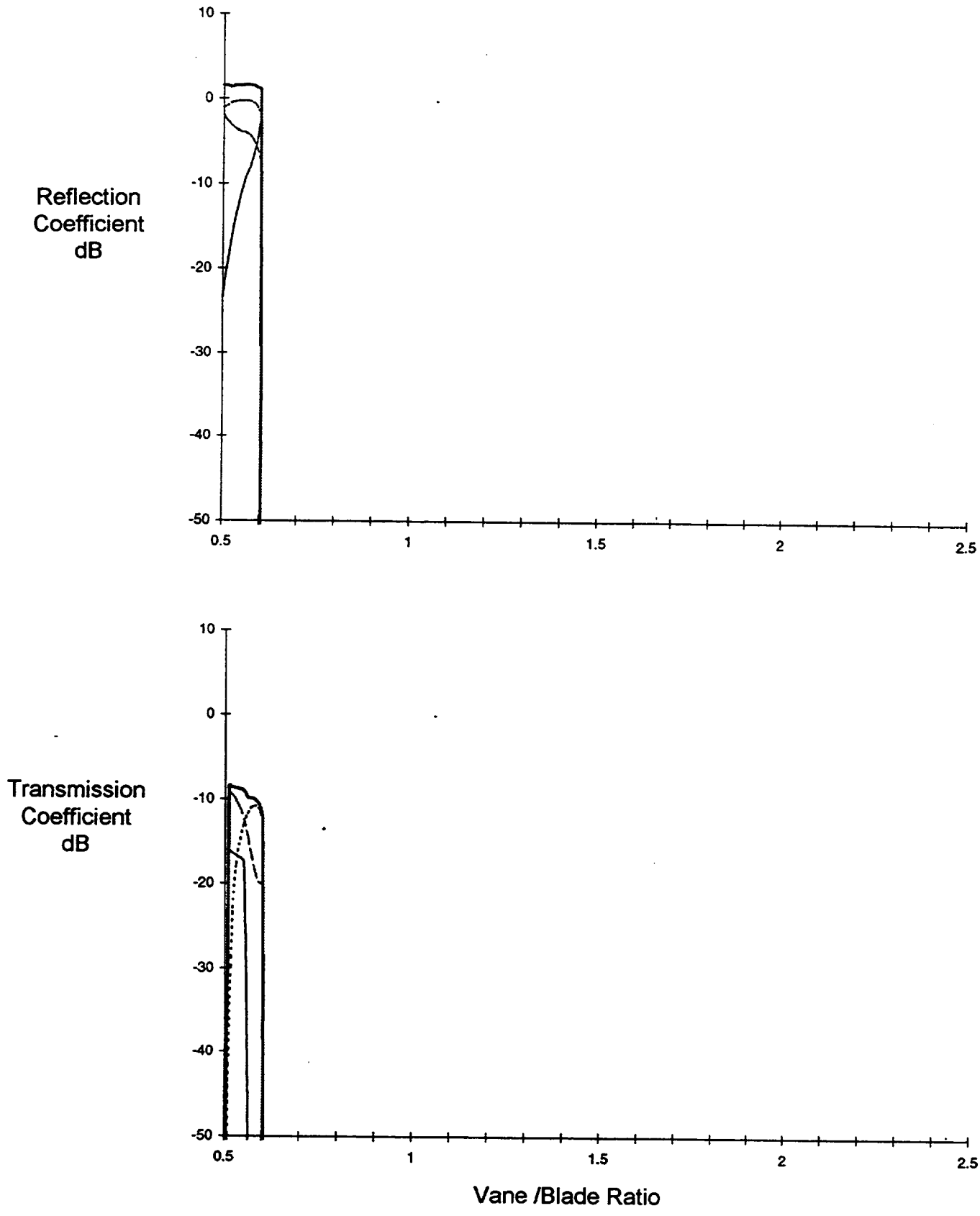

Figure 26a

Stator Scattering - Mid Speed Case
Input Mode Order: *n=1, k=3* Output Modes: *n=1; k'=1,2,3*

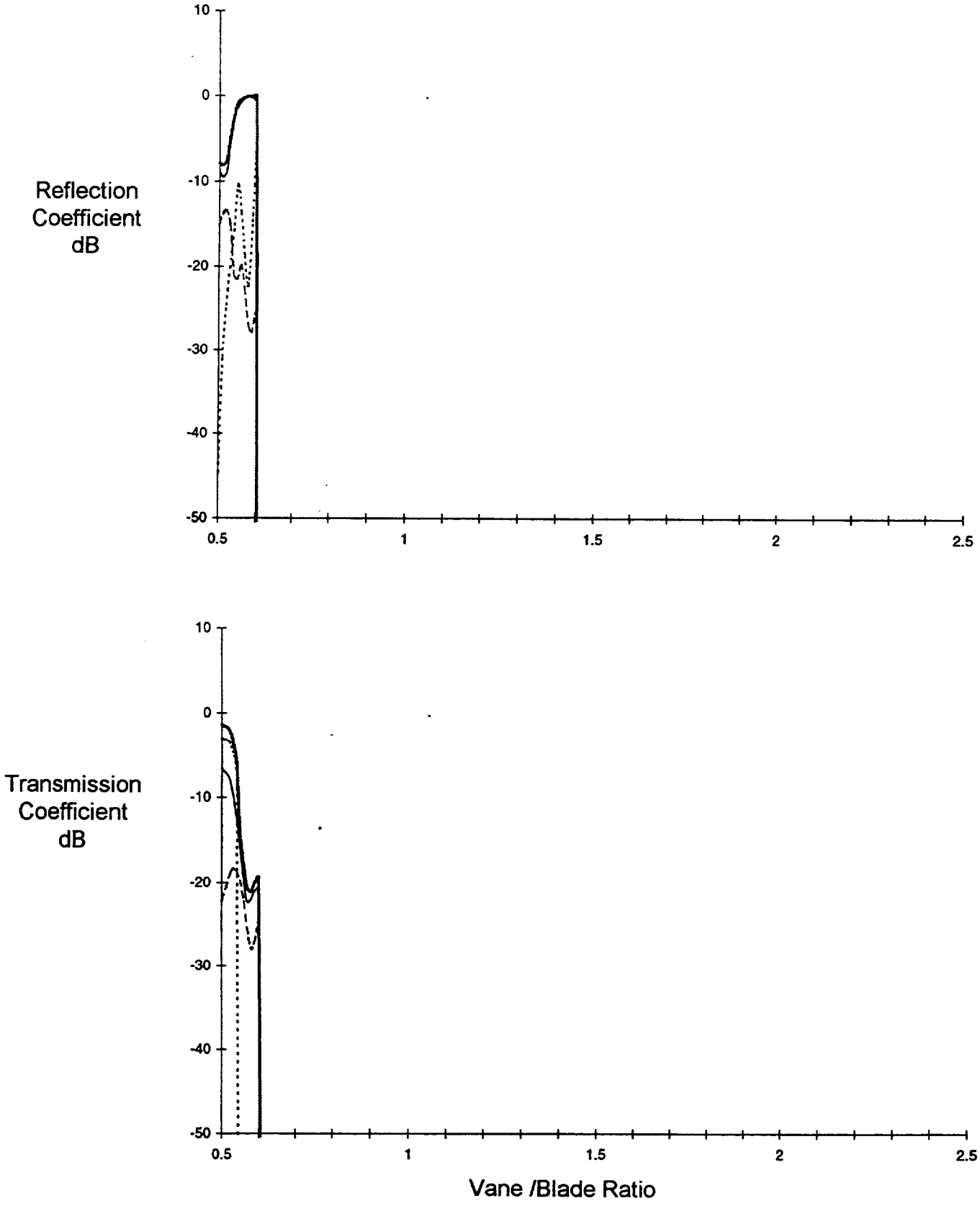

Figure 26b

Rotor Scattering - Mid Speed Case
Input Mode Order: *n=2; k=1* Output Modes: *n'=1,2,3; k=1*

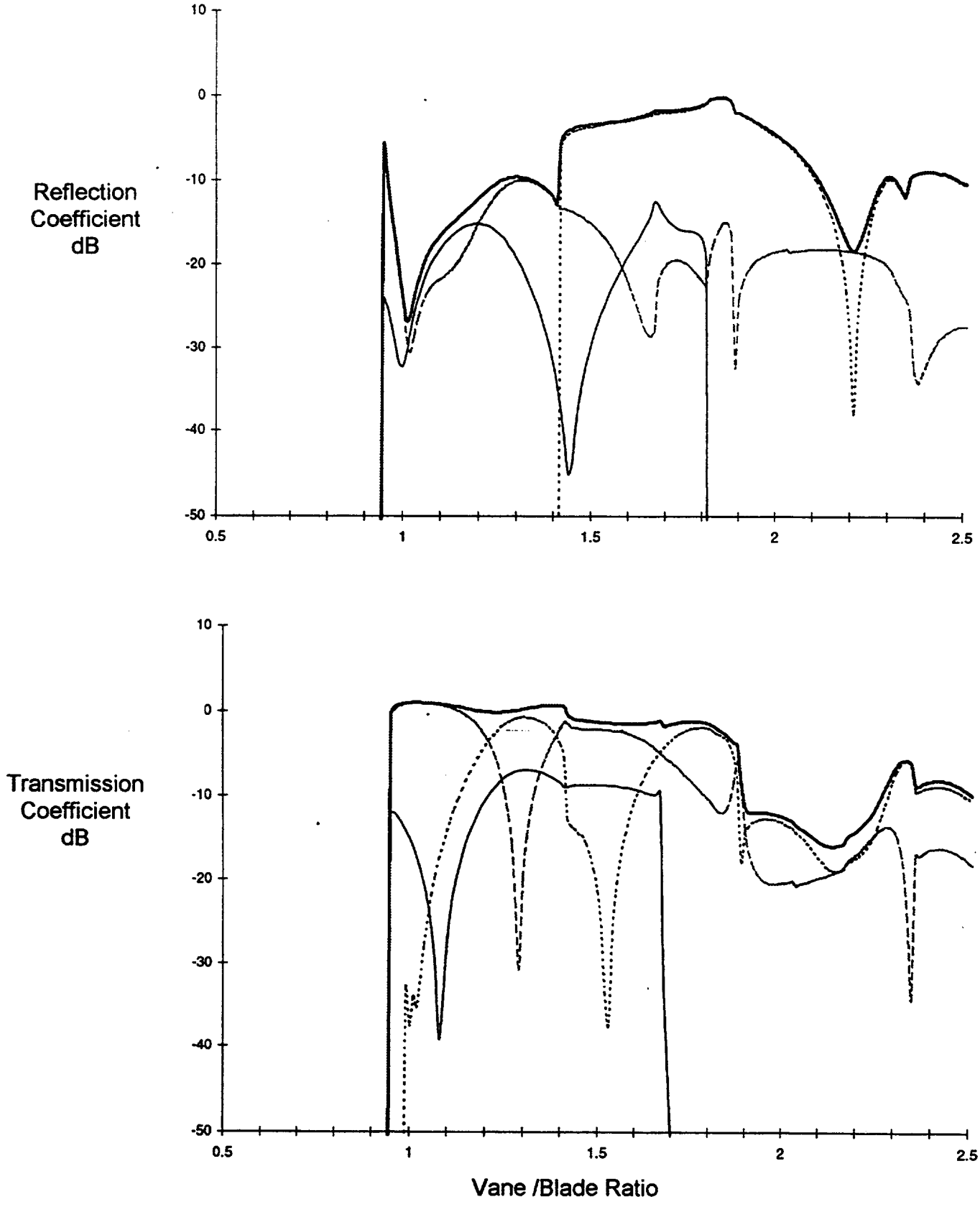

Figure 27a

Stator Scattering - Mid Speed Case
Input Mode Order: *n=2, k=1* Output Modes: *n=2; k'=1,2,3*

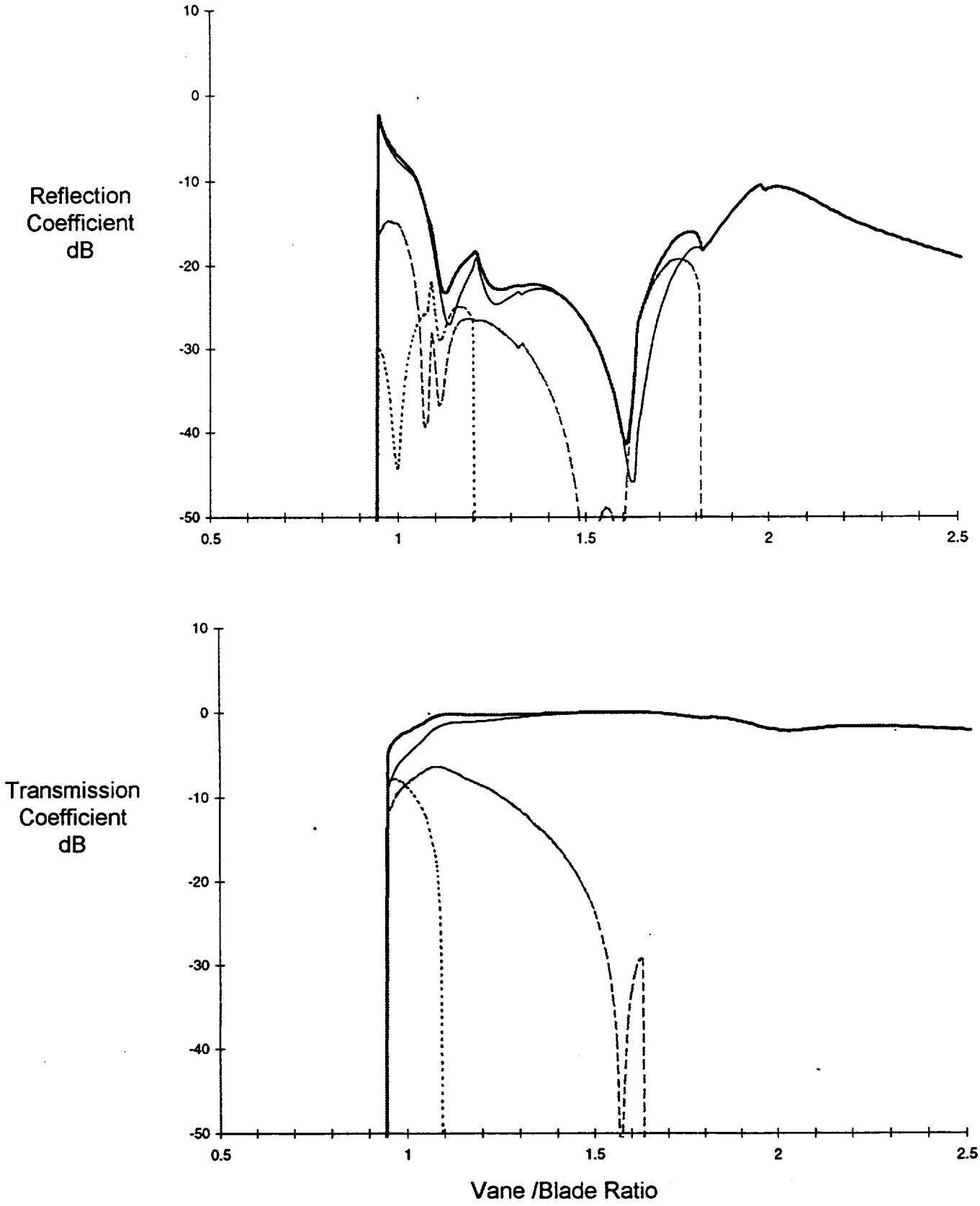

Figure 27b

Rotor Scattering - Mid Speed Case
Input Mode Order: *n=2; k=2* Output Modes: *n'=1,2,3; k=2*

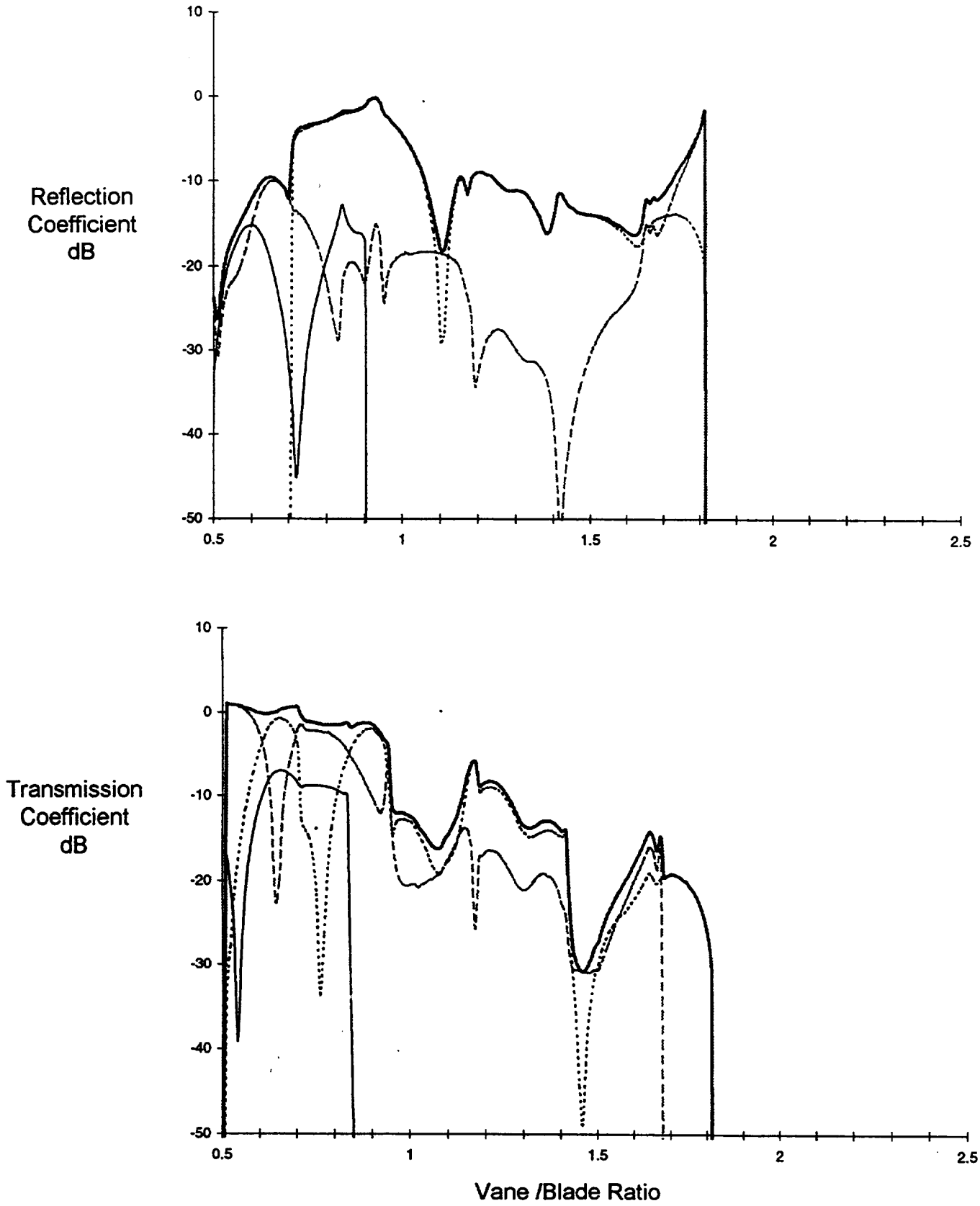

Figure 28a

Stator Scattering - Mid Speed Case
Input Mode Order: *n=2, k=2* Output Modes: *n=2; k'=1,2,3*

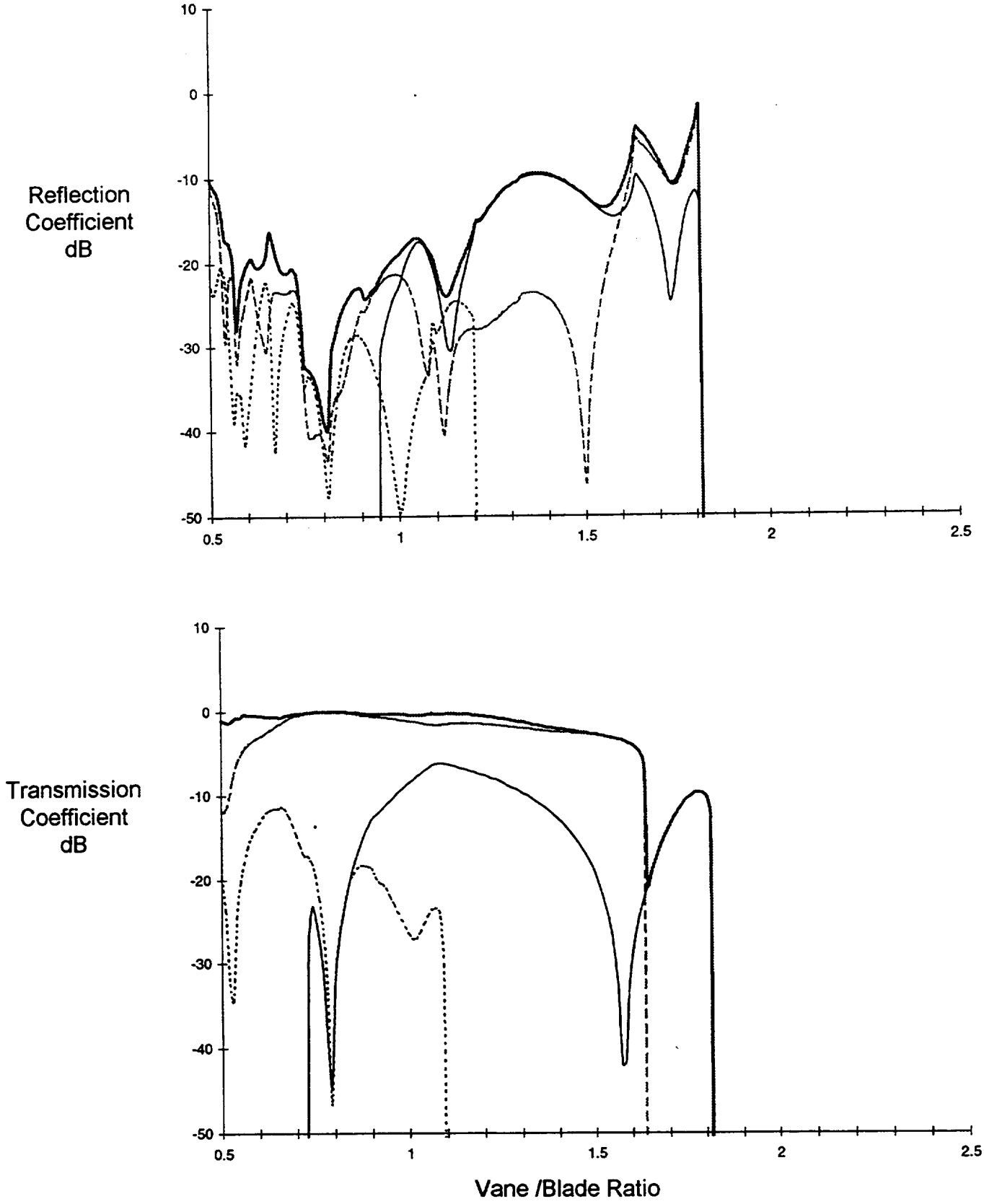

Figure 28b

Rotor Scattering - Mid Speed Case
Input Mode Order: *n=2; k=3* Output Modes: *n'=1,2,3; k=3*

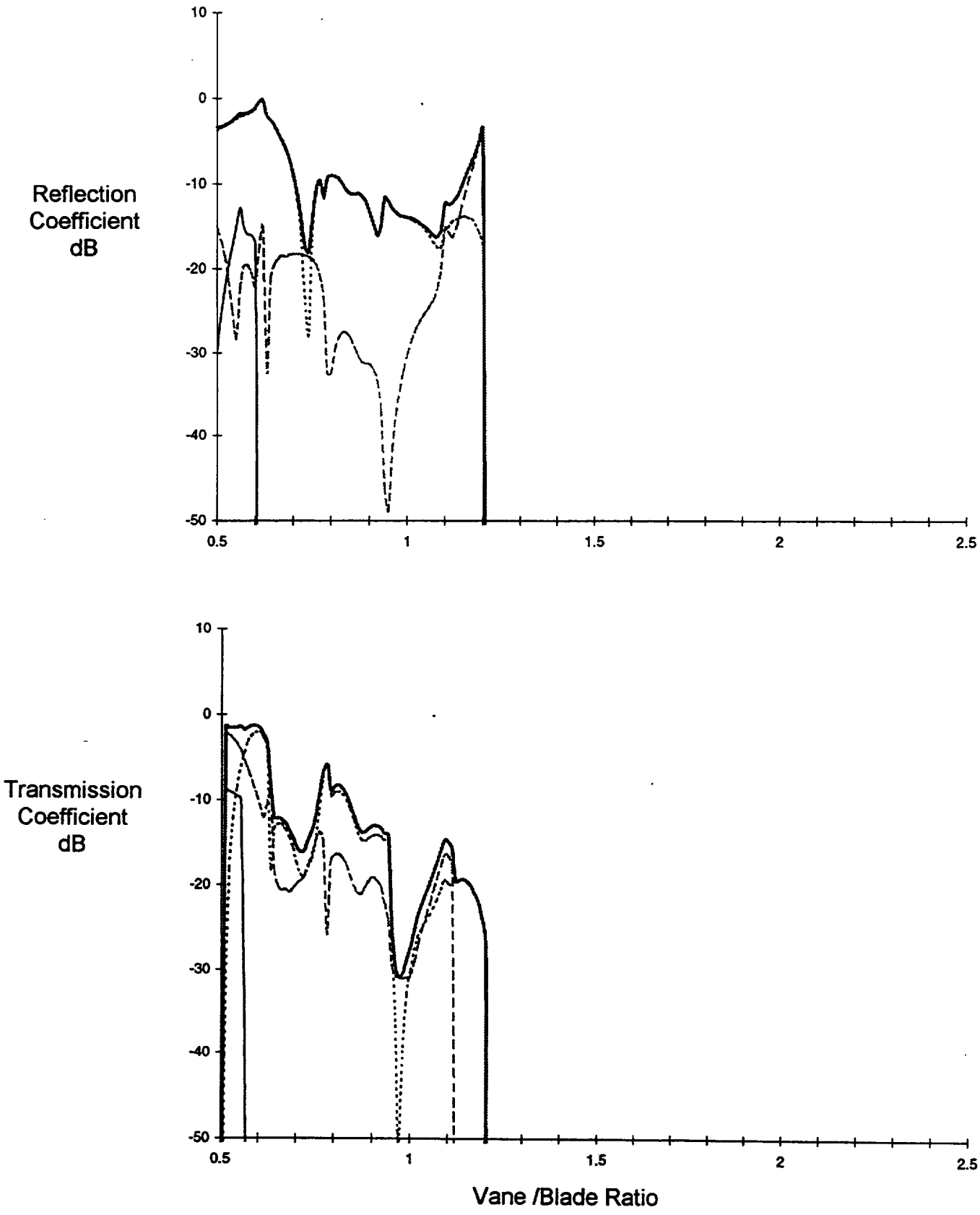

Figure 29a

Stator Scattering - Mid Speed Case
Input Mode Order: *n=2, k=3* Output Modes: *n=2; k'=1,2,3*

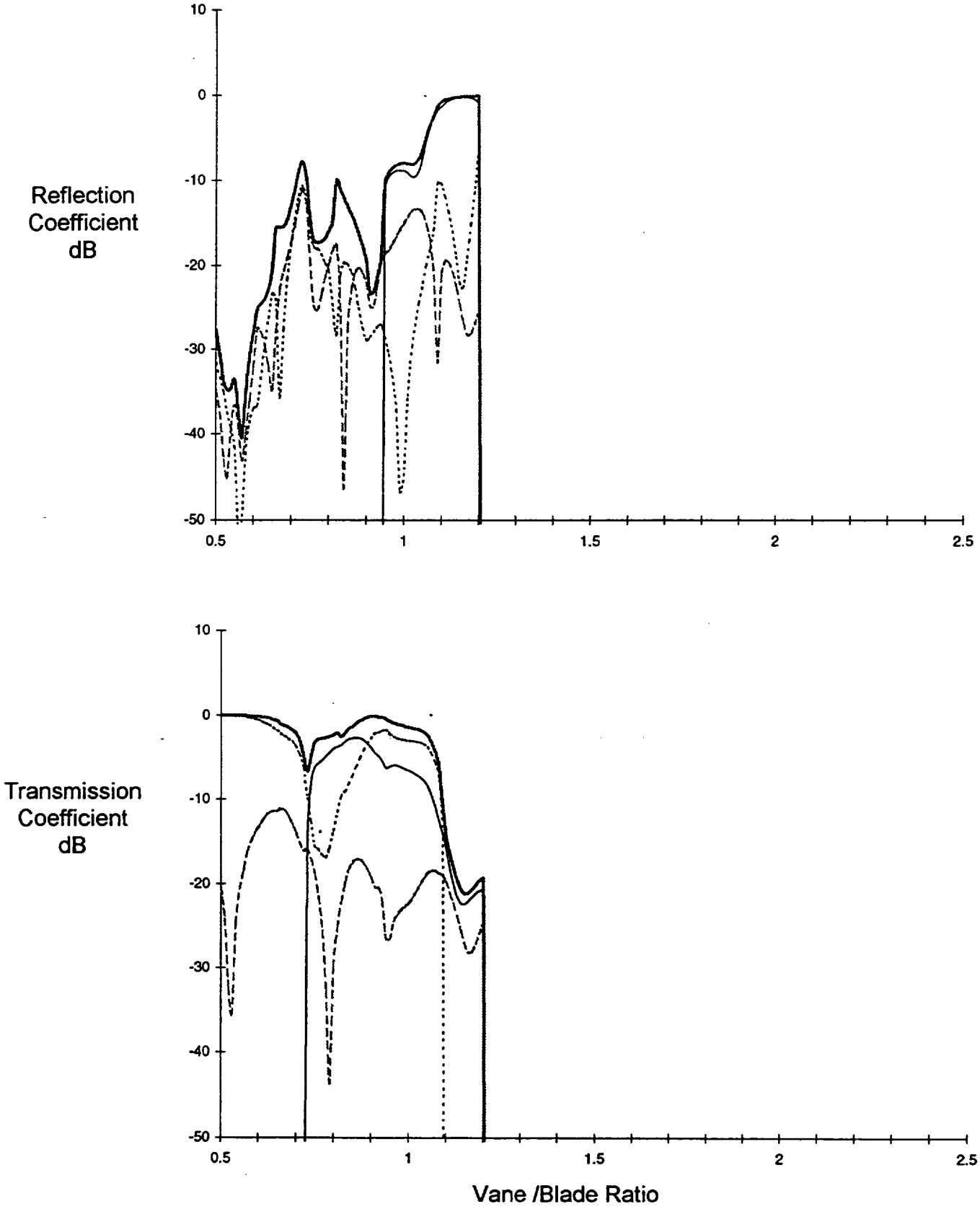

Figure 29b

Rotor Scattering - Mid Speed Case
Input Mode Order: *n=3; k=1* Output Modes: *n'=1,2,3; k=1*

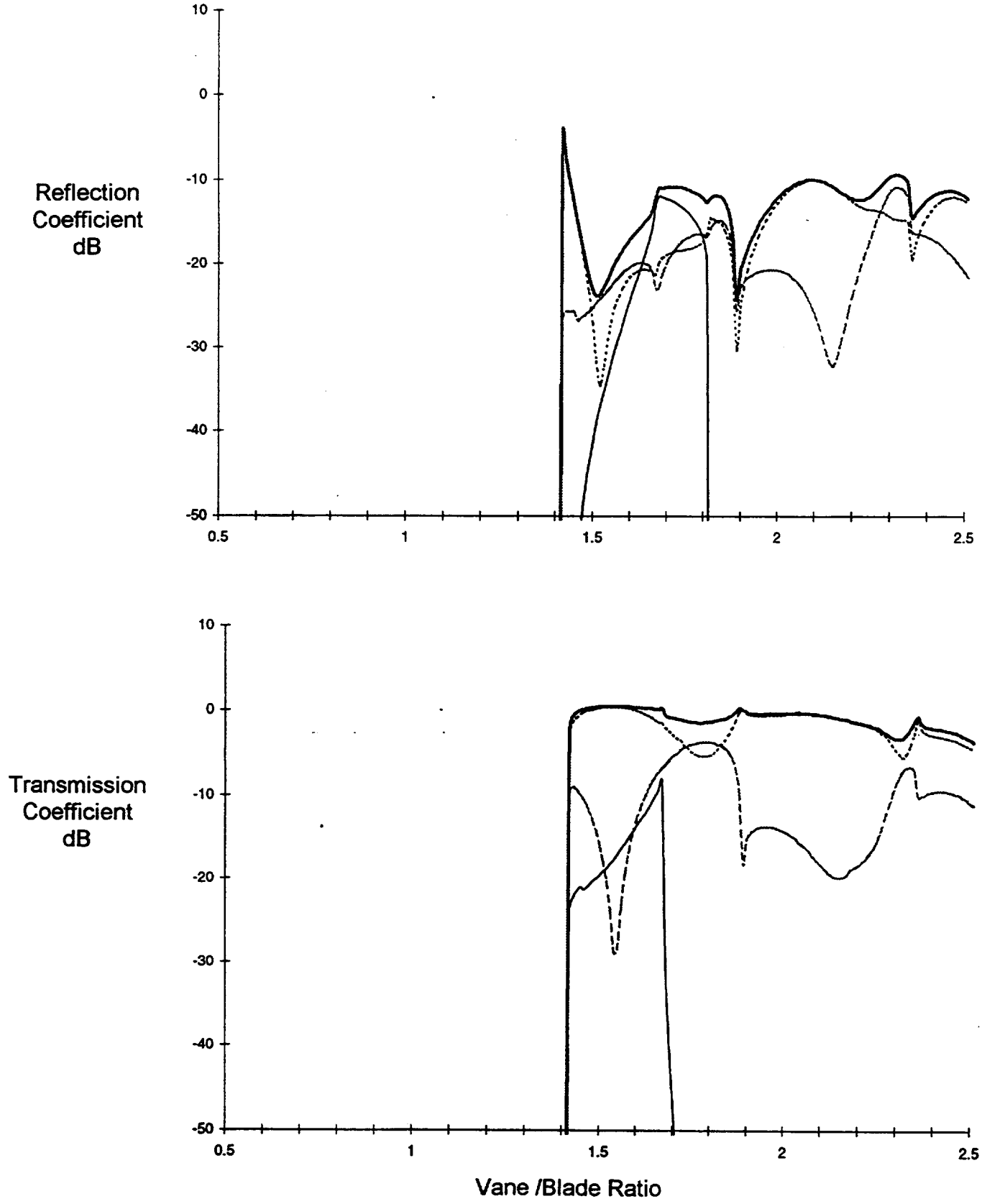

Figure 30a

Stator Scattering - Mid Speed Case
Input Mode Order: *n=3, k=1* Output Modes: *n=3; k'=1,2,3*

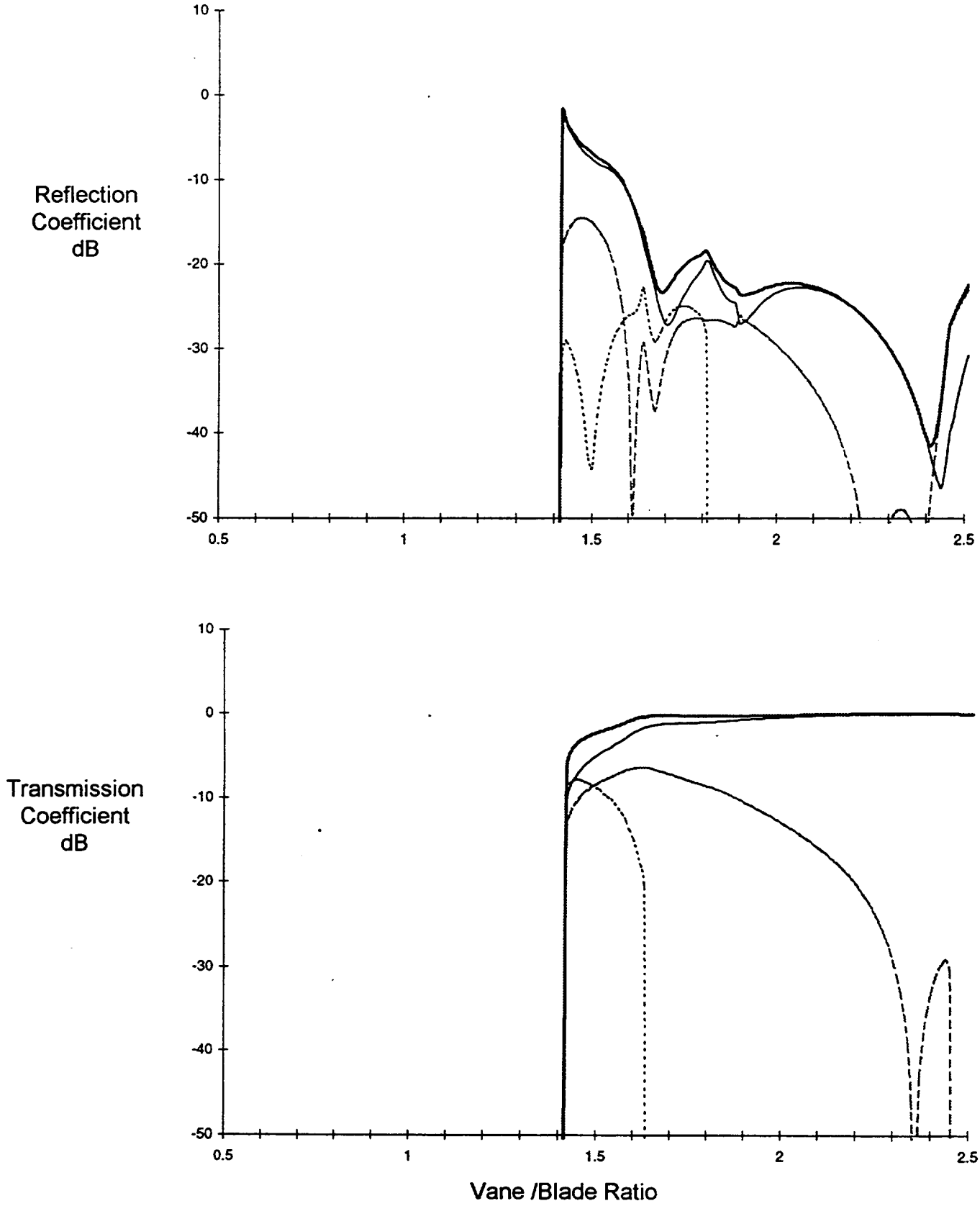

Figure 30b

Rotor Scattering - Mid Speed Case
Input Mode Order: *n=3; k=2* Output Modes: *n'=1,2,3; k=2*

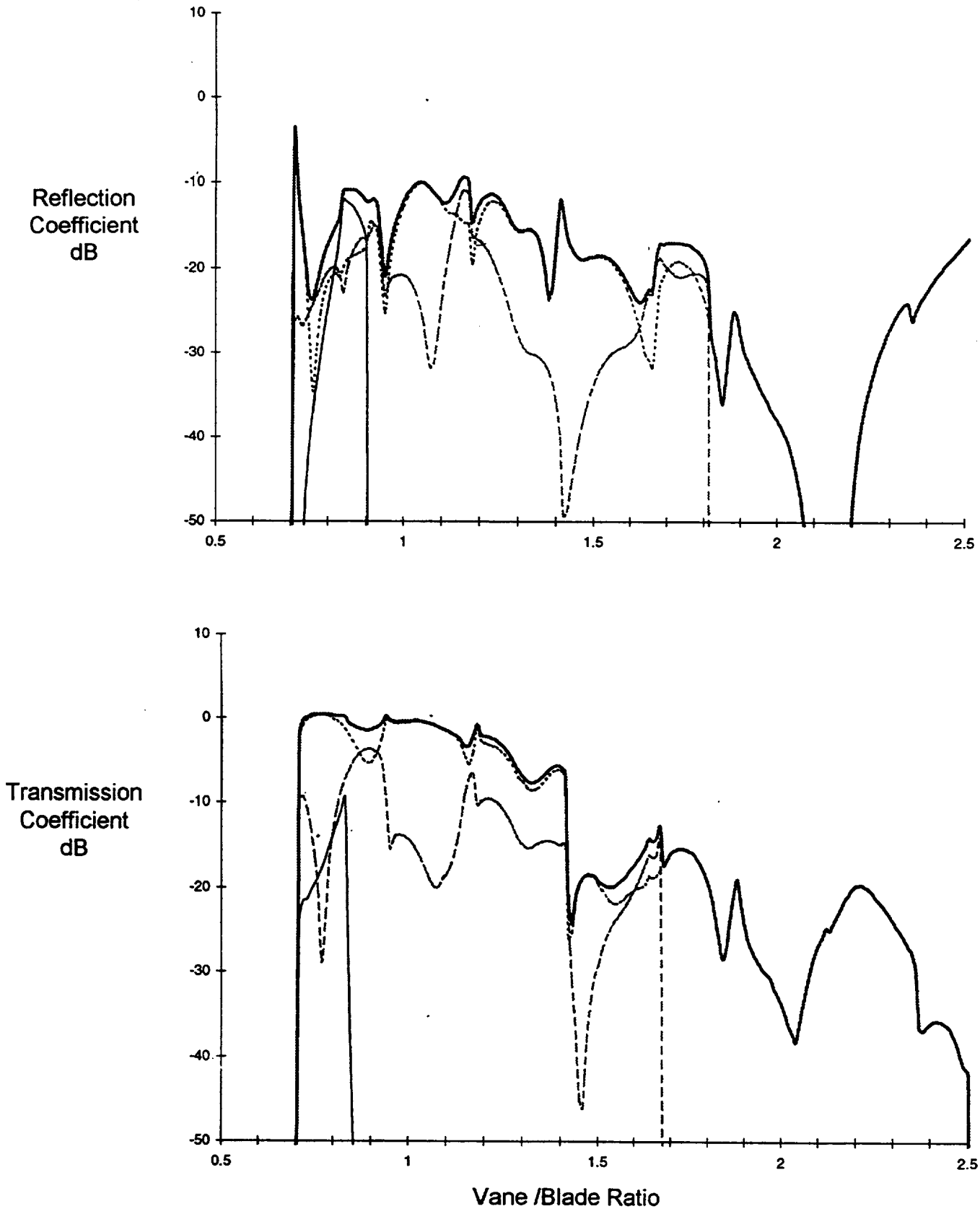

Figure 31a

Stator Scattering - Mid Speed Case
Input Mode Order: *n=3, k=2* Output Modes: *n=3; k'=1,2,3*

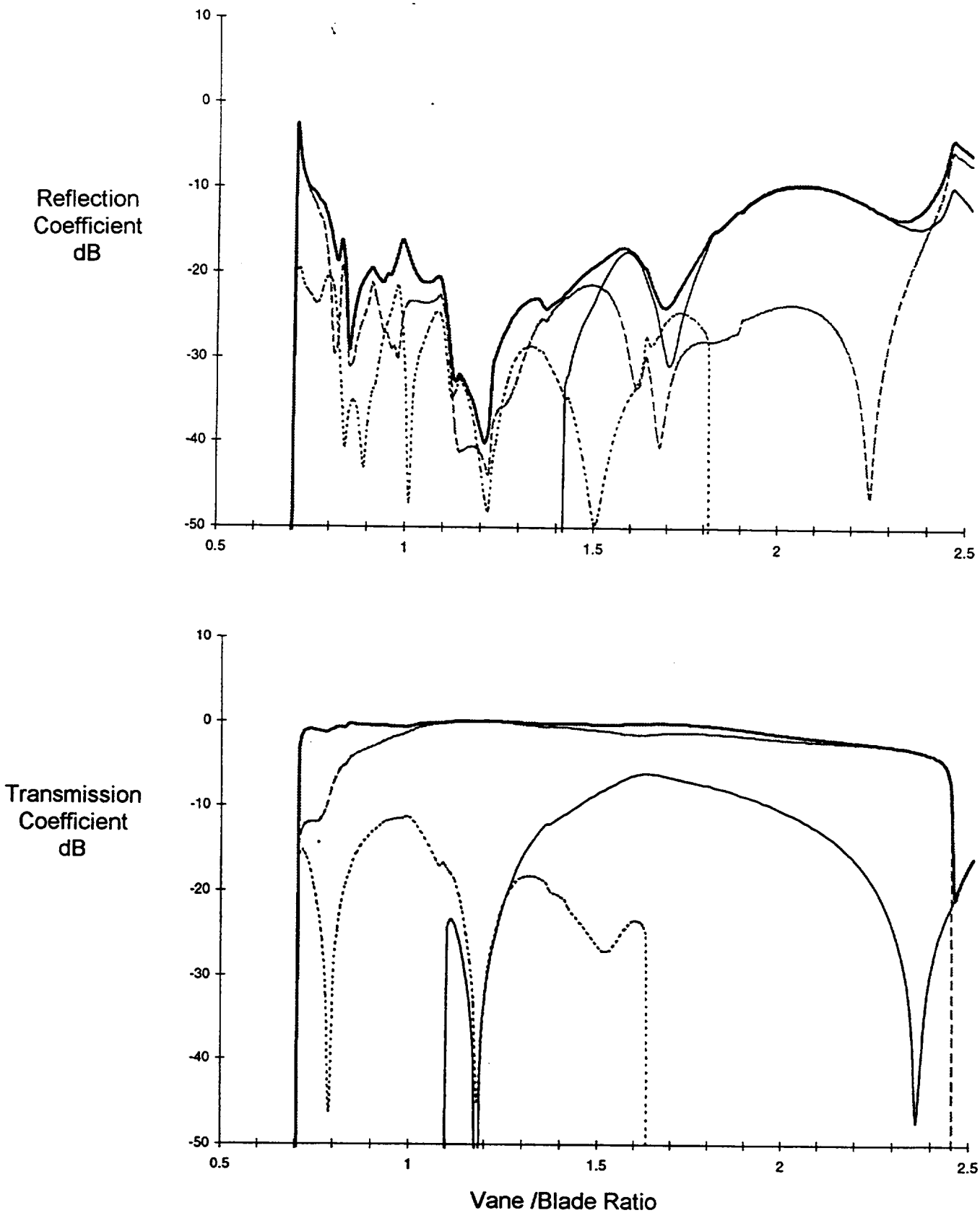

Figure 31b

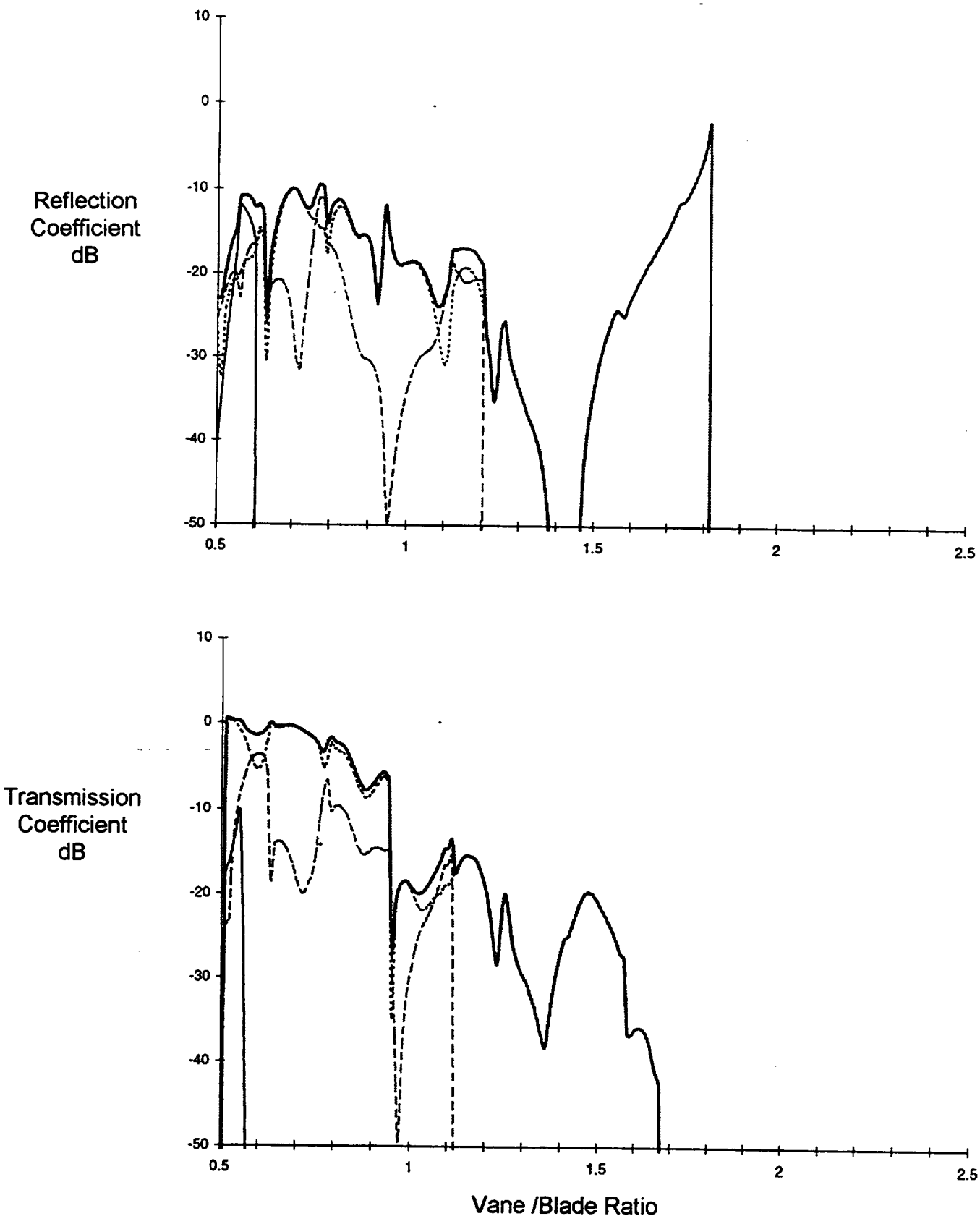
Rotor Scattering - Mid Speed Case
Input Mode Order: n=3; k=3 Output Modes: n'=1,2,3; k=3
Reflection Coefficient dB
10
0
-10
-20
-30
-40
-50
0.5
1
1.5
2
2.5
Transmission Coefficient dB
10
0
-10
-20
-30
-40
-50
0.5
1
1.5
2
2.5
Vane /Blade Ratio

Figure 32a

Stator Scattering - Mid Speed Case
Input Mode Order: *n=3, k=3* Output Modes: *n=3; k'=1,2,3*

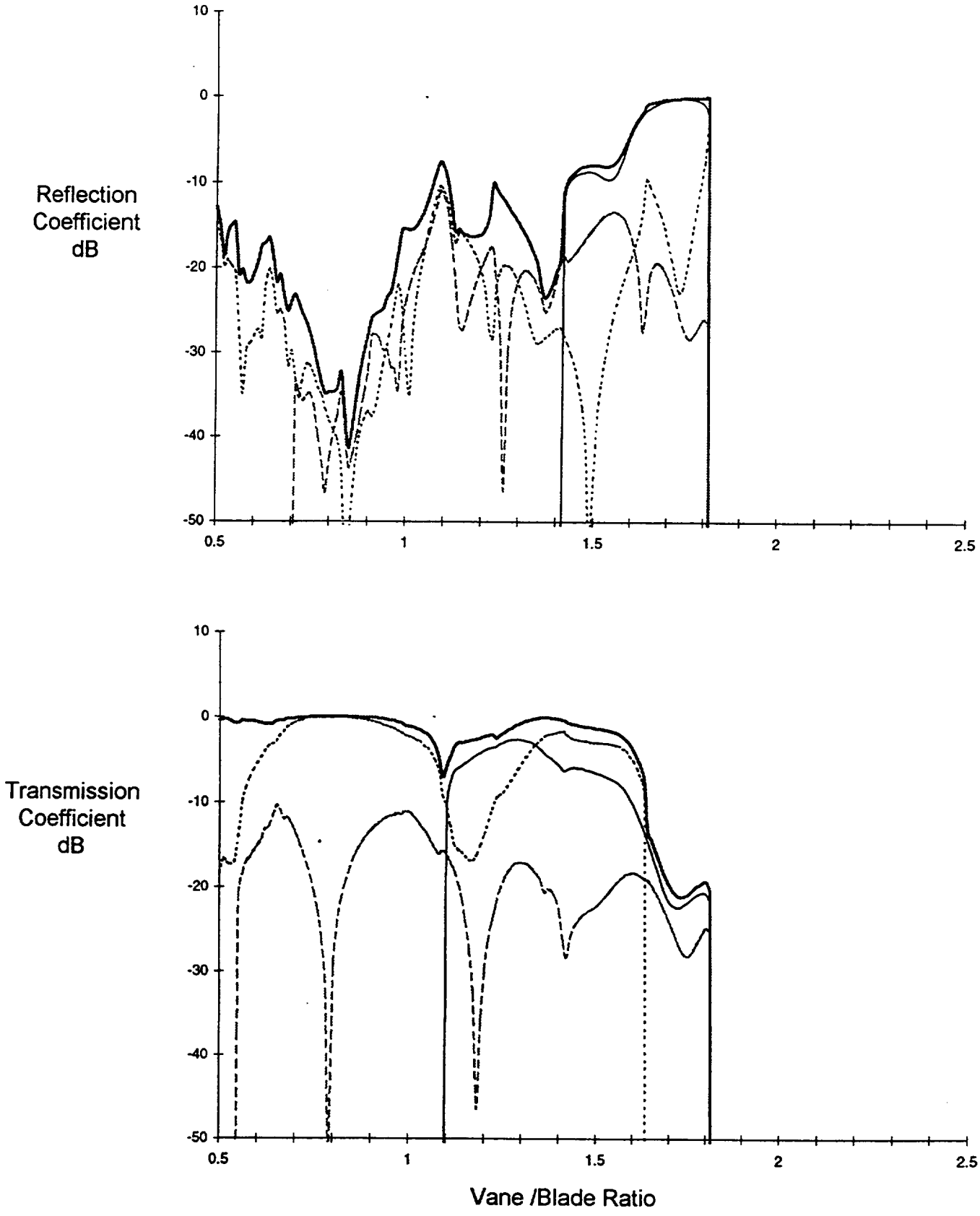

Figure 32b

APPENDIX B
ACTUATOR DISK THEORY

The role of actuator disks in the scattering theory is to account for turning of the mean flow at the rotor and stator through conservation of mass and momentum. In applying the conservation equations, the flow quantities are written as sums of steady and perturbation (or unsteady) parts. When the steady and unsteady parts are separated, the steady flow is considered prescribed (i.e. known from a separate aerodynamic analysis. These steady equations provide coefficients for the unsteady equations so that jumps in the mean flow cause jumps in the perturbation flow. The jumps lead to reflection and transmission coefficients that are found by inverting a linear system.

There are 3 wave types:

T=1: Upstream-going pressure waves
T=2: Downstream-going pressure waves
T=3: Vortical (downstream-going) waves

and 3 conservation equations:

Conservation of mass
Conservation of axial momentum
Conservation of tangential momentum

These are satisfied on a mode-by-mode basis using the standard wave set from the main text.

In the following sections, we present the standard wave sets, apply them to the conservation equations to develop the linear system, and show the solution method.

STANDARD WAVE SET

Forms of the standard waves are given in terms of the *defining* components and the *associated* components. Pressure waves are defined in terms of pressure; the velocity perturbations are the associated components. Vorticity waves are defined in terms of their axial velocity components; the tangential velocity is the associated component.

The defining form for the pressure waves is

$$T = 1,2 \qquad p_T^r(x,\phi,t) = p_o \sum_{n=-\infty}^{\infty} \sum_{k=-\infty}^{\infty} A_T^r(n,k) e^{i[\alpha_T^r(n,k)(\bar{x}-\bar{x}_T^r)+\psi_{n,k}]} \qquad \text{(B-1)}$$

Vorticity waves are defined in terms of their axial velocity component

$$T = 3 \qquad u_T^r(x,\phi,t) = a_o \sum_{n=-\infty}^{\infty} \sum_{k=-\infty}^{\infty} A_T^r(n,k) e^{i[\alpha_T^r(n,k)(\bar{x}-\bar{x}_T^r)+\psi_{n,k}]} \qquad \text{(B-2)}$$

where

$$\psi_{nk} \equiv \beta_{nk}\phi + nB\Omega t \tag{B-3}$$

and

$$\beta_{nk} \equiv -(nB - kV) \tag{B-4}$$

The associated axial and tangential velocity components are given by

$$T = 1,2 \qquad u_T^r(x,\phi,t) = a_o \sum_{n=-\infty}^{\infty} \sum_{k=-\infty}^{\infty} A_T^r(n,k) U_{Tnk}^r e^{i[\alpha_T^r(n,k)(\bar{x}-\bar{x}_T^r)+\psi_{n,k}]} \tag{B-5}$$

and

$$T = 1,2,3 \qquad v_T^r(x,\phi,t) = a_o \sum_{n=-\infty}^{\infty} \sum_{k=-\infty}^{\infty} A_T^r(n,k) V_{Tnk}^r e^{i[\alpha_T^r(n,k)(\bar{x}-\bar{x}_T^r)+\psi_{n,k}]} \tag{B-6}$$

The superscripts r refer to conditions on either side of the actuator disk: $r = a$ on the upstream side of the actuator disk and $r = b$ on the downstream side. In the above equations $\bar{x}$ denotes axial distance normalized by radius R of the narrow annulus so that the α's are also non-dimensionalized by R. By applying the momentum equation, or looking up formulas in Smith's paper, the coefficients relating the defining and associated components are easily shown for the pressure waves to be

$$T = 1,2 \qquad \begin{cases} U_{Tnk}^r = \dfrac{p_o}{\rho_a a_o a_a}\left(\dfrac{-\alpha_{Tnk}^r}{\lambda_{Tnk}^r}\right) \\ V_{Tnk}^r = \dfrac{p_o}{\rho_a a_o a_a}\left(\dfrac{-\beta_{nk}}{\lambda_{Tnk}^r}\right) \end{cases} \tag{B-7}$$

and for the vorticity waves

$$T = 3 \qquad V_{Tnk}^r = \frac{-\alpha_{Tnk}^r}{\beta_{nk}} \tag{B-8}$$

We have defined

$$\lambda_{Tnk}^r = nBM_{Tip,r} + M_{x,r}\alpha_{Tnk}^r + M_{s,r}\beta_{nk} \tag{B-9}$$

where $M_{Tip,r} = \Omega R / a_r$ is the tip rotational Mach number based on the local sound speed and M_{xr} and M_{sr} are the axial and swirl Mach numbers.

CONSERVATION OF MASS

J. H. Horlock's book *Actuator Disc Theory* (McGraw-Hill, New York, 1978) gives the conservation equations applied here. The unlinearized mass flux is ρu. Matching this across the actuator disk can be expressed

$$(\rho u)_a = (\rho u)_b \tag{B-10}$$

We write this in terms of steady and unsteady parts (with the tilde's):

$$(\rho_a + \tilde{\rho}_a)(U_a + \tilde{u}_a) = (\rho_b + \tilde{\rho}_b)(U_b + \tilde{u}_b) \tag{B-11}$$

and focus on the first order unsteady terms, which become

$$\rho_a \tilde{u}_a + \frac{U_a}{a_a^2}\tilde{p}_a = \rho_b \tilde{u}_b + \frac{U_b}{a_b^2}\tilde{p}_b \tag{B-12}$$

after applying $\tilde{p} = \tilde{\rho} a^2$. Now, we define

$$C_a = \frac{a_o}{p_o}\left(\rho_a \tilde{u}_a + \frac{U_a}{a_a^2}\tilde{p}_a\right) \tag{B-13}$$

for matching at the actuator disk with a similar form C_b for region b. The normalization via a_o/p_o is for convenience. a_o and p_o are reference values for the sound speed and ambient pressure which will drop out of the formulas later.

We interpret equation 13 to apply on a mode-by-mode basis and express the perturbation quantities as the sum over the 3 wave types

$$\begin{aligned} C_a = {} & \frac{a_o}{p_o}\left[\rho_a a_o \frac{p_o}{\rho_a a_o a_a}\left(\frac{-\alpha_1^a}{\lambda_1^a}\right) + \frac{M_{x,a}}{a_a} p_o\right] A_1^a \\ & + \frac{a_o}{p_o}\left[\rho_a a_o \frac{p_o}{\rho_a a_o a_a}\left(\frac{-\alpha_2^a}{\lambda_2^a}\right) + \frac{M_{x,a}}{a_a} p_o\right] A_2^a \\ & + \frac{a_o}{p_o}\left[\rho_a a_o\right] A_3^a \end{aligned} \tag{B-14}$$

where the first line comes from the upstream-going pressure wave, the second from the downstream-going pressure wave, and the third from the vorticity wave. Because we are matching on a mode-by-mode basis, we have dropped the n,k subscripts and $\exp i\psi_{nk}$, which are common to all terms. All of the matching is at $x=0$; reference planes are shifted later via the exponentials in equations B-1 and B-2. We compress the notation and write equation B-14 as

$$C_a = C_{1a} A_1^a + C_{2a} A_2^a + C_{3a} A_3^a \tag{B-15}$$

where

$$\begin{aligned} C_{1a} &= \frac{a_o}{a_a}\left[\frac{-\alpha_1^a}{\lambda_1^a} + M_x^a\right] \\ C_{2a} &= \frac{a_o}{a_a}\left[\frac{-\alpha_2^a}{\lambda_2^a} + M_x^a\right] \\ C_{3a} &= \gamma \frac{p_a}{p_o}\left(\frac{a_o}{a_a}\right)^2 \end{aligned} \tag{B-16}$$

where γ , the ratio of specific heats, entered from $p_o = \gamma \rho_o a_o^2$. The same argument leads to the conserved quantity on the b side of the actuator disk :

$$C_b = C_{1b} A_1^b + C_{2b} A_2^b + C_{3b} A_3^b \tag{B-17}$$

Now we equate C_a and C_b. Furthermore, we identify the 3 waves approaching the actuator disk as input waves and place them on the right hand side of the equation and the 3 waves leaving the actuator disk as scattered waves and place them on the left side. The input waves are the upstream-going pressure wave on the b side and the downstream-going pressure wave and the vorticity wave on the a side. The scattered waves are on the upstream-going wave on the a side and the downstream-going pressure and vorticity waves on the b side.

$$C_{1a} A_1^a - C_{2b} A_2^b - C_{3b} A_3^b = C_{1b} A_1^b - C_{2a} A_2^a - C_{3a} A_3^a \tag{B-18}$$

This is the first of the actuator disk equations and represents conservation of mass for the implicit n, k mode.

CONSERVATION OF AXIAL MOMENTUM

We treat conservation of axial momentum in similar fashion. The unlinearized conservation equation is

$$L \sin \alpha_m + (p + \rho u^2)_a = (p + \rho u^2)_b \tag{B-19}$$

where the first term is the axial component of loading on the disk. The critical step here is to separate the total loading on the blade row into the steady part, which is handled via the actuator disk, and the unsteady part, which is handled via unsteady cascade theory. Then, when we express the variables in equation B-19 in terms of steady and unsteady parts, the unsteady loading (on the actuator disk) is by definition equal to zero and the first order perturbation equation is

$$(1 + M_{xa}^2)\tilde{p}_a + 2\rho_a U_a \tilde{u}_a = (1 + M_{xb}^2)\tilde{p}_b + 2\rho_b U_b \tilde{u}_b \tag{B-20}$$

We define

$$F_a = \frac{1}{p_o}\left[(1 + M_{xa}^2)\tilde{p}_a + 2\rho_a U_a \tilde{u}_a\right] \tag{B-21}$$

and expand it in the 3 wave types, as before

$$F_a = F_{1a} A_1^a + F_{2a} A_2^a + F_{3a} A_3^a \tag{B-22}$$

where

$$F_{1a} = (1 + M_{xa}^2) + 2M_{xa}\left(\frac{-\alpha_1^a}{\lambda_1^a}\right)$$

$$F_{2a} = (1 + M_{xa}^2) + 2M_{xa}\left(\frac{-\alpha_2^a}{\lambda_1^a}\right) \tag{B-23}$$

$$F_{3a} = 2\gamma \frac{p_a}{p_o}\frac{a_o}{a_a} M_{xa}$$

The equations for the b side of the actuator disk are the same with b's substituded for the a's. By using the scheme described above for identifying source waves and scattered waves, the equation for conservation of axial momentum becomes

$$F_{1a}A_1^a - F_{2b}A_2^b - F_{3b}A_3^b = F_{1b}A_1^b - F_{2a}A_2^a - F_{3a}A_3^a \tag{B-24}$$

CONSERVATION OF TANGENTIAL MOMENTUM

The unlinearized equation for transverse (y direction) momentum is

$$-L\cos\alpha_m + (\rho uv)_a = (\rho uv)_b \tag{B-25}$$

Using the same arguments as in the discussion of axial momentum, the first order conserved quantity can be written

$$G_a = \frac{1}{p_o}[\rho_a U_a \tilde{v}_a + \rho_a V_a \tilde{u}_a + M_{xa}M_{sa}\tilde{p}_a] \tag{B-26}$$

or, in terms of the 3 wave types, as

$$G_a = G_{1a}A_1^a + G_{2a}A_2^a + G_{3a}A_3^a \tag{B-27}$$

where

$$G_{1a} = M_{xa}\left(\frac{-\beta_{nk}}{\lambda_1^a}\right) + M_{sa}\left(\frac{-\alpha_1^a}{\lambda_1^a}\right) + M_{xa}M_{sa}$$

$$G_{2a} = M_{xa}\left(\frac{-\beta_{nk}}{\lambda_2^a}\right) + M_{sa}\left(\frac{-\alpha_2^a}{\lambda_2^a}\right) + M_{xa}M_{sa} \tag{B-28}$$

$$G_{3a} = \gamma \frac{p_a}{p_o}\frac{a_o}{a_a}\left[M_{xa}\left(\frac{-\alpha_3^a}{\beta_{nk}}\right) + M_{sa}\right]$$

and the conservation equation for tangential momentum has the same form as the other 2 conservation equations

$$G_{1a}A_1^a - G_{2b}A_2^b - G_{3b}A_3^b = G_{1b}A_1^b - G_{2a}A_2^a - G_{3a}A_3^a \tag{B-29}$$

SOLUTION OF LINEAR SYSTEM

By "solution" here, we mean finding the scattered waves for specified input waves. To this end we assemble equations B-18, B-24, and B-29 into matrix form

$$\begin{bmatrix} C_{1a} & -C_{2b} & -C_{3b} \\ F_{1a} & -F_{2b} & -F_{3b} \\ G_{1a} & -G_{2b} & -G_{3b} \end{bmatrix} \begin{bmatrix} A_1^a \\ A_2^b \\ A_3^b \end{bmatrix} = \begin{bmatrix} C_{1b} & -C_{2a} & -C_{3a} \\ F_{1b} & -F_{2a} & -F_{3a} \\ G_{1b} & -G_{2a} & -G_{3a} \end{bmatrix} \begin{bmatrix} A_1^b \\ A_2^a \\ A_3^a \end{bmatrix} \tag{B-30}$$

Solution to this equation is

$$\begin{bmatrix} A_1^a \\ A_2^b \\ A_3^b \end{bmatrix} = \begin{bmatrix} C_{1a} & -C_{2b} & -C_{3b} \\ F_{1a} & -F_{2b} & -F_{3b} \\ G_{1a} & -G_{2b} & -G_{3b} \end{bmatrix}^{-1} \times \begin{bmatrix} C_{1b} & -C_{2a} & -C_{3a} \\ F_{1b} & -F_{2a} & -F_{3a} \\ G_{1b} & -G_{2a} & -G_{3a} \end{bmatrix} \begin{bmatrix} A_1^b \\ A_2^a \\ A_3^a \end{bmatrix} \tag{B-31}$$

or simply

$$\begin{bmatrix} A_1^a \\ A_2^b \\ A_3^b \end{bmatrix} = \begin{bmatrix} K_{11} & K_{12} & K_{13} \\ K_{21} & K_{22} & K_{23} \\ K_{31} & K_{32} & K_{33} \end{bmatrix} \begin{bmatrix} A_1^b \\ A_2^a \\ A_3^a \end{bmatrix} \tag{B-32}$$

APPLICATION TO ACOUSTIC ELEMENTS

The objective of this analysis is to create rotor and stator acoustic elements that can be represented in the coupling system of Figure 2 of Part 1. For example, when the stator cascade (with uniform flow corresponding to region 2) is combined with an actuator disk at the trailing edge to turn the flow from the θ direction to axial, the result is the stator acoustic element. This is done by using equation B-32, which amounts to 3 equations for the input/output behavior of the actuator disk, and a similar set of 3 equations for the input output behavior of the stator cascade. Setting the output of the cascade (on the downstream side) to the input of the actuator disk (on the upstream side) and the output of the actuator disk to the input of cascade permits us to eliminate 3 equations. The remaining 3 equations represent the input/output characteristics of the combined stator element.

APPENDIX C
CHANNEL RESONANCE CONDITIONS

When waves at the same frequency travel upstream and downstream in the channel between 2 adjacent vanes, a standing wave pattern forms. If the distance between nodes matches the channel length (the chord), a resonance could occur that might have an effect on reflection and transmission curves. In this appendix, we derive formulas to predict the vane/blade ratios for this condition for stators and rotors.

From equation 16 in Part 1, we can deduce that the axial wavenumbers for 1 dimensional waves in a flow of Mach number M are given by

$$\alpha_{1,2} = \pm \frac{\omega / a}{1 \mp M} \tag{C-1}$$

Then the sum of a wave travelling upstream and a wave travelling downstream can be written

$$p = \cos(\alpha_1 x + \omega t) + \cos(\alpha_2 x + \omega t) \tag{C-2}$$

Since we are only finding the standing wave condition and not attempting to be general, we use unit amplitude waves. The mean square of the pressure can be obtained by squaring this expression and averaging over time with the result

$$\overline{p^2} = 1 + \cos\left(\frac{2\frac{\omega x}{a}}{1 - M^2} \right) \tag{C-3}$$

The resonance condition occurs when the phase of the cosine equals 2π, 4π, etc. at x = b , i.e. for

$$\frac{2\frac{\omega b}{a}}{1 - M^2} = 2\pi q \tag{C-4}$$

where q is an integer. For the stator the radian frequency is $\omega = nB\Omega$ and the chord can be expressed as

$$b = \frac{1}{G}\frac{2\pi R}{V} \tag{C-5}$$

where G is the stator gap/chord ratio. Substitution into the Equation C-4 gives the desired formula for the stator

$$\frac{V}{nB} = \frac{M_T}{(1 - M^2)\frac{q}{2}G} \tag{C-6}$$

Similar analysis for the rotor leads to

$$\frac{B}{kV} = \frac{M_T}{(1 - M'^2)\frac{q}{2}G_r} \tag{C-7}$$

where M' is relative Mach number in the rotor blade passages and G_r is rotor gap/chord. These formulas are used in Section 2.2 of the text to generate Table 8.

APPENDIX D
CALCULATION OF MEAN FLOW PARAMETERS

Analysis in this report recognizes 3 regions of mean flow:

Region 1	Upstream of rotor	axial
Region 2	Between rotor and stator	swirling
Region 3	Downstream of stator	axial

Background (or mean) flow values of Mach number, pressure, and speed of sound in each of these regions are required for the acoustic and unsteady aerodynamic models. This appendix presents the scheme for calculation of the mean flow, including the FORTRAN code listing and a sample case. Much of the documentation is included with the listing.

Flow regions and some of the associated notation is sketched below.

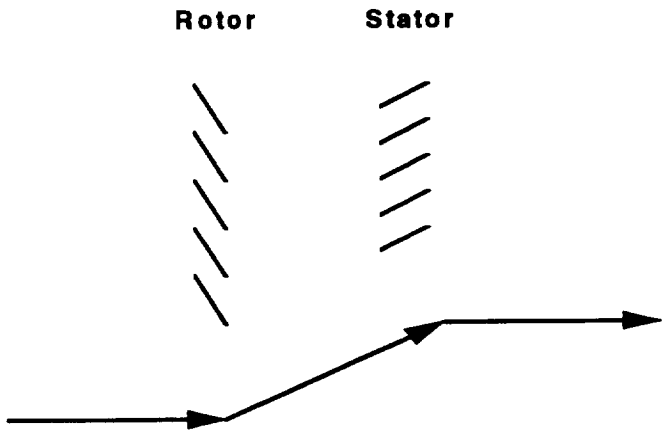

Operation of the system is as follows. Upstream total pressure and temperature are fixed at sea level, standard day values. The user specifies inflow axial Mach number, rotor rotational Mach number (based on speed of sound from region 1), and pressure ratio. The remaining quantities are then computed with 1D isentropic (lossless) flow equations and the standard equation for action of the rotor:

$$\Delta(\text{tangential velocity}) = \frac{C_p}{\text{wheel speed}} \times \Delta(\text{total temperature})$$

where C_p is the specific heat at constant pressure. Steps in the procedure can be followed easily in the code listing.

Calling Routine

The code is written as a subroutine. The calling main program immediately below was written for testing purposes. It is followed by the background flow subroutine. Sample I/O is shown at the end of this appendix.

```
      PROGRAM CALLMEANFLOW

      IMPLICIT DOUBLE PRECISION (A-H, O-Z)
      DIMENSION A(3), P(3)
      DOUBLE PRECISION MX(3),MY(3),MT(3),M1,MT1

      WRITE(*,*) 'Input M1, MT1, PR'
      READ(*,*) M1,MT1,PR
      CALL MEANFLOW(M1,MT1,PR,  P,A,MX,MY,MT )
      WRITE(*,1)  MX(1), MX(2), MX(3)
      WRITE(*,2)  MY(1), MY(2), MY(3)
      WRITE(*,3)  MT(1), MT(2), MT(3)
      WRITE(*,4)  A(1),  A(2),  A(3)
      WRITE(*,5)  P(1),  P(2),  P(3)
1     FORMAT(1X,'MX1, MX2, MX3 = ', 3F10.3)
2     FORMAT(1X,'MY1, MY2, MY3 = ', 3F10.3)
3     FORMAT(1X,'MT1, MT2, MT3 = ', 3F10.3)
4     FORMAT(1X,' A1,  A2,  A3 = ', 3F10.3)
5     FORMAT(1X,' P1,  P2,  P3 = ', 3F10.3)

      END
```

Background Flow Code

```
      SUBROUTINE MEANFLOW(M1,MT1,PR,  P,A,MX,MY,MT )
c.. This routine computes the mean (or background) flow parameters needed for
c.  acoustic calculations in 3 regions: 1-> upstream of rotor, 2-> between
c.. rotor and stator, 3-> downstream of stator.
c.. Calculations based on rotor action being given by delta T0=U*Cy2/Cp,
c.. one dimensional isentropic flow, equation of state (to get speed of sound),
c.. continuity, and assumption of zero losses. Coding by D. Hanson, Consulting on
c.. aero theory by M. Devries


c                        rotor        stator
c                          \           /
c    Regions:     1         \     2     /            3
c                          \           /
c
c                                      ----------------->
c                                    ^
c                                  /
c         axial                   /          axial
c         flow                  /swirl       flow
c         upstream            /  region      downstream
c        ----------------->/
c
c
c  SET:  T01, P01, M1
c      as inflow conditions
c
c  SPECIFY: Pressure ratio (PR) and rotor rotational Mach number (MT1)
c
c  COMPUTE:
c     T1, P1, A1             P2, T2        P3, T3, .....
```

```
      IMPLICIT DOUBLE PRECISION (A-H, O-Z)
      DIMENSION A(3), P(3)
      DOUBLE PRECISION MX(3),MY(3),MT(3),M1,M2,M3,MT1,M2OLD,M3OLD

c.. Input based to be based on Sea level standard day conditions

      GAM = 1.4D0           ! Ratio of specific heats
      R   = 1716.59D0       ! Gas Constant
      Cp  = 6008.09D0       ! Specific heat @ constant pressure

      Tstd = 518.67D0           ! Sea level Standard Day - Degrees Rankine
      Pstd = 2116.22D0          ! Sea level Standard Day - pounds/sq.ft.
      Astd = SQRT(GAM*R*Tstd)   ! ft/sec   (from equation of state)

      T01 = Tstd            ! Inflow based on Sea Level Standard Day
      P01 = Pstd            ! Inflow based on Sea Level Standard Day

c.. Compute parameters for Region 1 (upstream of rotor - axial flow)
      F1  = 1 + (GAM-1D0)/2 * M1**2          ! 1D isentropic flow
      T1  = T01 / F1                         ! 1D isentropic flow
      P1  = P01 / F1**(GAM/(GAM-1D0))        ! 1D isentropic flow
      RHO1= P1/(R*T1)                        ! Gas law
      A1  = SQRT(GAM*R*T1)          ! equation of state
       U  = MT1 * A1                ! rotor tip Mach number based on region 1
      Cx1 = M1 * A1                 ! axial velocity (needed later for continuity)

c.. Compute parameters for Region 2 (between rotor and stator - swirl flow)
      P02 = PR * P01                          ! Pressure ratio from input
      DELTAT0 = T01 * ( PR**((GAM-1D0)/GAM) - 1D0) ! assumes 100% efficiency
      T02 = T01 + DELTAT0
      Cy2 = (Cp/U) * DELTAT0                  ! Equation for action of rotor

c..  Iterate on Mach number and continuity
      M2 = M1 * SQRT(Cx1**2+Cy2**2)/Cx1   ! First guess to start iteration loop
      write(*,*)'Iteration on Mach number in region 2'
      DO I = 1, 10
        F2 = 1 + (GAM-1D0)/2 * M2**2          ! 1D isentropic flow
        T2 = T02 / F2                         ! 1D isentropic flow
        P2 = P02 / F2**(GAM/(GAM-1D0))        ! 1D isentropic flow
        RHO2=P2/(R*T2)                        ! Gas law
        A2 = SQRT(GAM*R*T2)                   ! equation of state
        Cx2 = Cx1 * RHO1/RHO2                 ! continuity
        M2old = M2                            ! save for convergence check
        M2 = SQRT(Cx2**2+Cy2**2) / A2         ! new estimate of Mach number
        write(*,*) i, m2
        IF (ABS(M2-M2OLD) .LT. .0001D0) GOTO 10
      ENDDO
      WRITE(*,*) 'WARNING, M2 LOOP NOT CONVERGED IN MEANFLOW ROUTINE'
10    CONTINUE

      write(*,*) ' '            ! write swirl angle (from axis of rotation)
      THETA = ATAN(Cy2/Cx2)
      write(*,*) 'Flow angle = ', theta*180d0/3.14159265D0
      write(*,*) ' '

c.. Compute parameters for Region 3 (downstream of stator - axial flow)
      T03 = T02                         ! Assume zero losses
      P03 = P02                         ! Assume zero losses

c..  Iterate on Mach number and continuity
      M3 = M2 * COS(THETA)              ! First guess to start iteration loop
      write(*,*)'Iteration on Mach number in region 3'
      DO I = 1, 10
        F3 = 1 + (GAM-1D0)/2 * M3**2          ! 1D isentropic flow
        T3 = T03 / F3                         ! 1D isentropic flow
        P3 = P03 / F3**(GAM/(GAM-1D0))        ! 1D isentropic flow
        RHO3=P3/(R*T3)                        ! Gas law
```

```
        A3 = SQRT(GAM*R*T3)                    ! equation of state
        Cx3 = Cx2 * RHO2/RHO3                  ! continuity
        M3old = M3                             ! save for convergence check
        M3 = Cx3 / A3                          ! new estimate of Mach number
        write(*,*) i, m3
        IF (ABS(M3-M3OLD) .LT. .0001D0) GOTO 20
      ENDDO
      WRITE(*,*) 'WARNING, M3 LOOP NOT CONVERGED IN MEANFLOW ROUTINE'
20    CONTINUE
c.. Prepare values to return to calling routine
      A(1) = A1/Astd
      A(2) = A2/Astd
      A(3) = A3/Astd
      P(1) = P1/Pstd
      P(2) = P2/Pstd
      P(3) = P3/Pstd
      MX(1) = M1
      MX(2) = M2 * COS(THETA)
      MX(3) = M3
      MY(1) = 0D0
      MY(2) = M2 * SIN(THETA)
      MY(3) = 0D0
      MT(1) = MT1
      MT(2) = MT1*A1/A2
      MT(3) = MT1*A1/A3

      RETURN
      END
```

Sample Case

Type a.out to get:

```
Input M1, MT1, PR
```

Enter values for axial Mach number, tip rotational Mach number, and pressure ratio:

```
      .510   .772    1.278
```

Hit "Enter" to do the calculation with the result:

```
 Iteration on Mach number in region 2
   1    0.49069069566595
   2    0.47318442132157
   3    0.46959417475541
   4    0.46887728952648
   5    0.46873493006882
   6    0.46870669130413

 Flow angle =      30.501298137168

 Iteration on Mach number in region 3
   1    0.39084584049871
   2    0.38850434236162
   3    0.38809172279216
   4    0.38801929795917
 MX1, MX2, MX3 =       0.510      0.404      0.388
 MY1, MY2, MY3 =       0.000      0.238      0.000
 MT1, MT2, MT3 =       0.772      0.743      0.738
  A1,  A2,  A3 =       0.975      1.014      1.020
  P1,  P2,  P3 =       0.837      1.099      1.152
```

REPORT DOCUMENTATION PAGE

Form Approved
OMB No. 0704-0188

1. AGENCY USE ONLY (*Leave blank*)	2. REPORT DATE	3. REPORT TYPE AND DATES COVERED
	March 1999	Final Contractor Report

4. TITLE AND SUBTITLE

Acoustic Reflection and Transmission of 2–Dimensional Rotors and Stators, Including Mode and Frequency Scattering Effects

5. FUNDING NUMBERS

WU–538–03–11–00
NAS3–26618

6. AUTHOR(S)

Donald B. Hanson

7. PERFORMING ORGANIZATION NAME(S) AND ADDRESS(ES)

United Technologies Corporation
Pratt and Whitney Division
400 Main Street
East Hartford, Connecticut

8. PERFORMING ORGANIZATION REPORT NUMBER

E–11599

9. SPONSORING/MONITORING AGENCY NAME(S) AND ADDRESS(ES)

National Aeronautics and Space Administration
John H. Glenn Research Center at Lewis Field
Cleveland, Ohio 44135–3191

10. SPONSORING/MONITORING AGENCY REPORT NUMBER

NASA CR—1999-208880
PWA 6420–107

11. SUPPLEMENTARY NOTES

Project Manager, Dennis L. Huff, NASA Lewis Research Center, organization code 5940, (216) 433–3913.

12a. DISTRIBUTION/AVAILABILITY STATEMENT

Unclassified - Unlimited
Subject Category: 71 Distribution: Nonstandard

This publication is available from the NASA Center for AeroSpace Information, (301) 621–0390.

12b. DISTRIBUTION CODE

13. ABSTRACT ***(Maximum 200 words)***

A reduced order modeling scheme has been developed for the unsteady acoustic and vortical coupling between blade rows of a turbomachine. The essential behavior of the system is governed by modal scattering coefficients (i.e., reflection and transmission coefficients) of the rotor, stator, inlet and nozzle, which are calculated as if they were connected to non-reflecting ducts. The objective of this report is to identify fundamental behavior of these scattering coefficients for a better understanding of the role of blade row reflection and transmission in noise generation. A 2D flat plate unsteady cascade model is used for the analysis with the expectation that the general behavior presented herein will carry over to models that include more realistic flow and geometry. It is shown that stators scatter input waves into many modes at the same frequency whereas rotors scatter on frequency, or harmonic order. Important cases are shown here the rotor reflection coefficient is greater than unity; a mode at blade passing frequency (BPF) traveling from the stator with unit sound power is reflected by the rotor with more than unit power at 2xBPF and 3xBPF. Analysis is presented to explain this unexpected phenomenon. Scattering curves are presented in a format chosen for design use and for physical interpretation. To aid in interpretation of the curves, formulas are derived for special condition where waveforms are parallel to perpendicular to the rotor.

14. SUBJECT TERMS

Acoustics; Turbomachinery; Noise; Fans

15. NUMBER OF PAGES

75

16. PRICE CODE

A04

17. SECURITY CLASSIFICATION OF REPORT	18. SECURITY CLASSIFICATION OF THIS PAGE	19. SECURITY CLASSIFICATION OF ABSTRACT	20. LIMITATION OF ABSTRACT
Unclassified	Unclassified	Unclassified	